UNIVERSITY OF OKLAHOMA

GRADUATE COLLEGE

ASSESSING MUDROCK CHARACTERISTICS, HIGH-RESOLUTION CHEMOSTRATIGRAPHY, AND SEQUENCE STRATIGRAPHY OF THE WOODFORD SHALE IN THE MCALISTER CEMETERY QUARRY, ARDMORE BASIN, OKLAHOMA

A THESIS

SUBMITTED TO THE GRADUATE FACULTY

in partial fulfillment of the requirements for the

Degree of

MASTER OF SCIENCE

By

IFUNANYA CYNTHIA EKWUNIFE
Norman, Oklahoma
2017

ASSESING MUDROCK CHARACTERISTICS, HIGH-RESOLUTION CHEMOSTRATIGRAPHY, AND SEQUENCE STRATIGRAPHY OF THE WOODFORD SHALE IN THE MCALISTER CEMETERY QUARRY, ARDMORE BASIN, OKLAHOMA

A THESIS APPROVED FOR THE
CONOCOPHILLIPS SCHOOL OF GEOLOGY AND GEOPHYSICS

BY

_____

Dr. Roger Slatt, Chair

_____

Dr. Matthew Pranter

_____

Dr. Fuge Zou

ACKNOWLEDGMENTS

First, I thank God for grace, love, blessings, spiritual support, and good health throughout my master's program. I am grateful for purpose and passion, for without these essential elements I would not be where I am.

My appreciation to one of the most amazing academic advisors in the world, Dr. Roger Slatt. I am truly honored to have worked with him. His support and encouragement carried me throughout my journey at the University of Oklahoma. What an impact he makes in the life of his students. His heart of Gold will never be forgotten.

This thesis would not be possible without the support of our great consortium members; BHP, New Field Exploration, Tapstone Energy, Southwestern Energy, Paisano Energy, Chaparral Energy, BP, Casillas Petroleum Corporation, Jones Energy, Jetta Corporation, Marathon Oil Corporation, Jetta Operating Company, Rebellion Energy, Chevron, ConocoPhillips, Longfellow Energy, Payrock Energy, Pathfinder Exploration, Tip Top Energy, Apache Corporation, Council Oak Resources, Ward Petroleum, Halliburton, Nostra Terra Oil and Gas Company, Potts-Stephenson Exploration Company, Chandler Engineering, Gastar Exploration, Vitruvian Exploration, and Central Sumatera Energy.

Thank you to my thesis committee members, Dr. Matthew Pranter and Dr. Fuge Zou. I appreciate the time taken from their busy schedules to be part of my thesis work.

Thank you to my research colleagues for great discussions, and suggestions. Muizz Matemilola, Jing Zhang, Richard Brito, Sayantan Ghosh, Carlos Molinares, David Duarte Coronado, Benmadi Milad, Daniela Becerra, and Henry Galvis, I appreciate every one of them. To the 'dad minion' himself, Dr. Bryan Turner, I thank him for sharing his knowledge on fieldwork and geochemistry, for this certainly added value to my research. To my field assistants, Sama Khawaja and Faryl Smith, I thank them for the hard work, dedication, and fun times out in the field.

Lastly, I thank my family for everything. My mother for being a rock in my life. My siblings for their effort and emotional support, and to my father, I say thank you for supporting my dreams and career. I know you are looking down, and you are proud of what I have achieved and who I have become. Thank you for giving me the opportunity to further my education. I will always make you proud.

TABLE OF CONTENTS

LIST OF TABLES

LIST OF FIGURES

ABSTRACT

The Late Devonian – Early Mississippian Woodford Shale is a significant unconventional play in the Midcontinent region. An approximately 365ft thick exposure of the Woodford Shale is present in the McAlister Cemetery Quarry. Mudrock samples were collected every stratigraphic foot and analyzed for its characteristics using outcrop gamma-ray variations, XRF elemental compositions, XRD mineralogy, hardness variations, petrographic and SEM analysis. Eight major lithofacies were defined for the Woodford Shale section, starting from most clay-rich to most siliceous, and decreasing degree of fissility: clayshales, mixed clayshales – mudshales, argillaceous mudshales, siliceous mudshales, siliceous mudstones, and radiolarian chert. Calcareous lithofacies defined include dolomitic mudstones and dolomitic mudshales.

The technique of chemostratigraphy relies upon the fact that stratigraphic variations in geochemistry can be useful for the interpretation of the changes in minor fluctuations in variables such as facies, paleo-redox conditions, organic paleoproductivity, carbonate paleoproductivity, and depositional cyclicity. Redox-sensitive elements were used for analyzing paleoenvironmental conditions such as bottom water redox conditions, water column metal-oxyhydroxide particulate shuttles, and the degree of water mass restriction. Using high-resolution chemostratigraphy paired with hierarchical clustering analysis (HCA), the study area presents an opportunity to better understand the paleodepositional conditions and to investigate the possibility for the subdivision of the Woodford Shale into more units and to compare their geochemical

character. Overall, the Woodford Shale showed stratigraphic geochemical variations associated with a decrease in the degree of basin restriction up-section.

The general sequence-stratigraphic model established for unconventional resource shales was applied to the Woodford Shale section for sequence stratigraphic interpretations. Using gamma-ray (GR) parasequences, the Lower and Middle Woodford Shale were deposited during a 2nd order transgressive cycle represented by increasing GR. The Upper Woodford Shale was deposited during a turn-around point, during a 2nd order regressive cycle. Additionally, fourteen 3rd order regressive-transgressive cycles were identified. In the Lower Woodford Shale, five 3rd order cycles were identified, four 3rd order cycles were defined in the Middle Woodford Shale, and five 3rd order cycles were defined in the Upper Woodford Shale.

Source rock evaluation demonstrates that the Woodford Shale is organic-rich. The Lower, Middle and Upper Woodford Shale possess average TOC values of 12.34 wt%, 11.2 wt%, 5.96 wt%; respectively. Type II kerogen is the most dominant (oil-prone), suggesting marine origin. Type I kerogen occurs in the Lower Woodford Shale, indicating lacustrine type deposition. Results from both calculated and measured Vitrinite reflectance shows that the Woodford Shale has low to moderate thermal maturity, and falls within the immature to early oil window.

CHAPTER I
INTRODUCTION

1.1. Scope of Thesis

A majority of wells drilled in North America are for unconventional resource plays. As shale plays continue to increase in importance, the ability to define stable stratigraphic frameworks using outcrop data becomes increasingly critical. Field-based studies or examination of outcrop analogs have long been an important aspect for the configuration of producing oil and gas fields in the subsurface. Outcrops have continued to play a central role in improving our understanding of the subsurface reservoir architecture. Outcrops have proven to be exceptional, especially when directly related to subsurface data (i.e., well logs, cores, seismic, e.t.c.) (e.g., Slatt et al., 2012; Becerra-Rondon, 2017; Brito et al., 2017; Galvis, 2017). In this research, outcrop studies allowed for the examination and evaluation of stratigraphic and sedimentological heterogeneities, which will eventually provide useful analogs for subsurface correlations.

In general, mudrocks can appear physically homogeneous; however, their geological, and geochemical properties can vary significantly. Assessing mudrock characteristics (both internal and external characteristics) is essential in understanding these variations. Using qualitative and semi-qualitative techniques such as petrography, scanning electron microscopy (SEM), x-ray fluorescence (XRF), x-ray diffraction (XRD), and outcrop gamma-ray (GR), the heterogenetic nature of mudrocks was demonstrated. As a result, a detailed lithofacies analysis was defined for the Woodford Shale at this popular and complete outcrop section.

Chemostratigraphy provides the opportunity to demonstrate geochemical variability. The technique relies on the fact that stratigraphic variations in geochemistry can be useful for the interpretation of the changes in minor fluctuations in variables such as facies, paleoredox conditions, paleoproductivity, and depositional cyclicity. The utility of chemostratigraphy within mudrock successions such as the Woodford Shale described in Tréanton (2014), Turner et al. (2015), Ekwunife (2015, 2016), Turner (2016), Turner et al., 2016, Becerra-Rondon (2017), Galvis (2017), and others. In this research, a multi-proxy approach was applied in order to: (i) highlight the geochemical variations in the Woodford Shale, (ii) reconstruct the paleoenvironmental setting of the Woodford Shale, (iii) delineate the degree of water mass restriction, and (iv) demonstrate the ability to go beyond the informal subdivision of the Woodford Shale sequence and to further subdivide the sequence into chemical facies/chemofacies (associated with changes in the concentrations of different elements) using multivariate statistics.

The concept of sequence stratigraphy is now an accepted approach for correlating organic-rich black shales (e.g., Singh, 2008; Slatt and Rodriguez, 2012; Slatt et al., 2012). Using the generalized sequence-stratigraphic model of unconventional resource shales in Slatt and Rodriguez (2012), it was possible to (i) delineate 3rd order stratigraphic gamma-ray (GR) parasequences and their component systems tracts, and (ii) construct a sequence stratigraphic framework based on defined GR parasequences. Additionally, source rock evaluation was conducted on the Woodford Shale section using organic-richness, kerogen type, and thermal maturity deduced from TOC and Rock-Eval data.

The Woodford Shale outcrop at the McAlister Cemetery Quarry is significant for such a study as it contains an extensive, well-preserved exposure of the complete section

of the Woodford Shale. Results from this study are expected to provide insight and to better understand geological/geochemical factors that might have influenced the depositional conditions of the Woodford Shale.

1.2. Previous Research

The Woodford Shale has historically been of great interest, initially for its role as a hydrocarbon source rock, and more recently for its reservoir potential. Since the first description of the Woodford Shale (Taff, 1902), comprehensive studies have been conducted on McAlister Cemetery Quarry (Kirkland et al., 1992; Serna-Bernal, 2013; DeGarmo, 2015) as well as nearby outcrops (Blackford, 2007; Miceli, 2012; Ellis, 2013; Fishman, 2013, Galvis, 2017, Becerra-Rondon, 2017), all detailing both the sedimentologic and stratigraphic features of the Woodford Shale. In southern Oklahoma several authors agree with the concept that the Woodford Shale is not a single depositional package, but instead is characterized by cyclical deposition that resulted in a sequence with intervals that are quartz-rich, high in organic matter concentration, and high radioactivity (up to 300 cps) (Landis, 1962; Hester et al, 1990; Kirkland et al, 1992; Krystyniak, 2005; Aufill, 2006; Blackford, 2007; Slatt 2012-2013-2016).

Taff (1902) was the first to highlight the characteristics of the Woodford Shale based on studies in southern Oklahoma (Murray, Carter, Marshall, Johnson, and Atoka Counties). He described the Woodford Shale as thinly interbedded chert and black shales, with a total thickness that ranges from 500 - 700 feet, mainly resting unconformably on the Silurian Hunton Group. Landis (1962), based on studies also in southern Oklahoma (Arbuckle Mountains), recognized that the largest uranium content in the Woodford Shale is related to the uraniferous asphaltic material associated with the highly folded and

brecciated strata. Hester et al. (1990) from work in northwestern Oklahoma (Anadarko Basin) was able to recognize that the Woodford Shale was not one depositional package, and subdivided the Woodford Shale, based on log responses, into informal lower, middle, and upper members. It is important to point out the log character of the Woodford Shale can differ from basin to basin based on lateral and vertical heterogeneities liberated from depositional conditions, even though the Woodford Shale looks similar in gross character.

Kirkland et al. (1992) documented the first study at the McAlister Cemetery Quarry. Along with the work done in the western Arbuckle Mountains, they identified that the Woodford Shale accumulated at a slow rate in water that was several hundred feet deep in a broad, thermally stratified tropical or subtropical, intracratonic sea. Krstyniak (2005), analyzed the gamma-ray intensity and resistivity of the Woodford Shale in southern Oklahoma (Carter and Murray Counties). Krstynaik's study recognized that the lower and middle members of the Woodford Shale have higher gamma-ray intensity and resistivity, and that the upper member has lower gamma-ray counts, lower resistivity, and is characterized by interbedded chert and shale. Aufill et al. (2006) documented difficulties in correlating formation radioactivity with TOC in the Woodford Shale. It was recognized that gamma-ray magnitude does not always correspond with organic richness. The anoxic or euxinic conditions postulated to be the requirement for source rock formation (Demaison and Moore, 1980), did not completely prevail in the deposition of the Woodford Shale.

Blackford (2007) interpreted and mapped the informal stratigraphy of the Woodford Shale from well logs, identifying the three informal stratigraphic units across the Arkoma basin. Isopach maps indicated that the upper unit is the least favorable in

thickness, and the lower unit is highly variable due to the in-filling of paleo-depressions in the underlying Hunton Group surface (Infante-Paez et al., 2016). The radioactivity response of the Woodford Shale (southern Oklahoma) analyzed in Boardman (2009) indicates that the total radioactivity is driven by uranium enrichment and that the preservation of non-metabolized remains of phytoplankton within fine-grained clastic and biogenic sediments provided the Woodford with an immense capacity to generate oil at thermal maturity.

Slatt et al., (2016) from studies in central and southern Oklahoma demonstrated the impact of paleotopography on the thickness of the Lower Woodford Shale. It was identified that the Woodford Shale tends to be thicker in paleotopographic lows (incised valleys and paleokarst) of the Hunton Group or Sylvan Shale. McCullough (2014), in the study of the Woodford Shale in the Cherokee Platform (central Oklahoma), identified that the Woodford Shale was deposited within two linear trends that correspond to eroded and missing sections on the underlying Hunton Group. These trends coincide with incised valleys that were carved out of the underlying Hunton Group by erosional processes that occurred a falling stage of sea level prior to the deposition of the Woodford Shale.

Using evidence from GR log patterns, pollen index, and Ti/Al and Si/Al geochemical patterns, Molinares-Blanco (2013) suggested that the Lower and Middle Woodford Shale correspond to a 2nd order Transgressive System Tract (TST) and the Upper Woodford to a 2nd order Highstand System Tract (HST). Serna-Bernal (2013) from studies of the Woodford Shale at the McAlister Cemetery Quarry (~ 400 feet thick), interpreted that the lower member of the Woodford Shale was deposited during a 2nd

order TST. The middle member was deposited during the transition from TST to HST, representing the final stage of retrogradation and the onset of progradation.

Several organic geochemical studies have been conducted on the Woodford Shale. Type-II kerogen dominates the organic carbon content, with a lesser abundance of both type-I and type-III kerogens (Lewan, 1983). Miceli-Romero (2012) from work in southeastern Oklahoma (Pontotoc County) demonstrated the significant variability that occurs within shales. It was interpreted that the lower and the upper Woodford members were deposited under dysoxic to suboxic conditions and episodic photic zone anoxia while the middle member was deposited under anoxic conditions and persistent photic zone anoxia. DeGarmo (2015), using TOC and biomarkers suggested that two intervals within the Upper Woodford show a potential for subaerial exposure and paleoweathering. Evidence of influxes of weathered terrigenous organic matter appears to occur in all sections of the Woodford Shale, but could also be a product of modern exposure of quarry walls.

Several inorganic geochemical studies, using XRF analysis have been conducted on the Woodford Shale. Tréanton (2014), from studies in the Arkoma Basin, interpreted that the lower and middle Woodford Shale members record a marine environment that is hydrologically stratified and distal. The upper member records a more proximal environment that was influenced by wind-driven upwelling events that explain the presence of phosphates, and high biogenic silica content. McCreight (2014) concluded that the Woodford Shale in the Anadarko Basin was deposited under relatively short-lived periods of anoxic conditions, fluctuating with periods of oxic conditions. Turner et al. (2015) and Turner et al. (2016) concluded from work done in the Arkoma Basin that the

deposition of the lower and middle Woodford Shale members was occasionally interrupted by a sudden sedimentation event due to the movement of the shoreline position toward the ocean. The Woodford Shale records oscillating bottom water conditions through time, and this bottom water ventilation generally improves up-section. Localized paleotopographic depressions were conducive for organic matter preservation, and these depressions represent "sweet spots" for hydrocarbon exploration (Infante-Paez et al., 2016).

CHAPTER II

GEOLOGICAL CONTEXT

2.1. Regional Geology

The Southern Oklahoma Aulacogen (SOA) and Ardmore Basin Evolution

The first tectonic event that affected the southern Oklahoma region from the late Precambrian to Late Pennsylvanian was a continental rifting stage in the late Precambrian that separated North America from the proto-Afro-South American plate (Walper, 1977; Wickham 1978; Ataman, 2008). The SOA represents the failed arm of a triple junction (**Figure 1**).

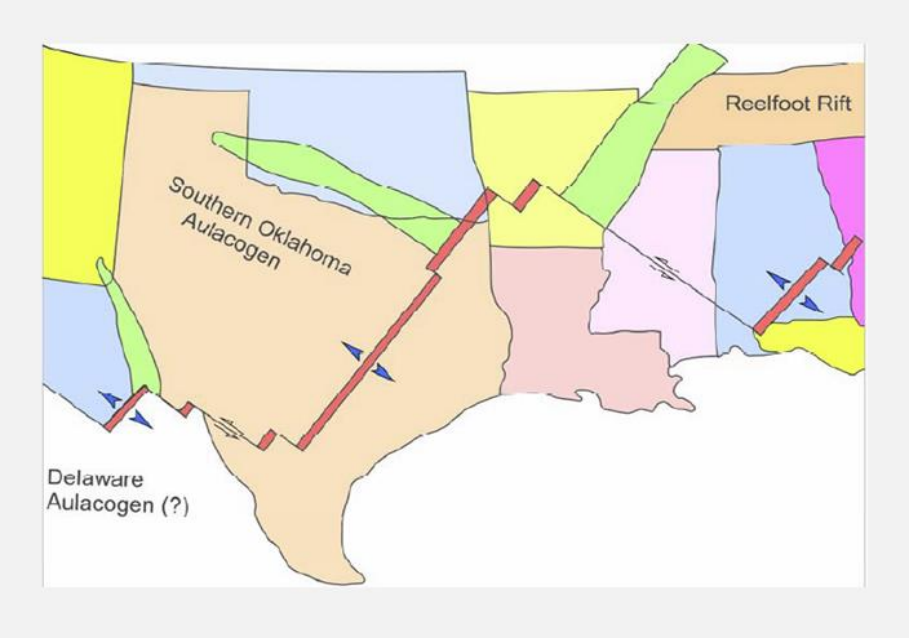

Figure 1. A plate tectonic model of the southern North America in the Cambrian Period (Adapted from Ataman, 2008: Modified from Suneson, 1996).

The SOA resulted in the development of normal faults and generated igneous rocks in the rifting stage (Hoffman et al., 1974). The rift cooled and began subsiding further with sediment accumulations. Later, the subsiding stage resulted in little folding and faulting. The deformation stage was the last stage in the evolution of the SOA (Ham, 1973) (**Figure 2**).

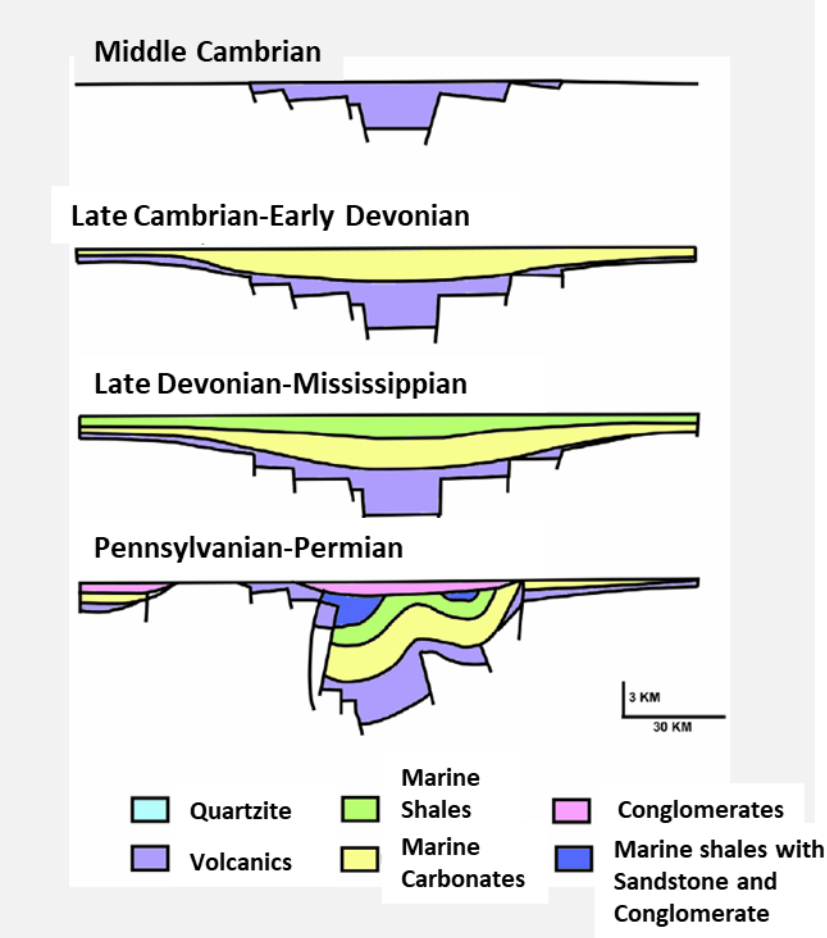

Figure 2. Structural development of the Southern Oklahoma Aulacogen; Rifting, Subsidence, and Deformation stages (Ataman, 2008: Modified from Bixler, 1993).

Orogenic activity in the SOA began with the Wichita Orogeny along the Wichita Mountains and Criner Hills in Late Mississippian time and ended with the Arbuckle

Orogeny in Virgilian time. The Wichita Uplift formed the Anadarko Basin; the Wichita Mountains and Criner Hills became intensely deformed during Morrowan time. The Wichita Orogeny continued during Early Atokan time and folded the Amarillo-Wichita-Criner trend (Hardie,1990).

The Arbuckle Orogeny, which occurred from Late Missourian to Early Permian time, represented a later pulse of deformation and reactivated the Wichita uplift, Hunton Anticline, Tishomingo Anticline and Criner Hills systems. Compression of the area between Tishomingo-Hunton and Criner Hills formed the northwest-southeast trending Ardmore Basin and the Arbuckle Anticline (Hardie, 1990) (**Figure 3**). Structural fingerprints of the orogenic events have been documented in Ghosh (2017a, 2017b).

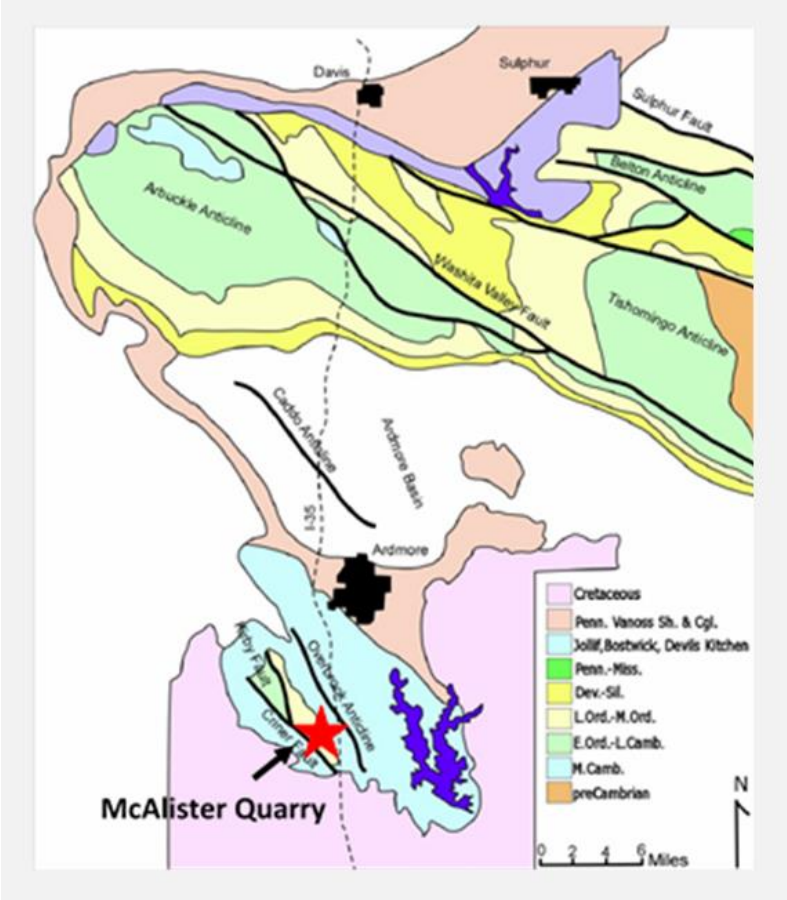

Figure 3. The structural expression for the region surrounding the study area. Structurally deformed rocks in the region range from Precambrian granite to Pennsylvanian conglomerate (Ataman, 2008: Modified from Grayson, 1985).

2.2. Woodford Shale

Stratigraphy

The Woodford Shale is laterally extensive in the subsurface throughout the state of Oklahoma. It extends throughout Oklahoma, Texas, Arkansas, Kansas, and New Mexico. In Oklahoma, it was deposited in what is now the Anadarko Basin, Arkoma Basin, Marietta Basin, Ardmore Basin, and Cherokee Platform. Laterally equivalent units of the Woodford Shale are the Chattanooga, New Albany and Ohio Shale Formations, which are also significant hydrocarbon source rocks and potential unconventional reservoirs (Kirkland et al., 1992). The Woodford Shale is an organic-rich, dark, siliceous mudrock with sporadic horizons of light-colored shales, phosphate nodules, cherty zones, and dolomitic zones, depending on stratigraphic position.

Typically, the Woodford Shale unconformably overlies the Ordovician-Devonian carbonates of the Hunton Group. Where the Hunton Group is absent; the Woodford Shale unconformably overlies the Sylvan Shale, Viola Limestone, or in rare occurrences, the Simpson Sandstone. The overlying strata is the Mississippian Sycamore Limestone or the Mississippian Limestone, as known in some parts of Oklahoma; the nature of the contact is transitional, and an unconformity in some areas. In the Ardmore Basin, the Woodford Shale is underlain by the Late Ordovician-Silurian-Devonian Hunton Group, with a contact marked by a major regional unconformity developed in the late Devonian. It is disconformably overlain by early Mississippian shales and limestones of the Sycamore Formation. Based on gamma-ray logs (radioactivity) and lithology, the Woodford shale

has been informally divided into three members; lower, middle and upper (Kirkland et al., 1992) (**Figure 4**).

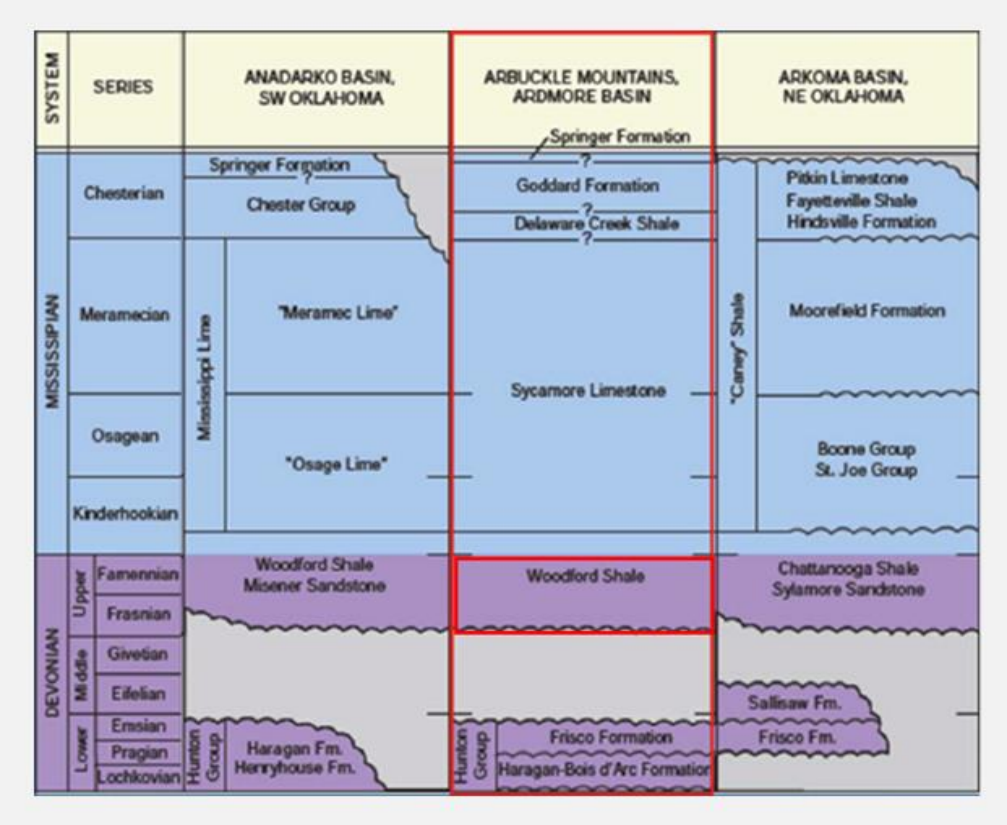

Figure 4. Stratigraphy of the Woodford Shale in the Ardmore Basin showing the overlying and underlying strata, the Hunton Group and the Sycamore Limestone respectively. (Modified from Comer, 2008).

The Lower Woodford Shale is predominately clay-rich and fissile, with minor thin highly siliceous beds that increase upsection.The Middle Woodford Shale has the highest radioactivity and organic richness and has been observed to be the most laterally extensive unit (Lambert, 1993). It is dominated by fissile shales, siliceous mudstones, and sporadically distributed dolomite beds. Remarkable features that are evident in this part of the section are the bitumen-filled fractures, where the level of thermal maturity has been attributed to pre-orogenic burial and syn-orogenic heating (Cardott, 1990).The

Upper Woodford Shale is characterized by interbedded chert and fissile shale beds that contain variable amounts of clays and carbonate minerals. The Upper Woodford Shale is dominated by phosphatic nodules and has the lowest radioactivity and organic-richness (Kirkland et al., 1992; Paxton et al., 2008).

The Lower Woodford Shale has been interpreted as deposition proximal to a shoreline during marine transgression. The Middle Woodford Shale, with the greatest areal extent of the three members occurred during deposition more distal from the shoreline during continued transgression. The Upper Woodford Shale was deposited closer to shore during a sea level fall (Cardott, 2005; Slatt et al., 2012).

Paleogeographic Setting

The Woodford Shale is a marine shale deposited in the early Paleozoic (Late Devonian to Early Mississippian) in a shallow, epicontinental sea in the western continental margin of North America close to a paleolatitude between 15º and 30º south latitude (Witze and Heckel, 1989; Comer 2005). The deposition of the Woodford Shale is related to equatorial or near equatorial latitudes, over an extensive intra-cratonic sea that was deeper toward the southeast and shallower to the northwest (Kirkland et al., 1992; Comer, 2005) (**Figure 5**). The Woodford Shale was deposited in dysoxic to anoxic redox conditions (Miceli-Romero and Philp, 2012; Amorocho, 2012).

Comer (2012) proposed a depositional environment that was dominated by upwelling as a result of aridity and high evaporation rates within the shallow epicontinental seaway that existed across the southern U.S. Similar geographic conditions are observed in modern marine upwelling centers where trade winds are driven by high dynamic episodes of circulation. The primary control for upwelling in modern systems is

atmospheric conditions, however, other controls may include, water temperature stratification, coastal topography, and bathymetry (Parrish, 1982; Anderson, 2015).

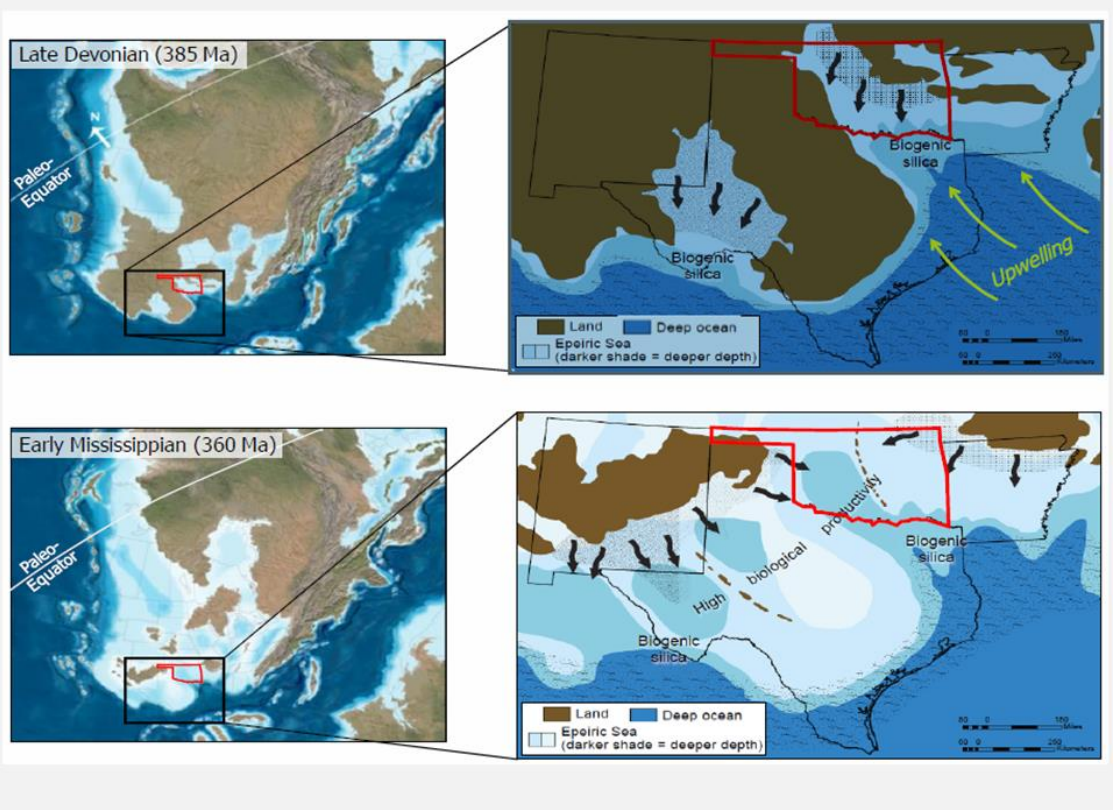

Figure 5. Paleogeography map of North America at the beginning of the Late Devonian and Early Mississippian, showing the extensive epeiric sea covering most of the area of Oklahoma, deeper portions are interpreted toward the southeast (Adapted from Galvis, 2017: Modified from Comer, 2008).

Paleotopography

Paleotopography is important to the distribution of the Woodford Shale facies. The Woodford Shale is stratigraphically variable due to the paletopographic expression developed pre-Woodford Shale deposition. Before the deposition of the Woodford Shale, the underying strata, the Hunton Limestone was subaerially exposed, forming a global unconformity beneath the Woodford. Incised valleys formed, deeper valleys were carved

into the less resistant Sylvan Shale, while shallower or no valleys were carved into the resistant limestones. Karst features on the unconformity surface of the limestones also produced topographic lows/irregularities.

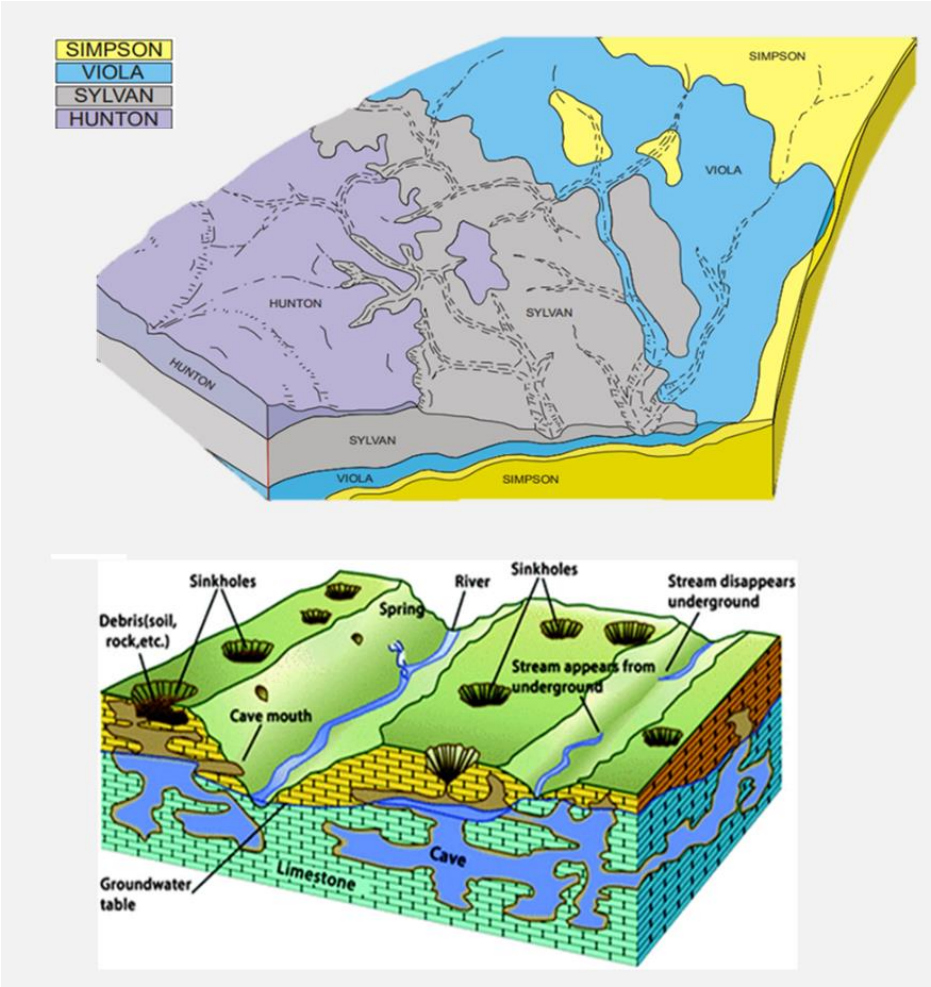

Figure 6. Top: Unconformity surface subject to erosional incision prior to Woodford Shale Deposition (Modified from Kuykendall and Fritz, 2001). **Bottom:** A generalized model of surface features on a carbonate unconformity (including incised valleys, collapsed caves, and karst sinkholes. Adapted from Infante-Paez et al., 2016: After Grotzinger and Jordan, 2010.

These paleotopographic expressions resulted in the stratigraphic variability of the Woodford across Oklahoma.The Woodford shale is underlain by different strata in

different areas of Oklahoma, specifically the Hunton Group (carbonates), the Sylvan shale, the Viola Limestone, and the Simpson Sandstone. The thickness of the Woodford Shale varies according to which of the strata underlies it. The Woodford Shale is thicker where it is underlain by the Sylvan Shale, and thinner when underlain by the Hunton Group or Viola Limestones (Althoff 2012; McCullough, 2014; Infante-Paez et al., 2016) (**Figur 6**).

2.3. Area of Study

Regionally, the study area, McAlister Cemetery Quarry, is located at the southern termination of the Ardmore Basin, close to the boundary with the Marietta Basin. Geographically, the McAlister Cemetery Quarry is located eight miles to the south of Ardmore, south of Carter County, Oklahoma, [Exit 24, I-35 South; NE 1/4, SW1/4, Sec. 36 T.5S., R1E] (Latitude N 34°04.868 Longitude W 97°09.395), elevation 846 ft. The outcrop is adjacent to the McAlister Cemetery, Ardmore, Oklahoma. Due to the excellent exposure of this outcrop, figuring out the location was fairly easy (**Figure 7**).

Locally, a complete section of the Woodford Shale, approximately 365ft, is exposed in the McAlister Cemetery Quarry (**Figure 8**). This complete characteristic of this specific outcrop is what makes it exceptional, as it presents the opportunity to perform detailed analysis. Here, the beds are striking N40^{o}W and steeply dipping 35^{o}NE. Also exposed is the underlying Late Ordovician-Early Devonian Hunton Group marked by an erosional unconformity, and the overlying Mississippian Sycamore Limestone, characterized by a transitional surface.

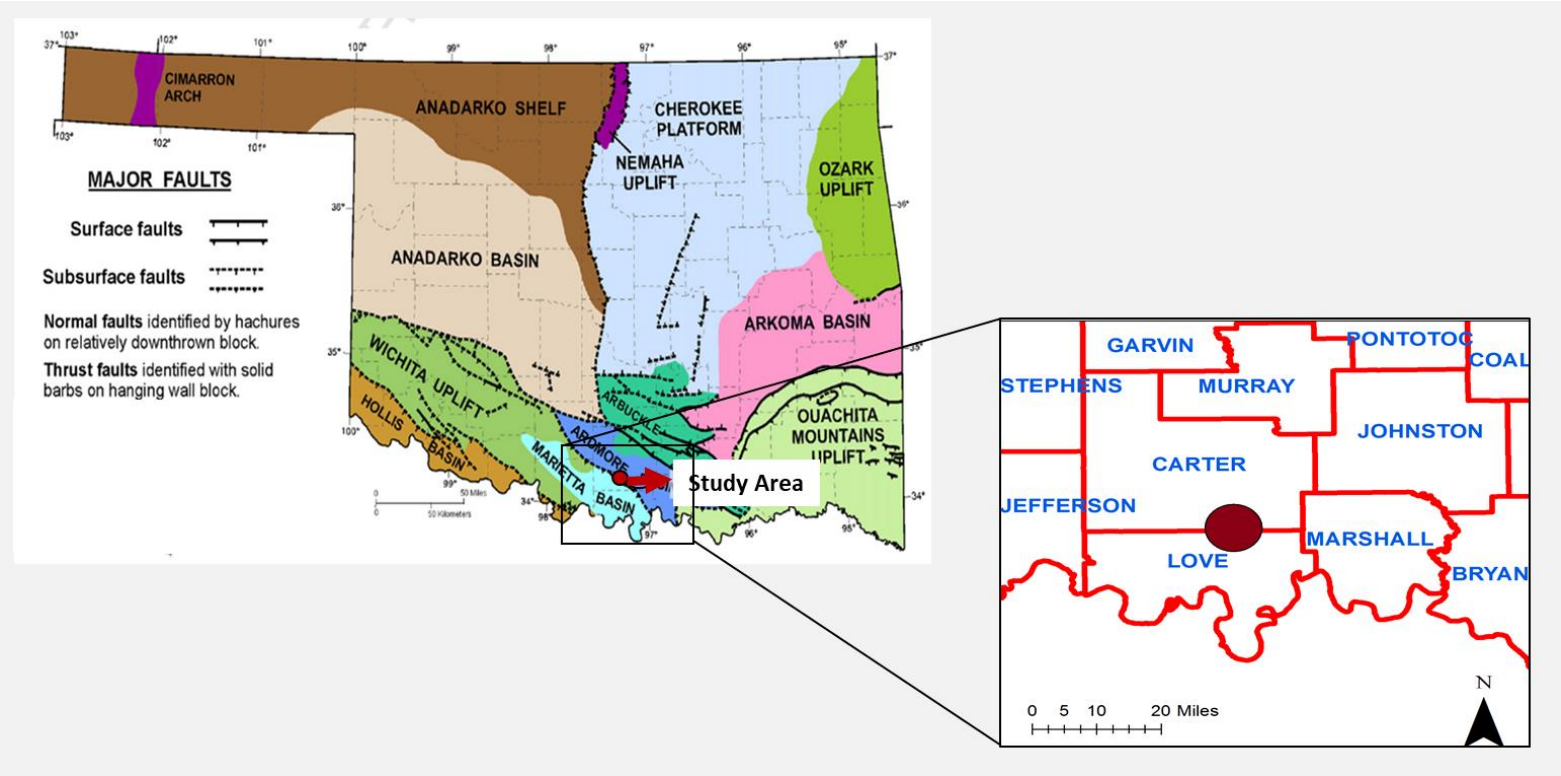

Figure 7. Study Area. **Left**: Map showing the structural provinces of Oklahoma, highlighting the area of study within the Ardmore Basin (modified from Cardott, 2012). Study area highlighted with a red circle. **Right**: Magnification of the study area, showing geographic proximity from I-35 South. Study area highlighted in with a red star.

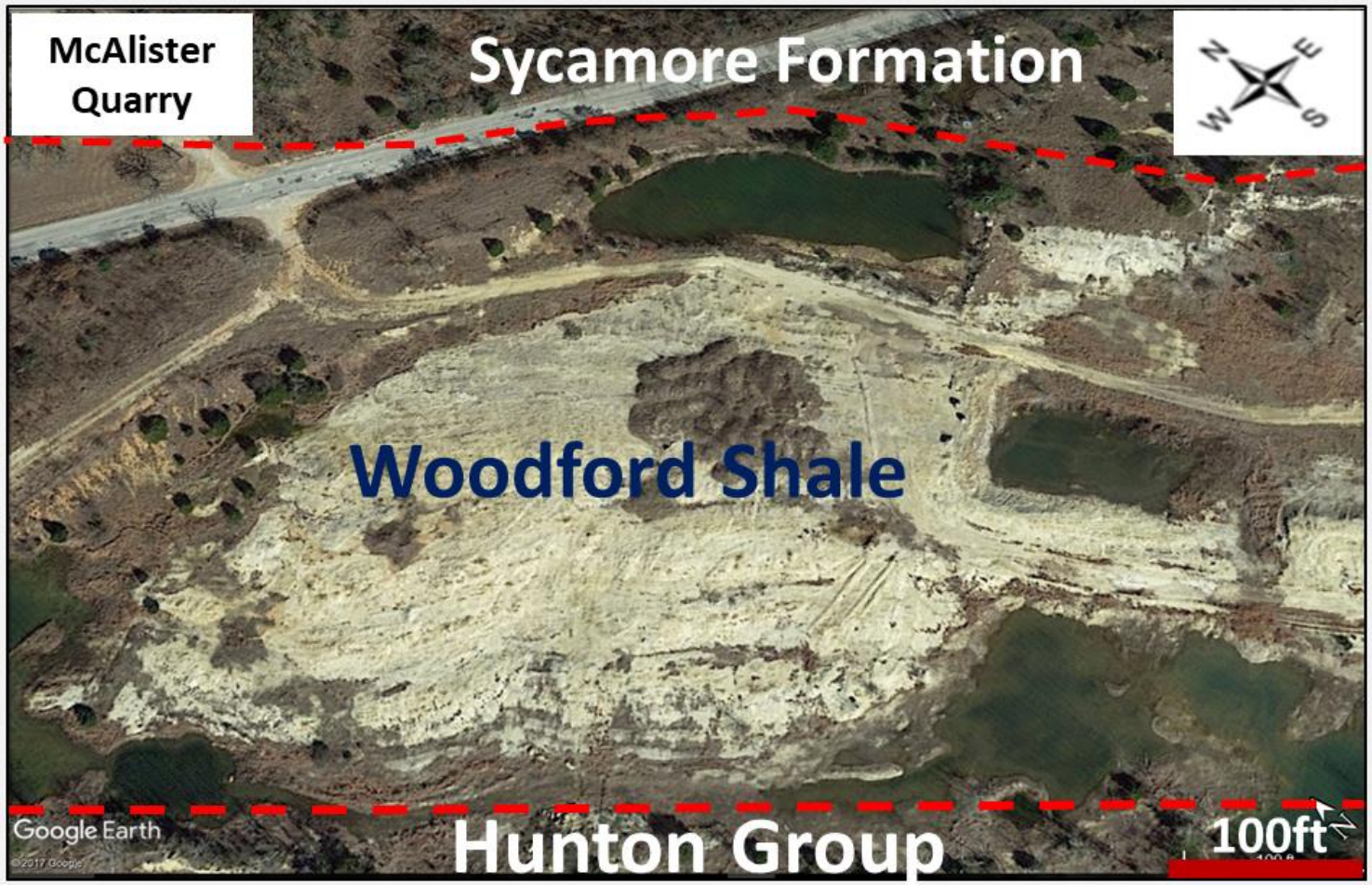

Figure 8. The Woodford Shale Outcrop at the McAlister Quarry.

CHAPTER III

METHODOLOGY

3.1. Mudrock Characterization

1. *Stratigraphic Measurement & Sampling Technique*

The study area was first located, and preliminary observations were determined before sampling commenced. Initial observations include; sample accessibility (good exposure or not), nature of the beds strikes and dips (variability throughout the section), top, base and contacts of formation (exposed or not), weathering profile (soft vs. hard rocks), observable structural deformation, surficial deposits, and potential hazards.

Data collection commenced with the measurement of the strike and dip angles of the beds, where measurable. Using a Jacob staff, the local dip angles were inputted into a Brunton Compass, and the true stratigraphic thickness of the section was measured at 5 feet intervals. Lateral movements while measuring were necessary due to the degree of weathering of the rocks exposed at the outcrop. A measuring tape was used to subdivide each 5 feet intervals into 1 feet intervals further. For effective analysis of the section, bright colored adhesive duct tape was used to create marker tabs for each interval and was held in place using an ungalvanized steel nail. The stratigraphic section measured included the complete section of the Woodford Shale, as well as 5 feet inclusion into the underlying and the overlying formations - the Hunton Limestone, and the Sycamore Formation, respectively.

Once the section was measured, test pits were dug at each marker tab for fresh sample collection. The depth of the test pits was dependent on the degree of weathering.

The nature of the sample in its weathered and fresh state observed was recorded as part of sample description. Hand samples were then collected along the section. Due to the number of analyses to be performed on the samples, at least two samples were collected per marker tab, maintaining dimensions of at least 2inch x 2inch x 2 inch for each sample. The samples were bagged in a gallon bag, labeled with the field location and stratigraphic position of the test pit.

2. *Mudrock Classification*

Mudrock classification for this study was constructed based on field observations as well as observations made from hand specimen scale. Mudrock classification was defined using mainly the textural attributes of mudrocks, which include the grain-size, and the fissility, or lack of fissility. Mudrock classification was further enhanced by utilizing results from XRD, XRF, and petrographic analysis for lithofacies classification.

Grain size	Mudrock Type	Massive (non-fissile)	Fissile
No connotation as to relative amounts of silt and clay	Mudrock	Mudstone	Mudshale
Silt predominant over clay	Siltrock	Siltstone	Siltshale
Clay predominant over silt	Clayrock	Claystone	Clayshale

Table 1: Mudrock (>50% silt and/or clay) classification (modified from Ingram, 1953; Potter et al., 2013).

Based on grain-size, without inference of relative percentages of silt/clay, and braking characteristics, two classifications are relevant: *Mudrock,* a fine-grained sedimentary rock composed of at least 50% of silt and clay, and *Clayrock,* mudrock

composed predominantly of clay-sized minerals. Fissility is the tendency for rocks to break along sheet-like planes of weakness that are parallel to the surface; four sub-classifications are relevant: *Mudstone* – non-fissile/massive mudrock; *Mudshale,* fissile mudrock; *Claystone*, massive clayrock; and *Clayshale*, fissile clayrock (Ingram, 1953) (scheme summarized in **Table 1**).

3. Fissility/Parting

The degree of fissility varies throughout the Woodford Shale section. Whether a rock is fissile or non-fissile depends on several factors; (1) the abundance of clay minerals. Rocks abundant in clay minerals will most likely display fissile characteristics. (2) The degree of preferred orientation of the clay minerals to be deposited with their sheet structures parallel to the depositional surface. Fissility is defined based on the following criteria; less than 0.5mm (papery parting) to more than 10 mm (slabby), intermediate thicknesses include (fissile, 0.5 to 1 mm; platy, 1 to 5 mm; and flaggy, 5 to 10 mm) (Ingram, 1953; Potter et al., 2012) (**Table 2**).

Stratification		Thickness	Fissile	Mudrock
Bedding	Thin	30cm	Slabby	Bedded Chert
	Very thin	3cm		Bedded Chert Mudstone
Lamination	Thick	10mm	Flaggy	Mudstone
	Medium	5mm	Platy	Mudshale
	Thin	1mm	Fissile	Mudshale
	Very thin	0.5mm	Papery	Clayshale

Table 2. Mudrock defined for the Woodford section and the terminology related to stratification and fissility/parting (Modified from Potter et al., 2012).

4. *Gamma-Ray Measurements (GR)*

GR measurements were used as a correlation tool, as well as for developing a sequence stratigraphic framework. GR is a good correlation tool, in that it can be correlated with lithofacies, TOC, elemental chemistry, and mineralogy. When building the sequence stratigraphic framework, GR variations was used to identify parasequence sets.

Gamma-ray data was acquired using a handheld portable Radiation Solutions R-125 Scintillometer^{TM}, to determine the GR profile of the stratigraphic section. The GR scintillometer measures the total counts (U, K, Th) at one-second intervals (units: counts per second, cps). The instrument was provided by the Institute of Reservoir Characterization at the University of Oklahoma. GR data were measured along the same sampling path, adjacent to the test pit. A total of five readings were taken for each measurement, averaging all five for a mean GR value (Slatt et al., 1992).

As a result of the degree of weathering and outcrop exposure, the GR measuring technique was variable throughout the section. For the Lower Woodford Shale, the measurement was taken on the ground level, and for portions of the Middle and Upper Woodford, the measurements were taken from the exposed walls. The mean GR values (cps) were plotted as a function of stratigraphic thickness (ft) of the section.

5. *Petrography and Scanning Electron Microscope (SEM) Analysis*

The principal objective of the petrographic analysis was to observe mineralogy and small-scale vertical heterogeneities within the lithofacies defined. SEM analysis

aided this technique by providing additional information on texture/fabric and pore-scale level analysis.

Fifty-two samples were selected, and prepared for petrographic analysis by Argile Analytica^{TM}, and National Petrographic^{TM}. The petrographic analysis was performed using a Zeiss Imager Z1 petrographic microscope. SEM analysis was conducted using an SFEI Quantum 250 Scanning Electron Microscope (SEM) with an attached Bruker Electron Dispersive Spectrometer (EDS). Analyses were conducted in the Thin Section Petrography and the Devon SEM Laboratory at the University of Oklahoma. Specifics for thin section preparation include; 25 x 50mm (1''x2'') section size, double carbonate staining, and coverslip exclusion. For the SEM Analysis, fifteen samples of interest were selected. Samples were sputter coated with a conductive material (gold-palladium) before analysis commenced.

6. ***X-Ray Diffraction (XRD) Bulk Mineralogy***

XRD data integrated into this study was taken from a previous master's thesis conducted by Serna-Bernal (2013). Twenty-one samples were analyzed for XRD bulk mineralogy by Prograding Rock Services Ltd ^{TM}. Mineralogical components determined from XRD analysis in weight percent (Wt%), are as follows; quartz, k-feldspar, plagioclase, dolomite, gypsum, pyrite, illite/mica, kaolinite, and apatite.

3.2. Organic Geochemistry - Source rock characterization

The organic geochemistry analysis was analyzed by the Organic Chemistry Group at the University of Oklahoma. Fifteen samples were geochemically analyzed using Leco TOC, and Rock-Eval pyrolysis methodologies to determine organic-richness, kerogen

type, and thermal maturity. Leco TOC to lithofacies, chemofacies, and GR to understand the implications on the depositional environment of the Woodford Shale. Analysis from Serna-Bernal, 2013, was also integrated.

The principle parameters obtained from the Rock-Eval pyrolysis include (Tissot and Welte, 1978);

S_1 = the amount of free residual hydrocarbon content (gas and oil) in the sample

S_2 = the amount hydrocarbons generated through thermal cracking of nonvolatile organic matter

S_3 = the amount of CO_2 (in milligrams CO_2 per gram of rock) produced during pyrolysis of kerogen.

T_{max} = The temperature at which the maximum release of hydrocarbons from cracking occurs during pyrolysis.

From these parameters, the following variables are calculated;

Hydrogen index (HI) = S_2 x 100/TOC (mg HC/g TOC)

Oxygen index (OI) = S_3 x 100/TOC (mg CO_2)/g TOC

Types of hydrocarbons generated =S_2/S_3: (0.00-5.00)

Normalized oil content S_1/TOC: = S_1 x 100/TOC

Production index (PI) (0.00-1.00)

The organic richness was using criteria proposed for source rock potential in Jarvie (1991). Kerogen type was determined using pseudo Van Krevelen diagram with Hydrogen Index (HI) and Oxygen Index (OI) (Tissot and Welte, 1978), and a second technique proposed by Cornford et al. (1998) to determine the kerogen types using TOC (wt%) and remaining hydrocarbon potential (S2, mg HC/g Rock). Kerogen types: organic

matter in lacustrine environments (Type I), organic matter derived from marine planktonic organism (Type II), organic matter derived from terrestrial plants transported into the marine environments Type III, and Type IV is primarily composed of vitrinite or inert material.

3.3. Sequence Stratigraphy

Slatt and Rodriguez (2012) have identified the commonalities in the stratigraphic characteristics of several unconventional resource shales from the comparison of stratigraphic sequences and gamma-ray logs (i.e., Barnett Shale, New Albany Shale, Marcellus Shale, Haynesville Shale, etc.), which has led to a unifying sequence-stratigraphic model. The sequence-stratigraphic model includes a basal regional sequence boundary (SB) and/or transgressive surface of erosion (TSE) followed by a transgressive systems tract (TST); a fining-upward clay-rich interval, capped by a high gamma-ray organic-rich shale. The transgressive deposits are topped by a maximum flooding surface (mfs) with associating condensed section (CS) and then overlain by a decreasing upward gamma ray pattern (see **Figure 9**).

This general sequence-stratigraphic model was applied to the Woodford Shale section for a sequence stratigraphic framework interpretation, where all components were identified (surfaces, and systems tracts). GR parasequence sets/stacking patterns were identified using GR log variations. “Upward-decreasing”/ “upward-shoaling GR parasequence characteristic of a gradual fall in sea-level (LST), or late highstand (HST). “Upward-increasing”/ “deepening-upward” GR parasequence characteristic of transgressive deposits during a time of rapid rise in relative sea-level (TST) (Singh, 2008).

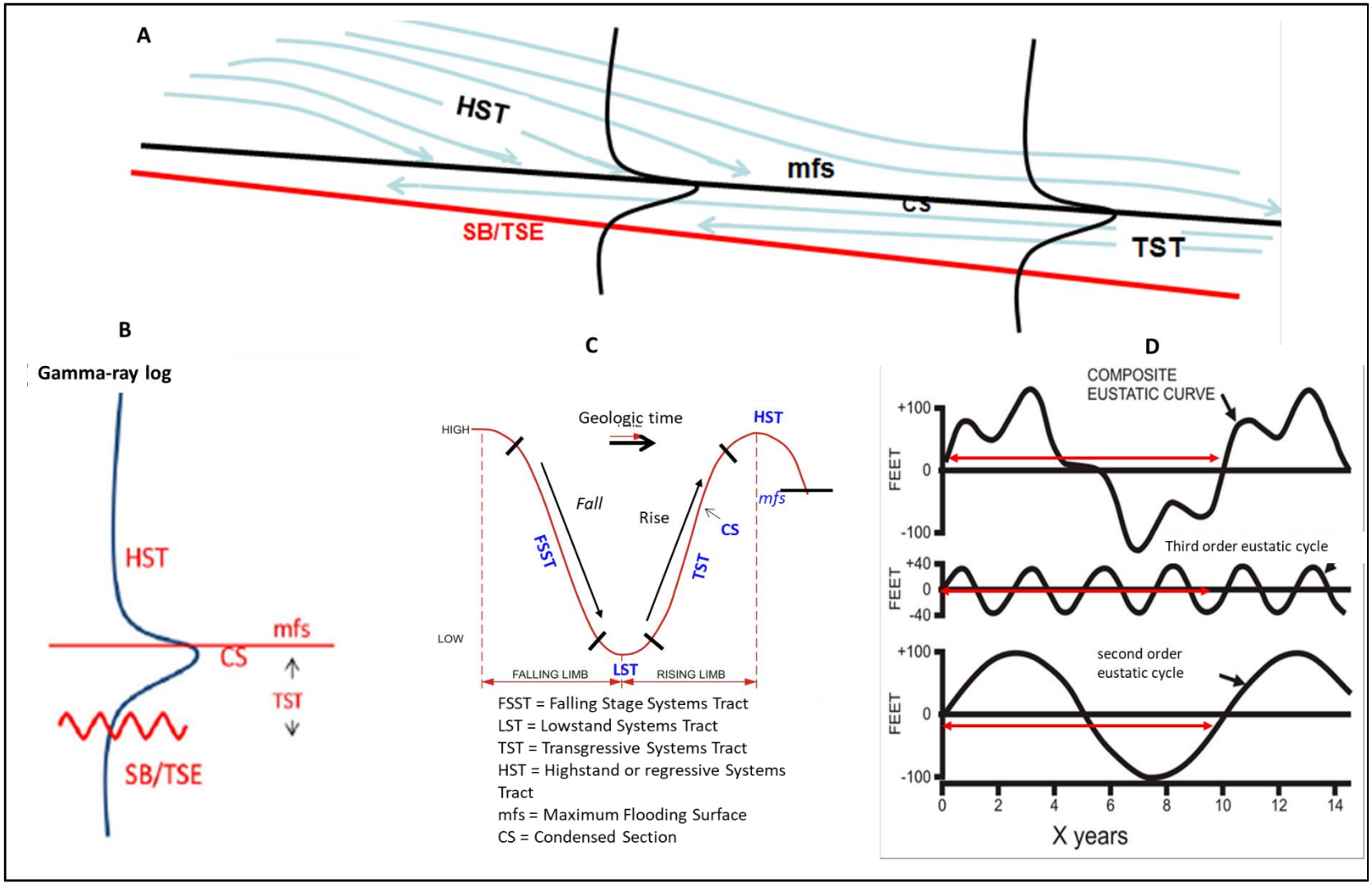
A
HST
mfs
CS
SB/TSE
TST
B
Gamma-ray log
HST
mfs
CS
TST
SB/TSE
C
Geologic time
HIGH
LOW
HST
Fall
Rise
mfs
CS
FSST
TST
FALLING LIMB
LST
RISING LIMB
FSST = Falling Stage Systems Tract
LST = Lowstand Systems Tract
TST = Transgressive Systems Tract
HST = Highstand or regressive Systems Tract
mfs = Maximum Flooding Surface
CS = Condensed Section
D
COMPOSITE EUSTATIC CURVE
+100
0
-100
FEET
Third order eustatic cycle
+40
0
-40
FEET
second order eustatic cycle
+100
0
-100
FEET
0
2
4
6
8
10
12
14
X years

Figure 9. The generalized sequence-stratigraphic model for unconventional resources shales. **A**. the generalized model, with associated components: SB, sequence boundary; TSE, transgressive surface of erosions; TST, transgressive systems tract; CS, condensed section; mfs, maximum flooding surface; HST, highstand systems tract. **B**. shows a conceptual gamma-ray log, showing the log responses of the different components (surfaces and systems tracts). **C**. the sea-level curve is showing the times within the sea-level cycle, in which the components formed. **D**. shows second-order and third-order eustatic cycles, with a composite eustatic curve of the two orders of cyclicity (Slatt, 2013a).

3.4.Elemental Geochemistry

1. Energy Dispersive X-Ray Fluorescence (XRF)

Three hundred and eighty-two samples were geochemically analyzed using the Brucker Tracer IV-SD Hand Held X-ray Fluorescence Spectrometer (HHXRF). The x-ray fluorescence (XRF) used for this study was provided by the Institute of Reservoir Characterization at the University of Oklahoma (**Figure 10**). The Brucker Tracer IV-SD is a handheld, portable, analytical device that measures the elemental concentrations of a material by displacing electrons from their atomic orbital position, thereby releasing energy that is characteristic of a specific element (Turner, 2016). The energy released is picked up, and is categorized by element. The analysis is completely non-destructive and provides within seconds data through the analysis screen while the sample is being analyzed.

To separately capture major elements and trace elements, two settings had to be employed; low energy and high energy. Major element analysis was performed for a count time of 90 seconds, at a 15kV accelerating voltage, with no filter to minimize the signal attenuation of the lighter elements such as Ca, Si, and Al. A minimum of 5 torr vacuum was used for major elements. Trace elements analyses were performed for a

count time of 60 seconds at 40 kV accelerating voltage, with a Ti-Al filter without a vacuum. Trace element analysis did require a filter, unlike the major elements, to eliminate the chance of lighter elements reaching the detector. No vacuum was required for this setting because heavier elements do not attenuate the signal in the short distance to the detector.

For each sample, major elements and trace elements were run separately, to avoid changing the settings multiple times. The same location on the sample was maintained using a sticker for both major and trace element analysis. To prevent contamination and obscurity of elemental concentrations, all samples were washed thoroughly, and cut using a rock saw to give a clean, smooth surface before XRF analysis. The raw data generated was processed using calibrations for mudrocks developed by Rowe et al. (2012). This method of analysis provided major and trace elemental data that were used in constructing the chemostratigraphic profile for the study area.

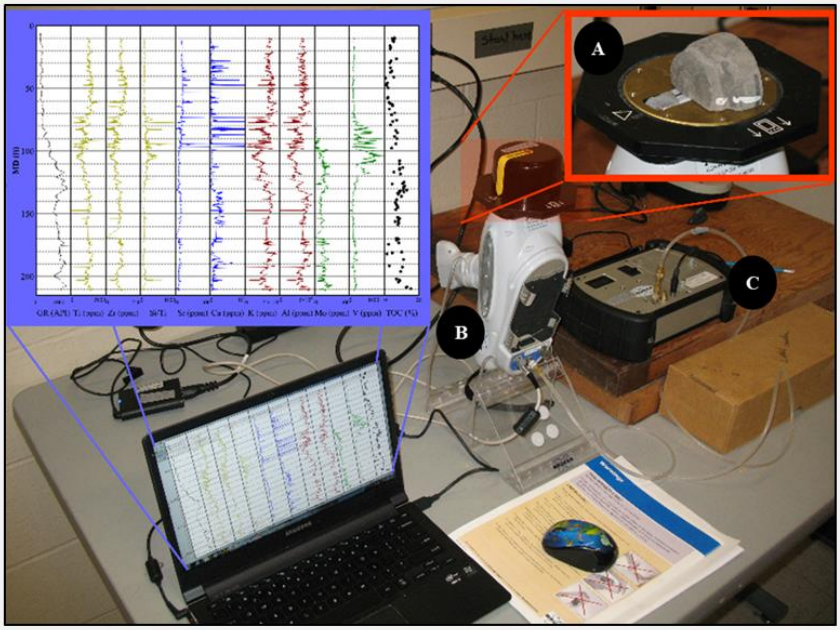

Figure 10 A-C. HHXRF operating instrument set-up. **A**: Sample placed on the window of the HHXRF. **B**: Bruker HHXRF. **C**: Vacuum pump (Photo courtesy of Bryan Turner (unknown source).

2. Chemostratigrahy - Geochemical proxies

Certain principal elements are used as proxies in developing a chemostratigraphic framework, and for inferring variations in a depositional environment such as sediment source (biogenic vs. detrital), organic paleoproductivity, carbonate productivity, and water column chemistry. Elements were subdivided into three categories of geochemical proxies; detrital proxies, carbonate proxies, and redox-sensitive elements (Vine and Tourtelot, 1970) (**Table 3**).

Element	**Indication**	**References**
Titanium (Ti), Zirconium (Zr), Aluminum (Al), Potassium (K)	Indicator of continentally derived sediments	Sageman and Lyons, 2004; Tribovillard et al., 2006
Silicon/Aluminum (Si/Al)	Indicator of detrital, and biogenic quartz.	Pearce and Jarvis, 1992; Pearce et al., 1999; Tribovillard et al., 2006.
Phosphorus (P)	Phosphate accumulation	Tribovillard et al., 2006
Calcium (Ca), Magnesium (Mg), Strontium (Sr)	Carbonates	Banner, 1995; Tribovillard et al., 2006.
Molybdenum (Mo), Vanadium (V), Uranium (U) Nickel (Ni), Cobalt (Co), Copper (Cu), Chromium (Cr), Zinc (Zn)	Redox-sensitive elements	Tribovillard et al., 2006

Table 3. Summary of geochemical proxies. Modified from Turner, 2016. Adapted from Pearce and Jarvis, 1992; Pearce et al., 1999; Banner, 1995 Sageman and Lyons, 2004; Tribovillard et al., 2006.

3. Pearson's Correlation Coefficient

To establish the linear relationship between elements, Pearson's correlation coefficient, *r* method was applied. Pearson correlation coefficient is a simple methodology that measures the degree to which two variables are linearly related. A best-fit line is defined by two variables, and *r* defines how far away the data points are from the defined best fit line. **Figure 11** shows the guidelines that have been proposed for interpreting Pearson's correlation coefficient.

	Coefficient, *r*	
Strength of Association	Positive	Negative
Small	.1 to .3	-0.1 to -0.3
Medium	.3 to .5	-0.3 to -0.5
Large	.5 to 1.0	-0.5 to -1.0

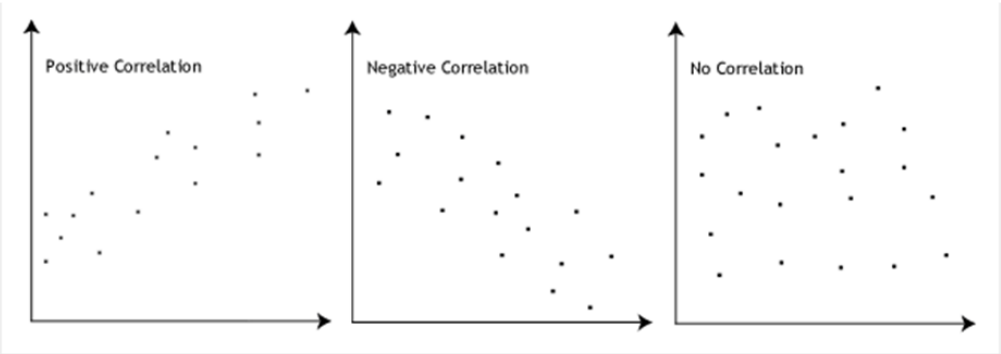

Figure 11. Guidelines for interpreting Pearson's correlation coefficient (statistics.leard.com)**.**

4. Hierarchical Clustering Analysis – Chemofacies Definition

Hierarchical cluster analysis (HCA) is a multivariate statistical approach that arranges items as a set of nested clusters organized in a dendrogram (hierarchical tree), based on similarity or distance between them. The goal is a case where intra-cluster distances are minimized, and inter-cluster distances are maximized (Turner, 2016). By using HCA, chemofacies were defined from XRF elemental data, to highlight geochemical variability within the stratigraphic section. All statistical analysis was conducted using a statistical analysis tool, Minitab.

Clusters are successively built by first selecting a clustering method, the distance measure, clustering algorithm, the linkage method, and the number of clusters. The clustering algorithm used was a hierarchical agglomerative algorithm. The result is a set of nested clusters, in which each cluster is successively nested in a larger group until one cluster is left.

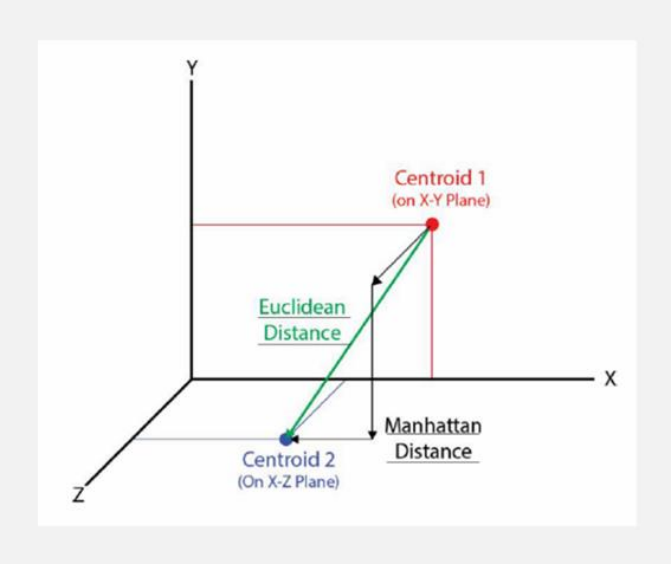

Figure 12. Distance measures in hierarchical clustering analysis, using three variables (x, y, and z). Euclidean distance (green) measures the straight-line distance. Manhattan

distance measures the sum of the distance along each axis at right angles (After Turner and Closs, 2009; Modified from Turner, 2016).

The selected distance measure calculates the distance or similarity between clusters. There are two ways of measuring the distance between clusters, Euclidian distance, and Manhattan distance. The Euclidean distance is the most commonly recognized, and it measures the straight-line distance between the center of two clusters. The Manhattan distance measures the sum of the distance along each axis at right angles (**Figure 12**). Manhattan distance is applicable where the variables are independent of each other. Euclidian distance takes into account the possibility of dependency among variables (Turner and Closs, 2009; Turner, 2016). For this analysis, the Euclidian distance was used.

There are several linkage methods for defining the distance from one cluster to another cluster. These most popular methods include; Single, Complete, Average, Centroid, and Ward's Method (**Figure 13**). The Single Linkage method is based on the minimum distance or the nearest cluster members of two separate clusters. Complete Linkage method is based on maximum distance or furthers neighbors of two separate clusters. Average Linkage method is based on the average of the distances between all pairs of objects. Centroid Linkage is the distance between the centroids of two separate clusters.

For Ward's Linkage method, the sum of squares is calculated for each cluster. Within the cluster distances, two clusters which have the smallest increase in the overall sum of squares are combined. This method considers population variability, by designating greater weight to populations with smaller variance. The later was used for

the analysis (Ward, 1963). Ward's approach has been shown to perform better than other procedures (Güler et al., 2002, Turner et al., 2016; Turner, 2016).

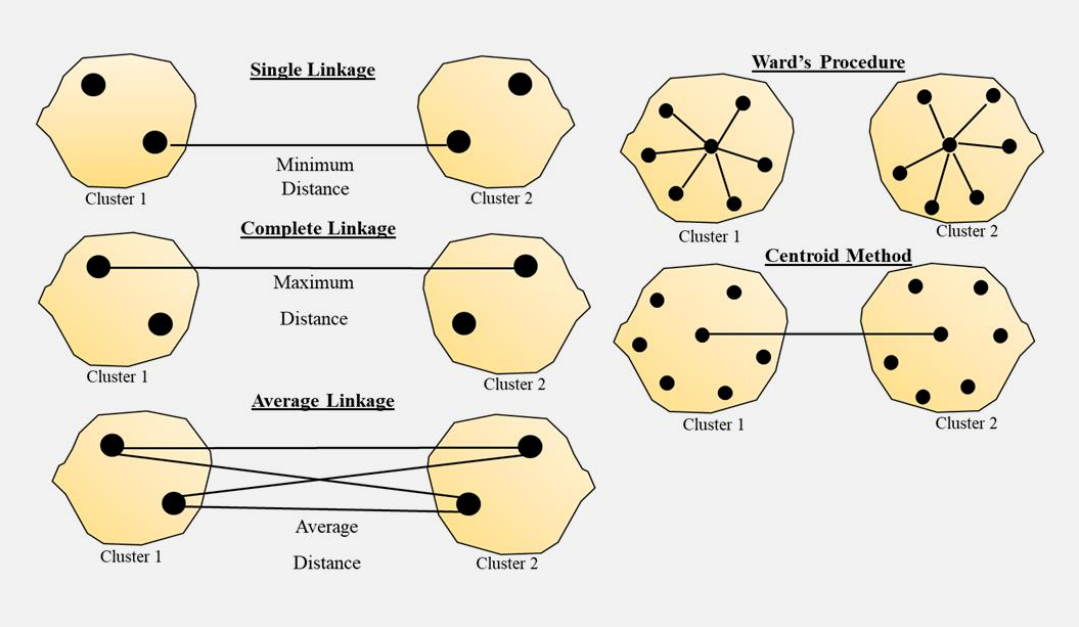

Figure 13. Schematic illustrating the popular linkage methods: Single, Complete, Average, Ward's, and Centroid Method. Modified from Kaushik, 2009.

CHAPTER IV

OUTCROP CHARACTERISRICS

4.1. Correlation with Previous Study

XRD and TOC dataset from a previous study at the McAlister Cemetery Quarry (Serna-Bernal, 2013) was utilized in this study. An initial attempt at incorporating this dataset proved problematic due to different sampling approaches. Therefore, to properly utilize the dataset a good correlation has to be established.

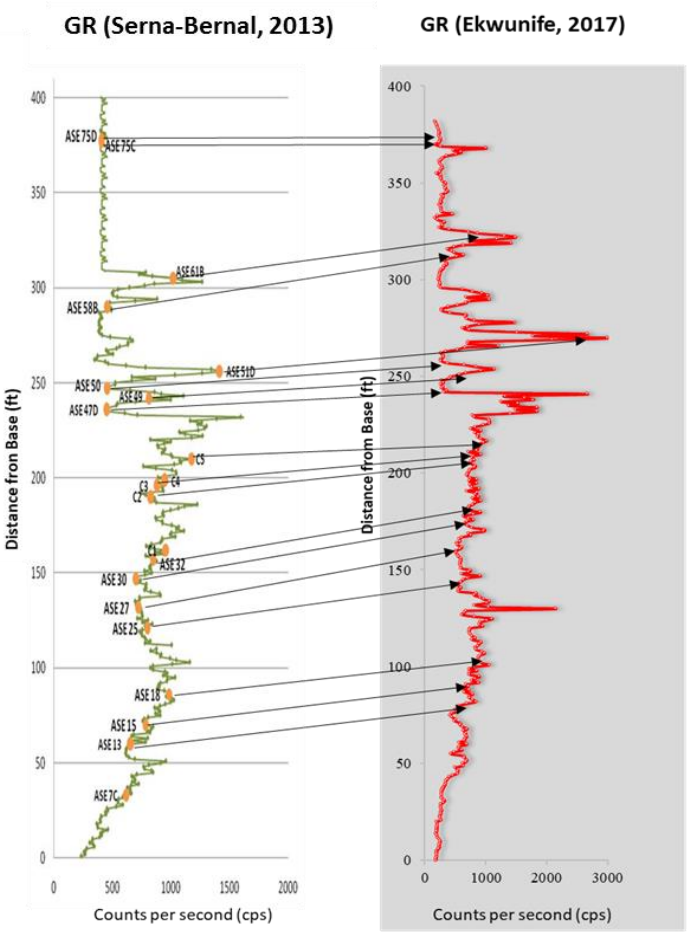

Sample	Serna's Depth (ft)	Ekwunife's Depth (ft)
ASE13	60.00	82.00
ASE15	70.00	107.00
ASE18	86.00	114.00
ASE25	121.00	147.00
ASE27	132.00	164.00
ASE30	147.00	178.00
ASE32	157.00	186.00
C2	190.00	211.00
C3	196.00	213.00
C5	210.00	217.00
ASE47D	236.00	244.00
ASE49	242.00	252.00
ASE 50	247.00	258.00
ASE51D	256.00	272.00
ASE58B	290.00	313.00
ASE61B	305.00	324.00
ASE75C	377.00	369.00
ASE75D	378.00	370.00

Figure 14: Correlation between previous study (Serna-Bernal, 2013) and the current study. **Left-Right**: GR from Serna-Bernal (2013) correlated to GR for section measured for this study, with depth-depth GR correlation.

A correlation was done primarily using GR profiles (**Figure 14**) assisted with XRF and XRD data. GR points and associated XRD mineralogy from Serna-Bernal (2013) was correlated with GR points and associated XRF measurements from this study. Although GR points were successfully matched from general trends, XRF data showed that not all lithofacies defined for this study accurately match with the XRD mineralogy obtain from Serna-Bernal (2013). Therefore, XRD and TOC data integrated into this was mainly restricted to understanding the general trend in the characteristics of the informal members, rather than individual lithofacies in the Woodford Shale. XRD and TOC data was only used where confidence in correlation was attained.

4.2 . Mudrock Classification and Lithofacies Defined

1. Mudrock Classification

Figure 15 shows the distribution of mudrock types within the informal members of the Woodford Shale. Included are the Upper Woodford Shale bleached facies, and bedded chert. Mudshales dominate the Lower and the Middle Woodford Shale, while bedded chert and bleached facies dominate the Upper Woodford Shale.

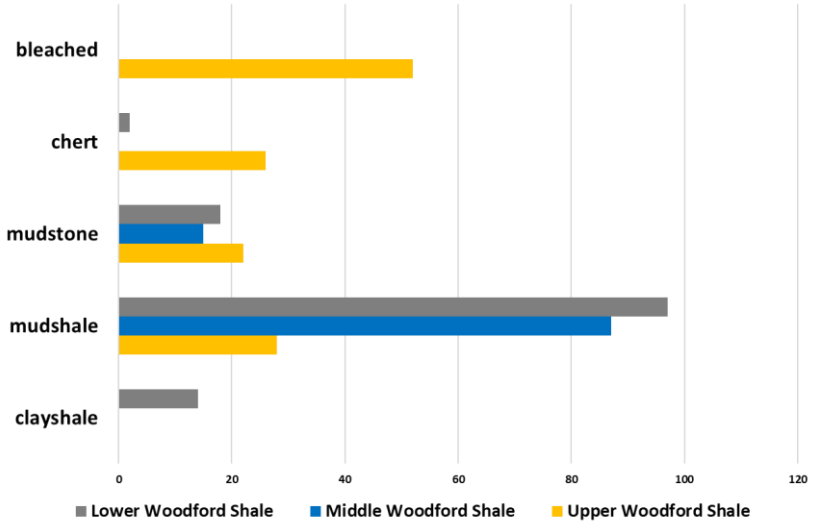

Figure 15. Mudrock types within informal Woodford Shale members. The Lower and the Middle Woodford Shale are dominated by mudshales. The Upper Woodford Shale is mostly bleached.

2. Lithofacies Defined

Using rock description (physical textures), petrographic analysis, XRF, XRD, eight major lithofacies were identified at the McAlester Cemetery Quarry, starting from the most clay-rich to the most siliceous: clayshales, mixed clayshale – mudshale, argillaceous mudshales, siliceous mudshales, siliceous mudstones, and radiolarian chert. Calcareous lithofacies defined include: dolomitic mudstones, and shales. Bleached facies from the Upper Woodford Shale was also defined.

Clayshale and Mixed Clayshale - Mudshale

These lithofacies have the highest clay content and the lowest silica content. In outcrop, due to high clay contents, they are soft and represent the least resistant lithofacies. They dominate the lowermost part of the Lower Woodford Shale and are indicative of the onset of the Woodford Shale deposition. In outcrop, clayshales are greenish, laminated, and usually, show papery (<0.5mm) parting. Mixed clayshale - mudshale in outcrop show interlayering of green clayshales and medium brown mudshales. They show planar to wavy thin laminations, and parting can range from papery (<0.5mm) to fissile (0.5mm), depending on the clayshale to mudshale ratio.

In thin section, the clayshales matrix is predominately organic poor and contains a significant amount of clay, and pyrite. Mixed clayshale - mudshale are dominated by clays and pyrite, which composes a significant amount of the entire matrix, especially in

the mudshale layer. Traces of carbonate minerals are common among several samples (**Figure 16 & 17)**.

Microfossils were observed in the clayshales. In the mixed clayshale - mudshale, microfossils present are flattened *tasmanites* cysts, with a few recrystallized by silica or carbonate minerals where not flattened, mainly evident within the mudshale layers. Conodonts are also present, and are observed within the clayshale layers. In some samples, burrows are recognized, infilled with green clayshales. Additionally, wavy laminations are common within these facies, which might suggest the influence of water currents during the time of deposition (**Figure 16 & 17**).

Bulk mineralogy of a mixed clayshale - mudshale in the Lower Woodford Shale from a sample from Galvis (2017) is: illite + kaolinite >70%.

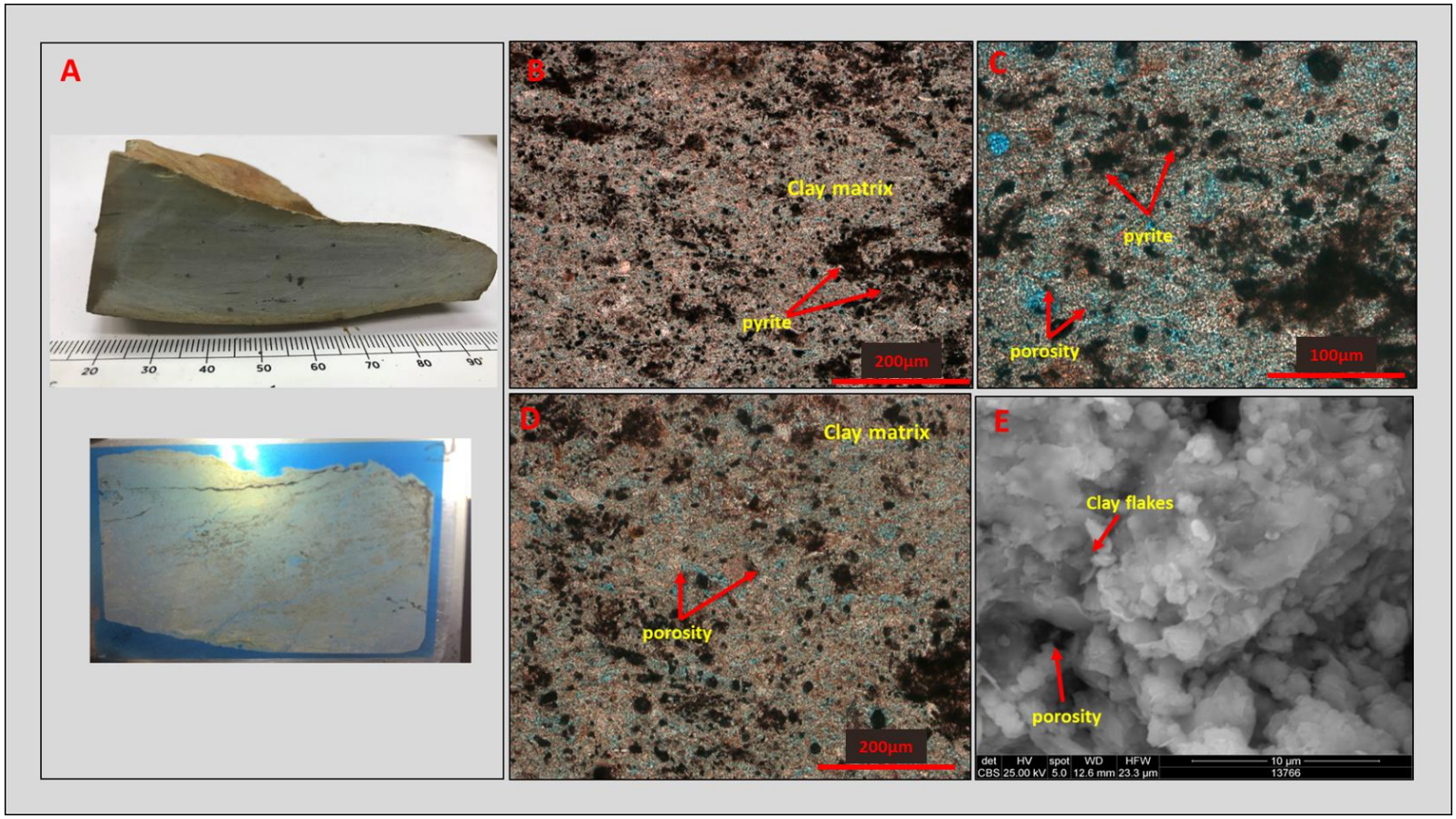

Figure 16. Clayshale lithofacies. **A**: Hand sample and thin section. **B-D**: Thin section photomicrographs. **E**: SEM images shows the predominately soft, wavy laminated, organic poor, clay rich fabric of clayshales. Pyrite minerals are abundant in this particular sample.

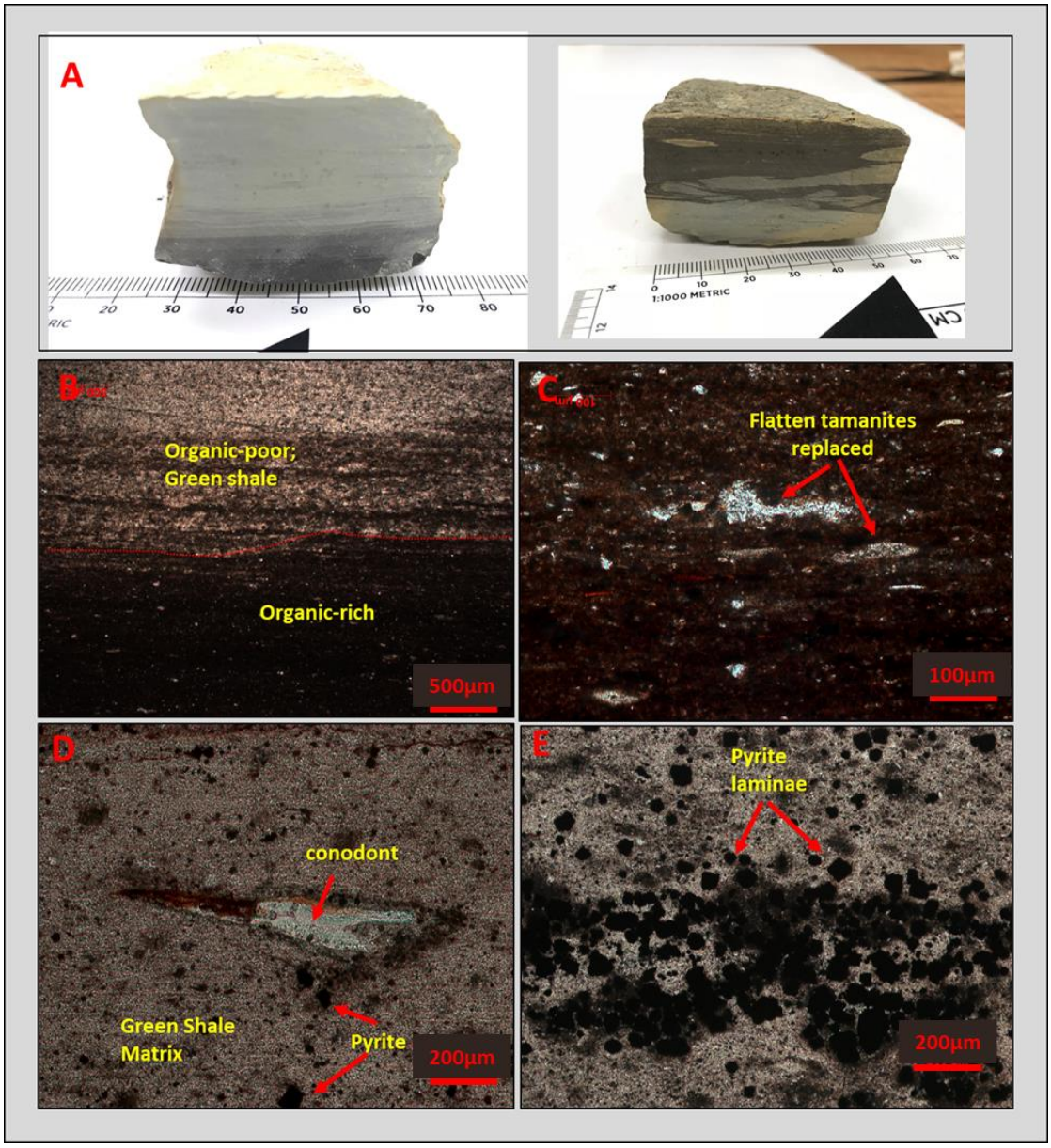

Figure 17. Mixed clayshale–mudshale lithofacies. **A**: Hand sample. **B-C**: Thin section photomicrographs. **D-E**: SEM images. The clayshale layer is predominately soft wavy laminated, and organic poor. The mudshale layer is slightly richer in organic content than clayshale layer.

Argillaceous Mudshale

In outcrop, argillaceous mudshales are dark orangish green (weathered), medium - dark brown (fresh), laminated, usually showing fissile (1-5mm) parting. This lithofacies dominates the uppermost Middle Woodford Shale. A yellow powdery substance, which has been interpreted as sulfates is typically observed between shale partings. Also, commonly found between shale partings, especially in the Middle Woodford Shale are black bitumen flakes.

In thin section the matrix is medium – dark brown; planar laminated mudshale. Clay minerals represent a majority of the matrix, occurring as fibrous crystals, and are aligned parallel to subparallel to the bedding in most instances. Diagenetic quartz and chalcedony are observed in some samples as an infill for several micro fossils. Pyrite is abundant, and present in the form of small euhedral crystals and oval framboids. Silt-sized aggregates composed of angular quartz and clay minerals are observed in some samples, although varying in different proportions from sample to sample. These aggregates, as well as clay minerals, contribute significantly to the laminations of the shales. Aggregates of the mineral dolomite are almost always present in analyzed samples, although in minor proportions. Organic materials in the form of stringers are also a significant percentage of the matrix and are dispersed throughout the matrix (**Figure 18**).

Microfossils present include several species of palynomorphs such as *Tasmanites* and spores. *Tasmanites* and spores are abundant within this lithofacies and are almost always flattened. In other observations, they are infilled with diagenetic quartz, and chalcedony. Specifically, flattened spores are mainly situated between the shale partings. Radiolarians are typically rare within this lithofacies, and where they occur, they are completely recrystallized (**Figure 18**).

Bulk mineralogy of an argillaceous shale in the Lower Woodford Shale is quartz (39%), clays (50%), dolomite (2%), pyrite (4%), k-feldspar (5%) (estimates taken from Brito, 2017). TOC content: 10 – 22 wt%.

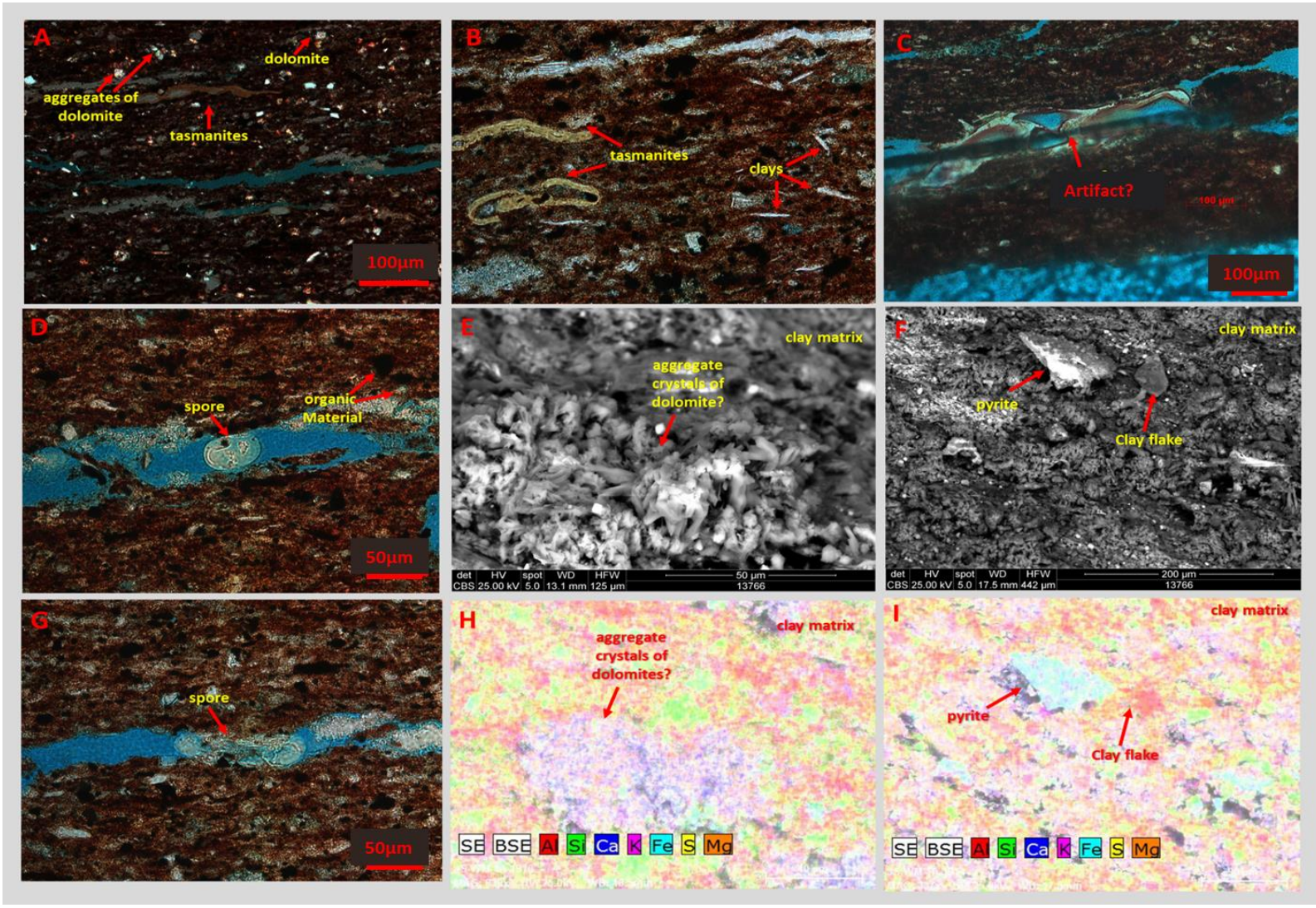
A
dolomite
aggregates of dolomite
tasmanites
100µm
B
tasmanites
clays
C
Artifact?
100µm
D
spore
organic Material
50µm
E
clay matrix
aggregate crystals of dolomite?
F
clay matrix
pyrite
Clay flake
G
spore
50µm
H
aggregate crystals of dolomites?
clay matrix
SE BSE Al Si Ca K Fe S Mg
I
clay matrix
pyrite
Clay flake
SE BSE Al Si Ca K Fe S Mg

Figure 18. Argillaceous mudshale lithofacies. **A**-**D, G**: Thin section photomicrographs. **E, F, H, I**: SEM images show matrix is clay rich, dominated by organic materials, silt-sized aggregates, minor dolomite aggregates, and several species of palynomorphs.

Siliceous Mudshale

In outcrop, siliceous mudshales are dark greenish orange (weathered), medium-dark brown (fresh), laminated, and usually show platy (0.5 – 1mm) parting.

In thin section, they are medium – dark, continuous, planar laminated shale. Typically, shale is dominated by two distinct layers, silt-sized aggregates dominated and diagenetic quartz dominated in a clay matrix. The silt-sized quartz dominated laminae are discontinuous (lenticular), incorporating clays and pyrite. The silt-sized aggregates and clay minerals represent a majority of the composition and are dispersed throughout the matrix. The silt-sized aggregates are lighter in color and appear to have more silt-sized detrital quartz grains than the rock matrix. Quartz grains are typically sub-angular to sub-rounded, present in monocrystalline and polycrystalline forms, varying in sizes. Clay minerals are typically fibrous and are aligned subparallel to the beddings in most instances. Clay minerals form a dominant portion of the silt-sized aggregates. Pyrite is present in the form of small euhedral, and oval framboids (**Figure 19)**.

Microfossils present include *tasmanites* and radiolaria. *Tasmanites* are flattened and may contain diagenetic quartz (as seen in the diagenetic quartz dominated layers), and in other cases pyrite (euhedral or framboid forms). Radiolaria have been replaced by chalcedony, and are dispersed throughout the matrix. Organic matter is disseminated throughout and appears in the form of organic stringers (**Figure 19)**.

These silt-sized aggregates have been documented in ancient black shales (e.g., Pike and Kemp, 1996, Milliken et al., 2007; Schieber, 2009), and have been interpreted as highly compacted tests of agglutinated foraminifera. The agglutinated foraminifera observed in the Woodford Shale samples are poorly sorted, structureless, and lacking chamber walls. Pike and Kemp (1996) attributed the structure to the disaggregation or compaction of foraminifera tests during diagenesis and lithification. That is, increasing compaction and diagenesis will disaggregate the foraminifera tests to structureless test over time. Milliken et al. (2007) also documented the occurrence of authigenic quartz as a cementing agent, owing to the microporous nature of the agglutinated tests (**Figure 19)**.

Bulk mineralogy of a siliceous mudshale in the Lower Woodford Shale is quartz (82%), illite/mica (9%), kaolinite (5%), pyrite (3%), k-feldspar (1%). TOC content: 15.5 wt.%.

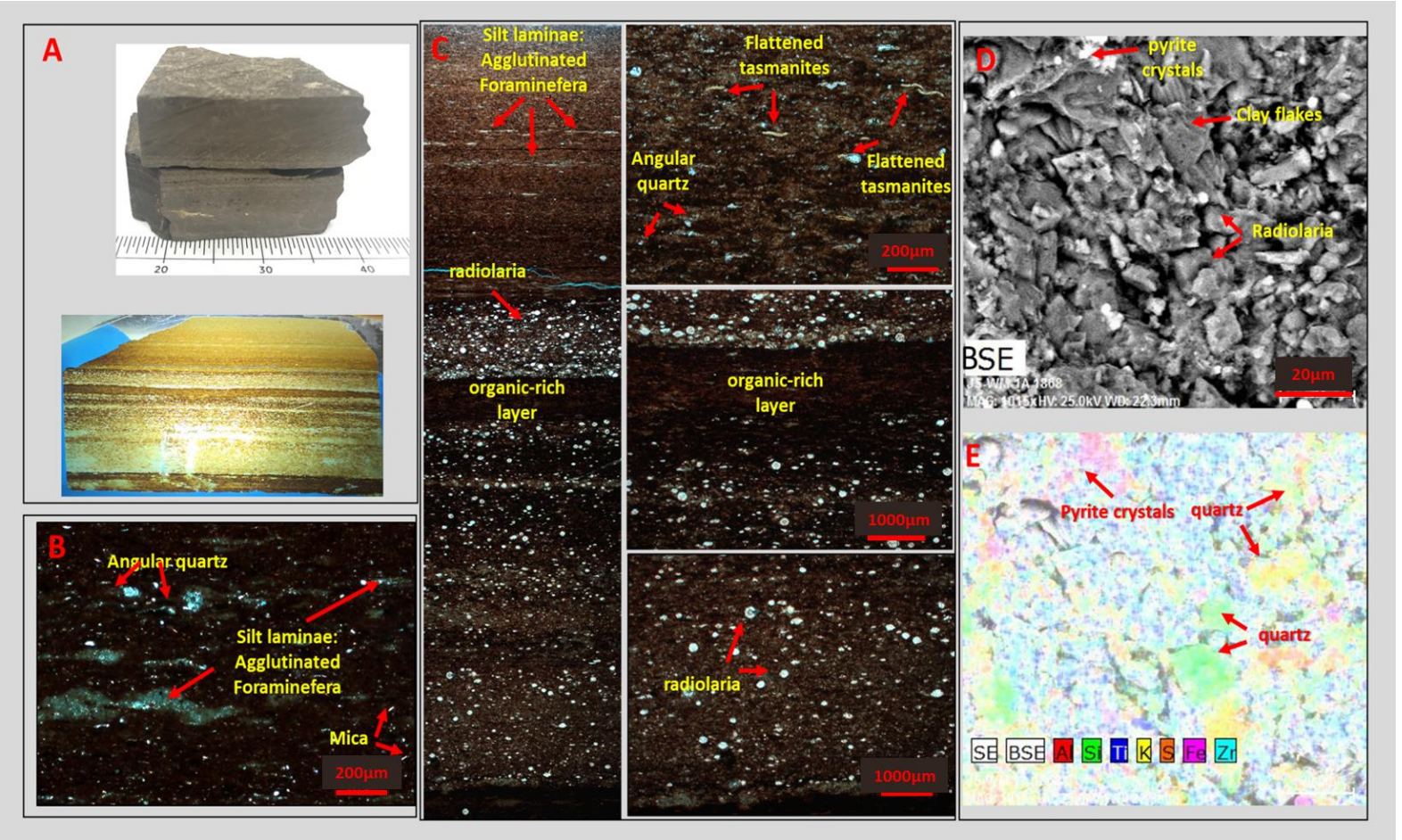

Figure 19. Siliceous mudshale lithofacies. **A**: Hand sample. **B-C**: Thin section photomicrographs. **D-E**: SEM images shows a siliceous mudshale samples is dominated by two distinct layers; a silt-sized aggregates (interpreted as agglutinated foraminifera) and diagenetic quartz dominated.The silt-sized quartz layers are discontinuous (lenticular), incorporating clays and pyrite. The diagenetic quartz layers are composed of radiolaria replaced by chalcedony.

Siliceous Mudstone

Siliceous mudstones are more siliceous than siliceous mudshales, and less siliceous than bedded cherts. In outcrop, they are dark greenish orange (weathered), medium-dark brown (fresh), hard, subtly laminated/massive, usually with flaggy (5-10mm) to slabby (>10mm) fissility, and fracture to blocky patterns. They tend to form the surficial resistant mounds in the Lower and Middle Woodford Shale outcrop, where they are typically associated with siliceous mudshales. In the Upper Woodford, they are generally associated with bedded cherts.

In thin section, they are medium–dark brown, with continuous, planar lamination (where laminations are discernable). The rock matrix is organic-rich, and dominated by abundant microfossils including *tasmanites* cysts, and radiolaria. In **Figure 20**, the total/partial replacement of *tasmanites* by chalcedony makes up a significant fraction of the matrix. Recrystallized radiolarian makes up a significant fraction of the matrix in other samples. The organic-rich fraction of the matrix is composed of disintegrated *tasmanites*. Microfossils are replaced by the mineral pyrite in some samples. Moderate contents of clays and detrital quartz are observed. No feldspars or rock fragments are present.

Figure 20 demonstrates the association of siliceous mudstones with mudshales, where the top of the sample is highly siliceous, and dominated by *tasmanites* cysts filled with diagenetic quartz, and chalcedony. The mudshale layer is dominated by flattened *tasmanites* cysts, with fewer *tasmanites* cysts in-filled with diagenetic quartz. Schieber (1996) suggests this textural observation can be an indicator of (1) diagenetic mobilization and precipitation of biogenic (radiolarian) silica into the voids spaces in the *tasmanites* cysts, (2) low sedimentation rates, and (3) the probable presence of biogenic

silica in the original sediments. The reverse would be the case for the mudshales, where the *tasmanites* cysts are flattened, and the matrix is less siliceous.

Bulk mineralogy of a siliceous mudstone in the Upper Woodford Shale is quartz (92%), illite/mica (7%), kaolinite (1%). TOC content: 11.7 wt.%.

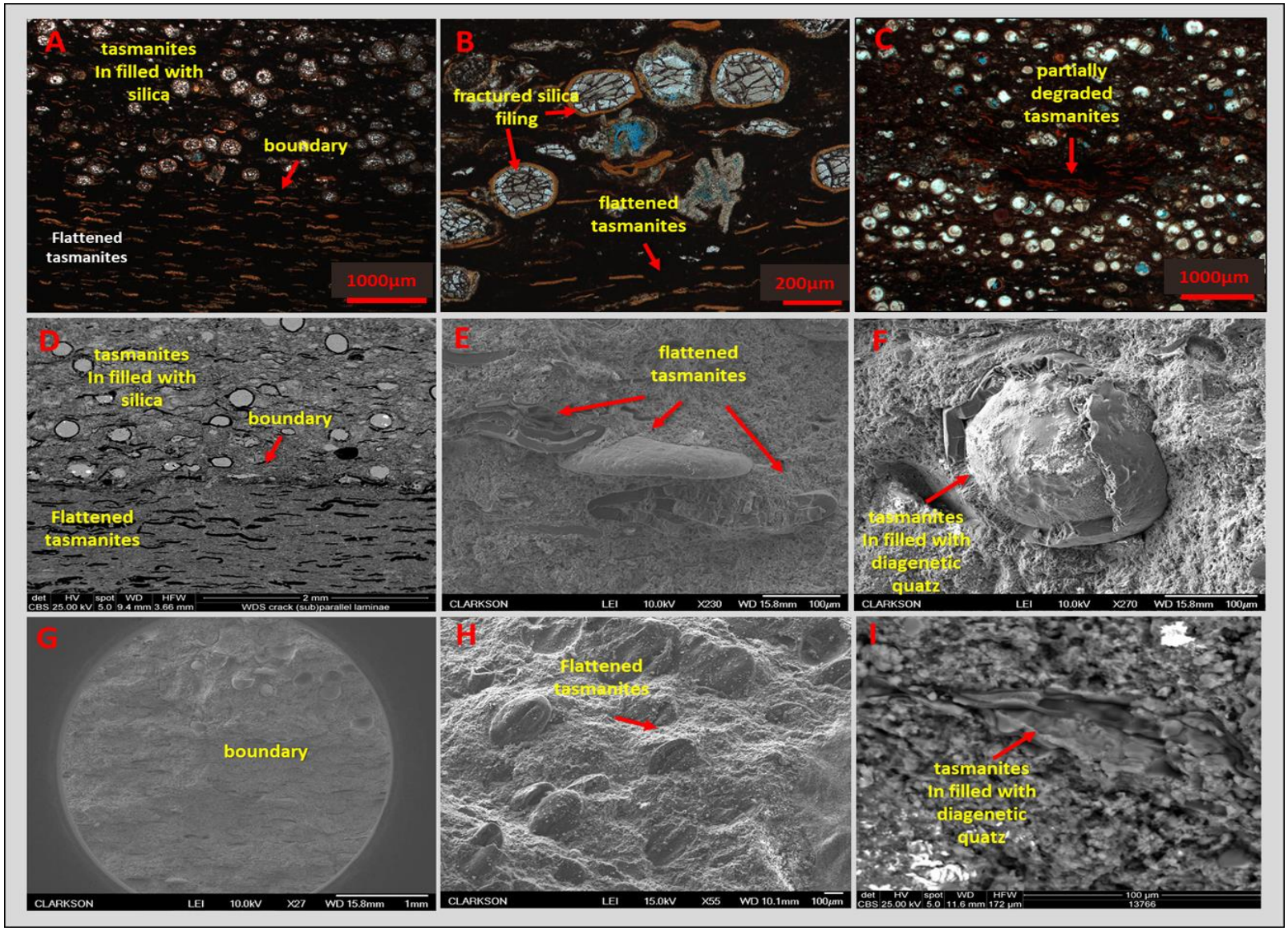
A
tasmanites
In filled with
silica
boundary
Flattened
tasmanites
1000µm
B
fractured silica
filing
flattened
tasmanites
200µm
C
partially
degraded
tasmanites
1000µm
D
tasmanites
In filled with
silica
boundary
Flattened
tasmanites
det HV spot WD HFW
CBS 25.00 kV 5.0 9.4 mm 3.66 mm
2 mm
WDS crack (sub)parallel laminae
E
flattened
tasmanites
CLARKSON LEI 10.0kV X230 WD 15.8mm 100µm
F
tasmanites
In filled with
diagenetic
quatz
CLARKSON LEI 10.0kV X270 WD 15.8mm 100µm
G
boundary
CLARKSON LEI 10.0kV X27 WD 15.8mm 1mm
H
Flattened
tasmanites
CLARKSON LEI 15.0kV X55 WD 10.1mm 100µm
I
tasmanites
In filled with
diagenetic
quatz
det HV spot WD HFW
CBS 25.00 kV 5.0 11.6 mm 172 µm
100 µm
13766

Figure 20. Siliceous mudstones lithofacies. The rock matrix is, organic-rich, and dominated by abundant microfossils including *tasmanites* cysts, and radiolaria. T*asmanites* cysts are filled with diagenetic quartz, and chalcedony. **A-C**: Thin section photomicrographs. **D-I**: SEM images shows the association of siliceous mudstones with mudshales that form the surficial resistant mounds observed in the outcrop.

Bedded Chert (Radiolarian)

Bedded Cherts are the most siliceous lithofacies and dominate the Upper Woodford Shale. They occur as intercalations between siliceous mudstones/mudshales. In outcrop, cherts are hard, brittle, vertically fractured, locally dark/light grey (can appear white when weathered), and exhibit conchoidal fractures. Chert beds in the Upper Woodford Shale are thick (>10mm) and can occur as flaggy (5-10mm) within other informal members. Phosphate nodules are dominant within the cherts of the Upper Woodford Shale, and are absent within other informal members. Mudstones are difficult to distinguish in cores as they tend to have similar colors due to lack of surface exposure. In outcrop, cherts can be easily distinguished from mudstones mainly based on color and fracture pattern. Mudstones usually have a darker fabric and fractures with a blocky pattern, while cherts are dark/light gray and fractures conchoidally (**Figure 21)**.

In thin section, cherts are massive to subtly laminated on the scale of 1mm. They are composed mainly of biogenic quartz in the form of recrystallized radiolarians, with negligible amounts of clays and carbonates. Quartz, which formed diagenetically early from recrystallization of radiolarian skeletal parts, occur as mosaic or granular microcrystalline chalcedony, infilling radiolarian tests, and composed much of the volume. Organic matter in cherts is present as amorphous organic materials and can fill micropores. Pyrite crystals are present mostly in association with radiolarians, as well as

dispersed around the matrix. Scour marks are rare but are evident in one sample, which might be indicative of bottom water currents during deposition. Microfractures filled with bitumen, quartz, or calcite are occasionally observed (**Figure 21)**.

Bulk mineralogy of a bedded chert in the Upper Woodford Shale is quartz (98%), illite/mica (2%). TOC content: 0.28 wt.%.

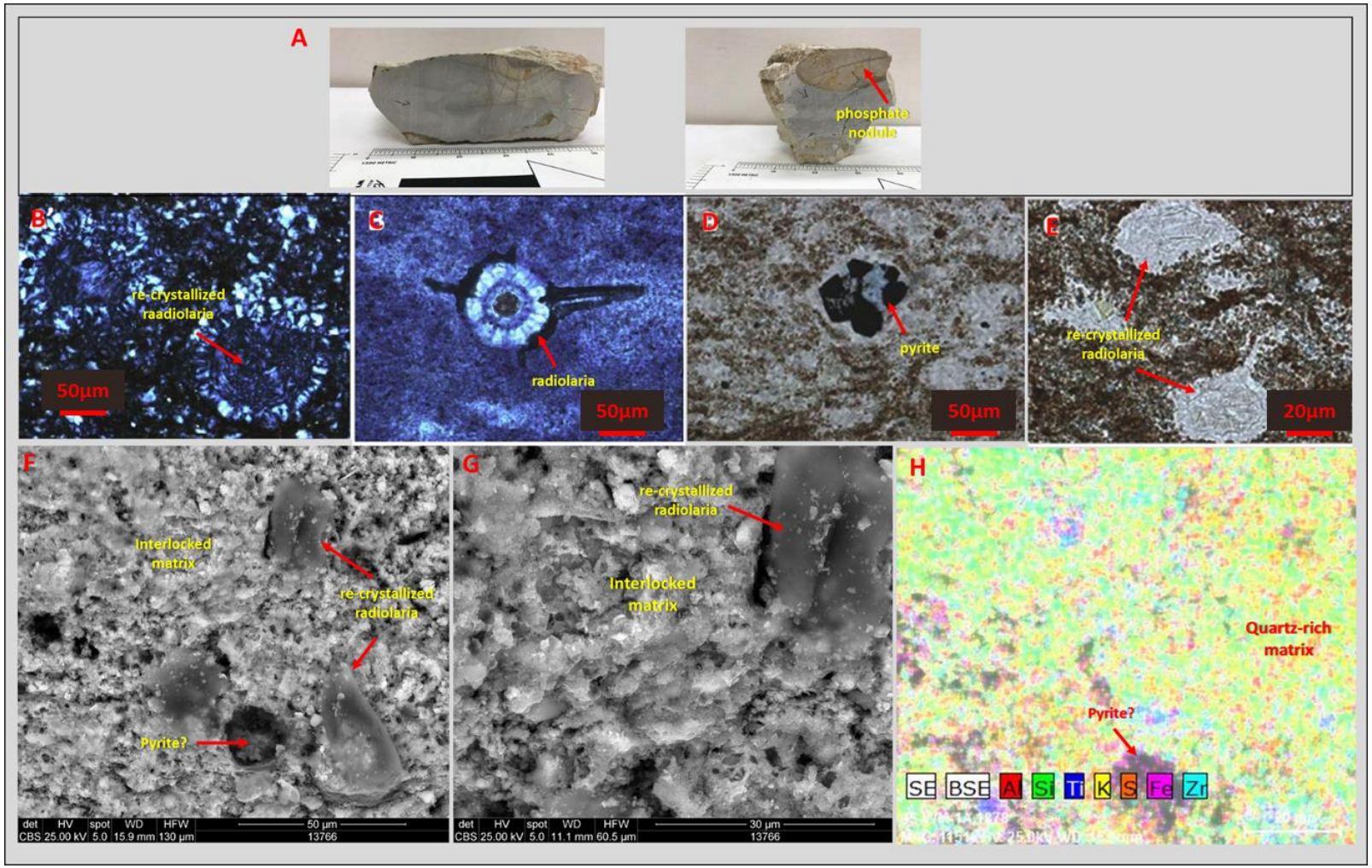

Figure 21. Bedded chert lithofacies. Cherts are composed mainly of biogenic quartz in the form of recrystallized radiolarians, with negligible amounts of clays and carbonates. A. Hand samples. B, C, D, E: Thin section photomicrographs (Modified from Serna, 2013). F, G, H: SEM images showing the recrystallized radiolarians resulting in an interlocking matrix of the chert.

Dolomite Mudstones and Mudshales

Dolomitic facies are primarily found in discrete beds throughout the Woodford section. Beds are commonly massive (mudstones), but rarely exhibit laminations (shales). In outcrop, dolomitic mudstones are light grey (weathered), dark brown-black (fresh), massive/slabby, crystalline, dense, hard, and typically exhibits conchoidal fractures. Where dolomitic facies are laminated, it is defined as dolomitic mudshales. Dolomitic mudshales are dark grey (weathered), dark brown-black (fresh), and exhibits a platy fissility. Dolomitic lithofacies display different degrees of dolomitization, where a bed can grade from dolomitic mudstones to dolomitic mudshales.

In thin section, the mineral dolomite occurs as aggregate crystals in its typical shape of rhombs and spherules, and in other cases as lens-shaped pods. Recognizable organisms are almost never present. Dolomitic mudstones have a dark brown matrix with micritic to silt size crystals of dolomite. No organisms are observed, but lens-shaped pods are commonly present in the mudstones and are similar in size and shape to recrystallized radiolaria observed typically in siliceous mudstones and bedded cherts. Thus, this is an indication of the original mudrock fabric and suggests a complete replacement for dolomite crystals. The clays and organic materials between crystals, and not within lens-shaped pods is a significant observation, as entrapment of clays and organic materials must have occurred in association with dolomite crystallization during replacement **(Figure 22)**.

Dolomitic mudshales have a dark brown matrix and are finely laminated with silt size discrete rhombs or spherules of dolomite dispersed throughout the matrix. Pyrite is dispersed throughout the matrix and is present in association with dolomite crystals as a

replacement or as pyritic laminae. The lense-shaped pods are absent in the mudshale; instead, recognizable organisms such as *tasmanites* are observed. *Tasmanites* are randomly oriented and are usually trapped between crystal boundaries. Kirkland et al. (1992) suggest that the discrete rhombs and spherules of dolomite that occur within dolomitic facies probably have an inorganic origin, and some may be the replacement of tests of a planktonic species **(Figure 22)**.

Bulk mineralogy of a dolomitic mudstone in the Middle Woodford Shale is dolomite (64%), quartz (35%), illite/mica (1%). TOC content: 4.05 wt.%. Bulk mineralogy for a dolomitic mudshale is: dolomite (38%), quartz (55%), illite/mica (11%), Plagioclase (2%). TOC content: 6.48 wt.%.

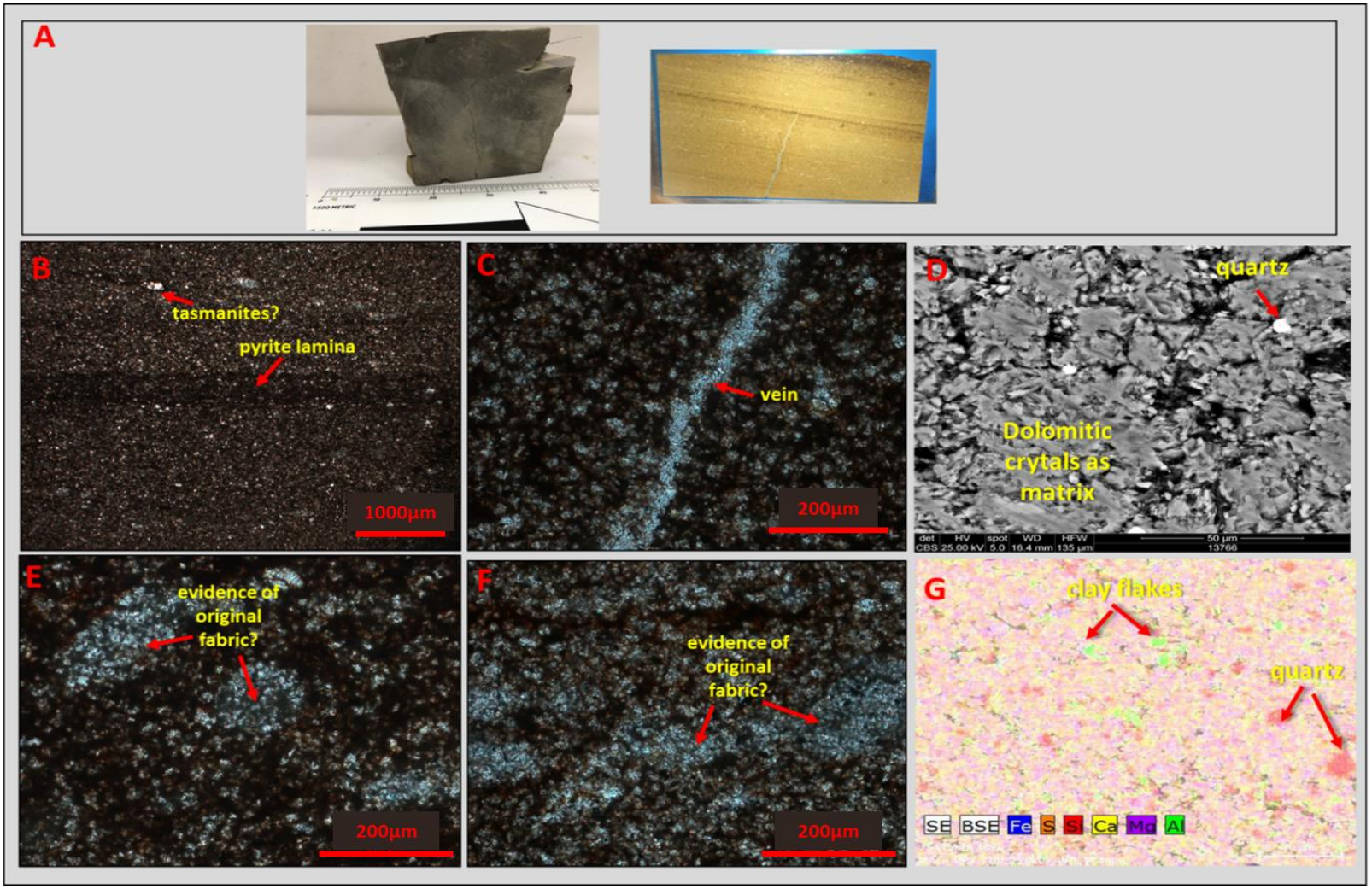

Figure 22. Dolomitic mudstones lithofacies. A. Hand sample and thin section. B, C, E, F: Thin section photomicrographs showing evidence of original fabric. The entrapment of clays and organic materials between crystals suggest entrapment must have occurred with dolomite crystallization during replacement. D, G: SEM images shows minor clays and quartz.

Bleached Facies

Bleached facies dominate the Upper Woodford Shale. Kirkland et al. (1992) has proposed that the appearance of these lithofacies can be attributed to Quaternary weathering, and its associated low organic matter content could be due to oxidation. The occurrence of these lithofacies, although not common, has been reported to occur in other localities by Kirkland et al., 1992.

In hand sample, these lithofacies appear lightweight, soft, and porous. Color is mostly white but can have a gray tint, or orangish stain as a result of iron oxidation. An indication of original lamination is observed in some samples, and in others, the fabric is structureless. In terms of texture, these lithofacies are powdery when dry and sticky when wet (**Figure 23**).

In thin section, they appear poorly crystallized, and in other cases, secondary porosity exists where crystalline minerals were initially present. Although the internal alteration of the fabric, the original bedding thickness is retained, and it can get as thick as bedded cherts and mudstones, and rarely as thin as mudshales. SEM analysis (EDS) shows that these facies despite their internal characteristics contain high percentages of silica within its matrix, with clay minerals dispersed throughout the matrix. This corroborates with interpretations from Kirkland et al. (1992) XRD analysis, which showed that the facies contain high percentages of silica and less clay in comparison to that of the average shale (**Figure 23**).

The only identifiable organism within these lithofacies are *tasmanites cysts.* The easily recognized orangish organic-rich walls usually associated with the *tasmanites cyst* which are almost completely absent, leaving only the quartz infill to retain the structure

that makes it identifiable. In accordance, the organic content within these lithofacies is as low as 0.07wt%, which is lower than the organic content of the green clayshales of the Lower Woodford Shale. However, organic materials can be observed in its matrix or within preserved *tasmanites cyst*, but thee occurrence is minimal. Radiolaria which is abundant in the Upper Woodford might also be present, but difficult to identify due to the weathered rock fabric. Phosphate nodules also occur with this lithofacies and appear bleached with internal fabric partially preserved or completely destroyed (**Figure 23**).

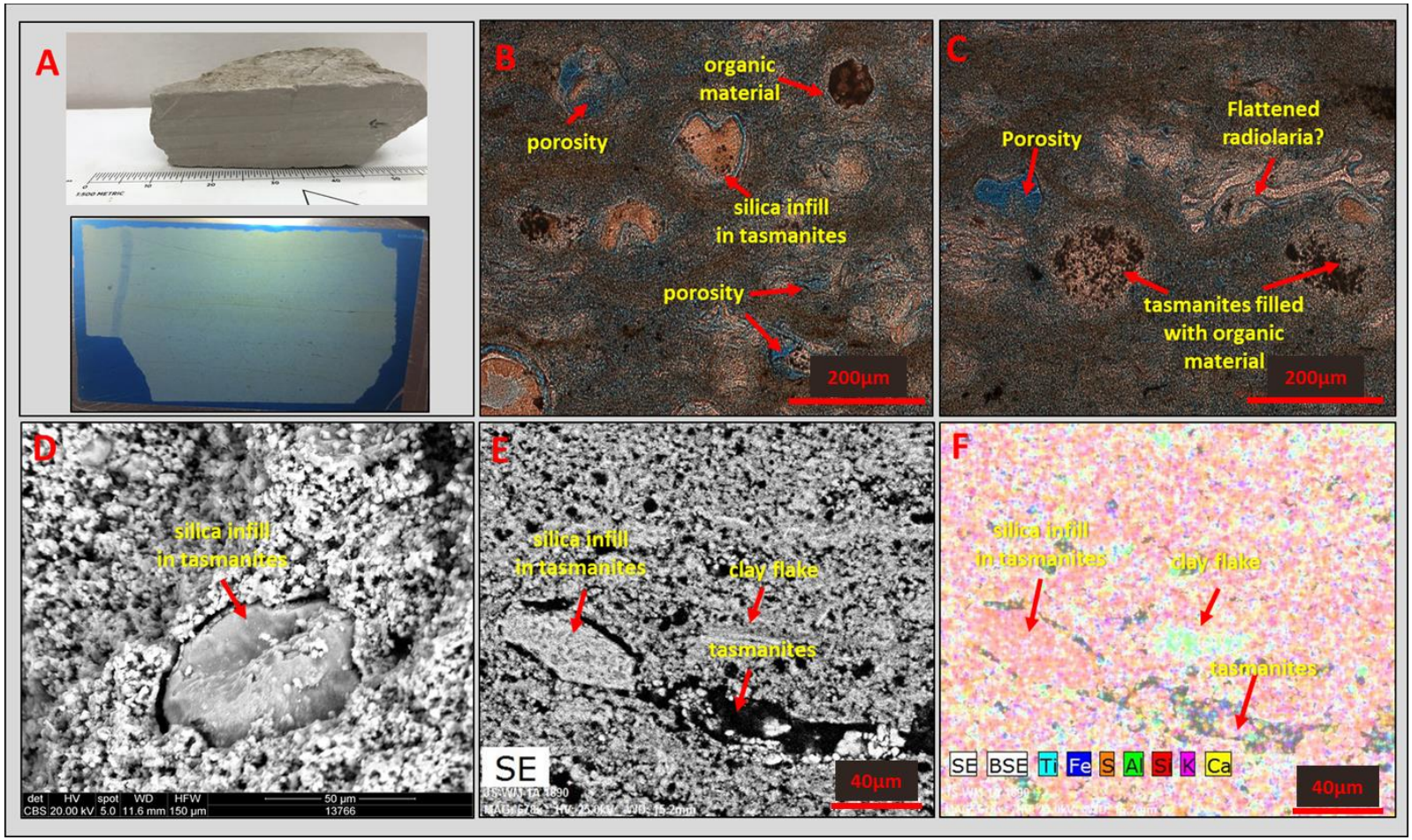

Figure 23. Bleached facies of the Upper Woodford Shale. Lithofacies are lightweight, porous, soft, poorly crystalline, with poorly preserved organisms. A: Bleached facies sample and thin section. B, C: Thin section photomicrographs showing the porous and structureless internal fabric. Traces of organic matter is evident. D-F: SEM images showing poorly preserved *tasmanites* infilled with silica. Clay flakes are dispersed throughout the matrix.

3. Lithofacies Defined and their Vertical Distribution

Figure 24 shows the lithofacies defined for the Woodford Shale section, and the distribution among the informal members. **Figure 25** shows the Woodford Shale outcrop at the McAlister Cemetery Quarry, with GR superimposed for an overlook of the variation in GR along the section.

The lowermost part of the Lower Woodford Shale, close to the Hunton Group – Woodford Shale contact is mainly composed of papery (<0.5mm) greenish clayshales. Because of its incompetent nature, this part of the section tends to form the surficial valleys/depressions in the outcrop. Up-section, as organic content increases slightly, there is a lithofacies change from green clayshales to a mixture of green clayshales and dark brown argillaceous-siliceous mudshales, and finally to interbeds of siliceous mudshales, mudstones, and argillaceous mudshales. As siliceous content increases, resistant surficial mounds occur where there is a consistent interbedding between siliceous shales and mudstones (**Figure 26**).

The Middle Woodford Shale is composed mainly of argillaceous mudshales in the uppermost part and siliceous shales and mudstones in the lowermost part. Resistant mounds also occur where there is a consistent interbedding between siliceous shales and mudstones (**Figure 27**). The Upper Woodford Shale is bleached and characterized by interbedded chert and shale/mudstone, with abundant phosphate nodules. This part of the section is highly resistant and exposed as the quarry walls. Dolomitic mudstones occur sporadically in the Upper Woodford Shale.

Within the overall section, there are characteristic patterns to the stratigraphic distribution of lithofacies relative to one another. Siliceous mudshales, followed by

siliceous mudstones are the most abundant lithofacies throughout the section and have been primarily distinguished based on the degree of outcrop fissility. Radioactivity and TOC are observed to be highest within these lithofacies. Siliceous mudshales are variably laminated, in some occurrences, laminations are distinct and easily identified, and in other cases, discerning laminations are difficult, as in siliceous mudstones which show a blocky pattern.

Clayshales exhibit a papery stratification, and dominates the lowermost part of the Lower Woodford Shale, and also marks the transition from the Upper Woodford Shale to the Sycamore Limestone. Radioactivity and TOC values are low within this lithofacies. In some cases, they are mixed with the underlying mudshales forming wavy, non-parallel laminations. In such instances, they are defined as mixed clayshale-mudshale. Argillaceous mudshales are fissile with a darker fabric than clayshales, and dominate the uppermost Middle Woodford Shale, with relatively high TOC.

Bedded cherts are typically the most abundant in the upper part of the section as interbeds between siliceous mudstones/mudshales, with bed thickness >10mm. This interbedding is present above the highest TOC and high gamma-ray spike close to the Middle-Upper Woodford Shale contact. They tend to have the lowest radioactivity, and TOC, and in general are hard and brittle, with an exception in areas that have been influenced by bleaching/weathering.

Usually, the stratigraphic distribution of dolomite mudstones/mudshales varies throughout the section. Dolomitic beds are preferentially distributed in the Middle Woodford Shale. Just as siliceous mudstones and mudshales, dolomitic mudstones are differentiated from mudshales based on the degree of fissility. Dolomitic mudstones

appear massive, and rarely show laminations. Dolomitic mudshales usually show some laminations (**Figure 28**).

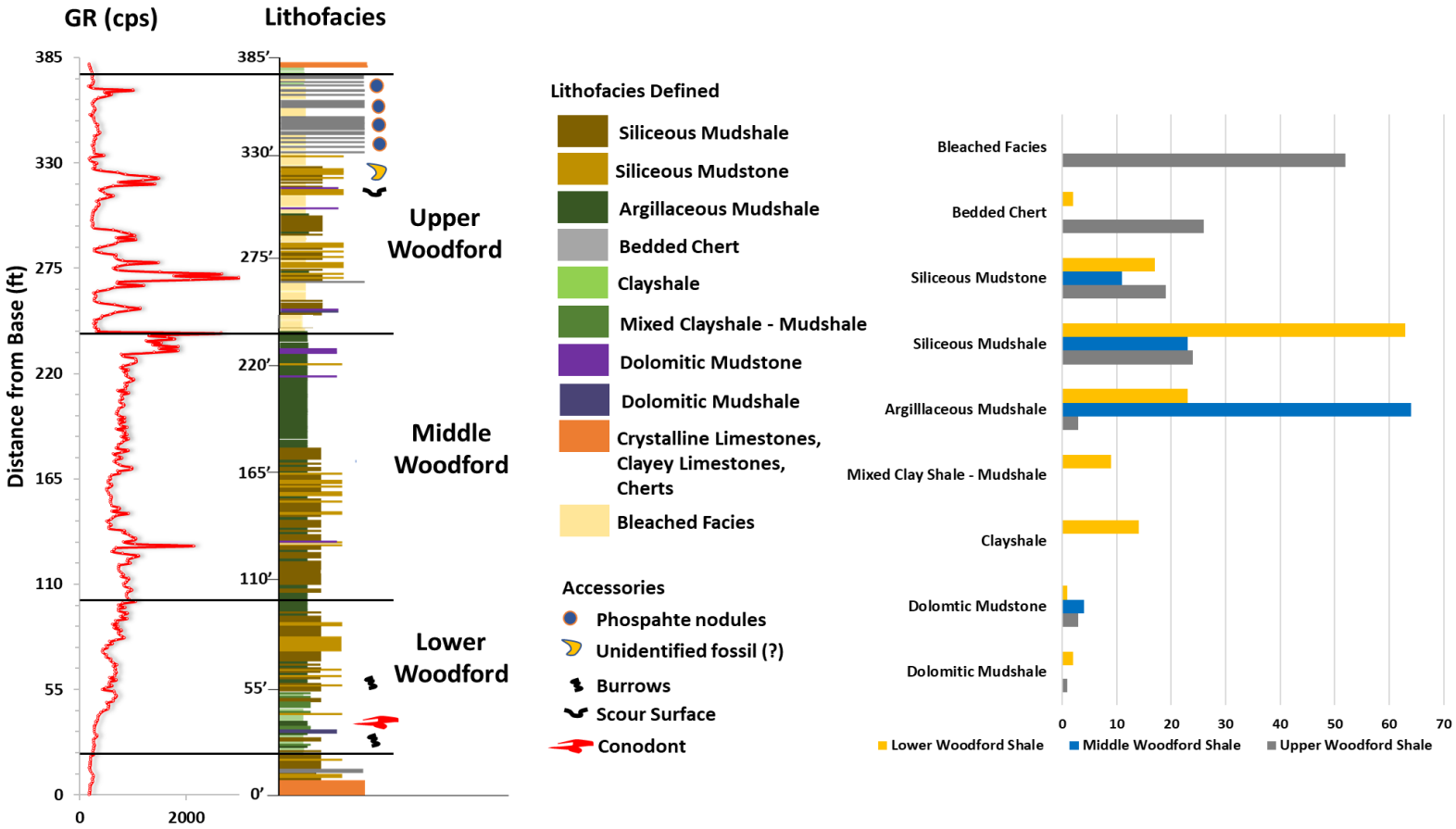

Figure 24. Distribution of lithofacies defined within the informal Woodford Shale members. Clay shales dominate the Lower Woodford Shale, as this is typical for the lowermost Lower Woodford Shale. The Upper Woodford Shale is mostly bleached, bringing down the abundance of cherts, mudstones, and mudshales, as this part of the section is typically characterized as interbeds between cherts and mudstones/mudshales.

Figure 25. Woodford Shale outcrop at the McAlister Cemetery Quarry, with GR superimposed, marking the boundaries of the informal members of the Woodford Shale.

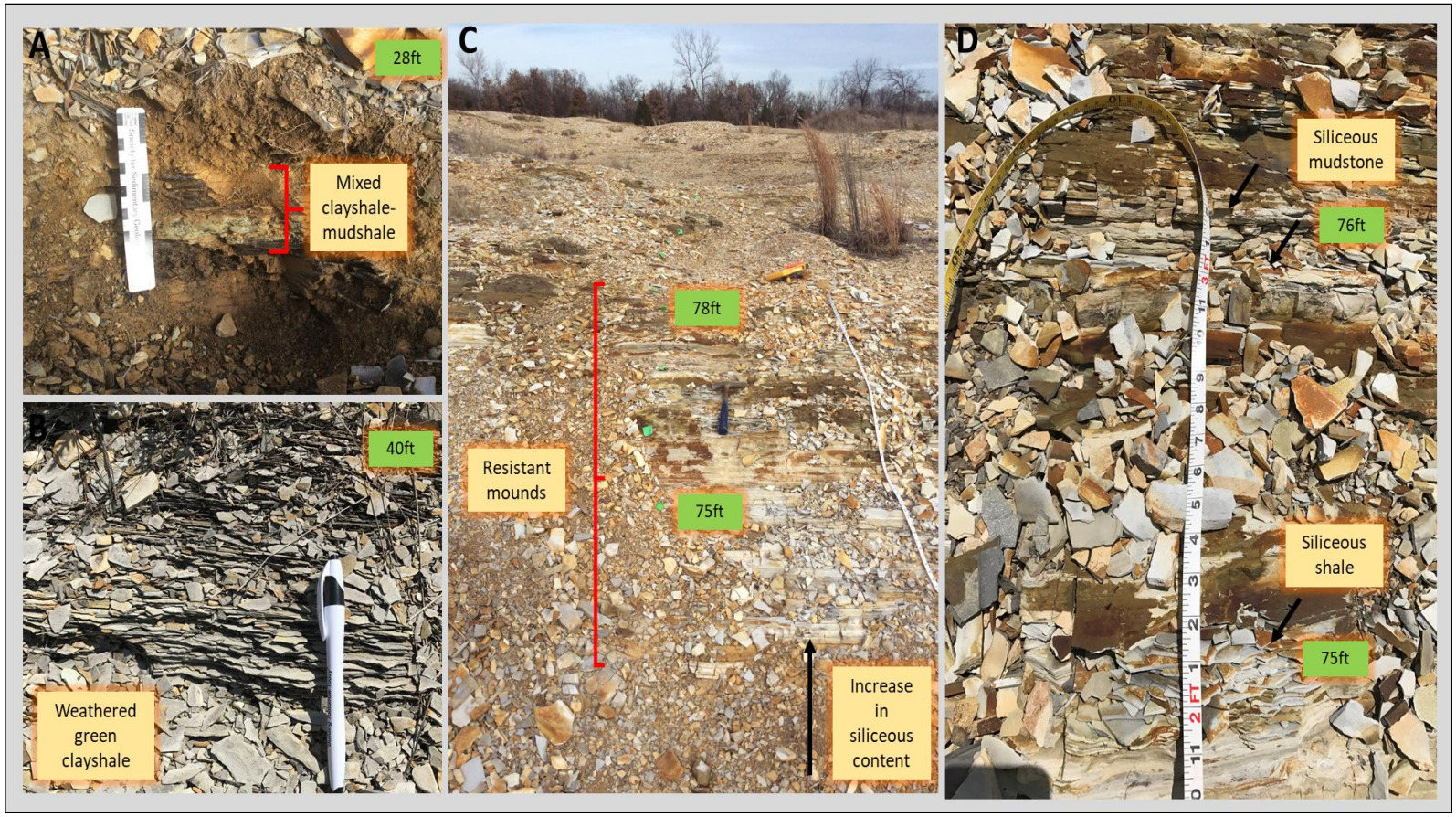

Figure 26. The lower Woodford Shale member. **A**. The lowermost Lower Woodford Shale green clayshales, and mixed clayshale-mudshale. **B**. Papery-fissile clayshales. **C.** Resistant mounds in the Lower Woodford Shale composed of interbeds of siliceous shales and mudstones. **D**. Closer view of resistant mounds.

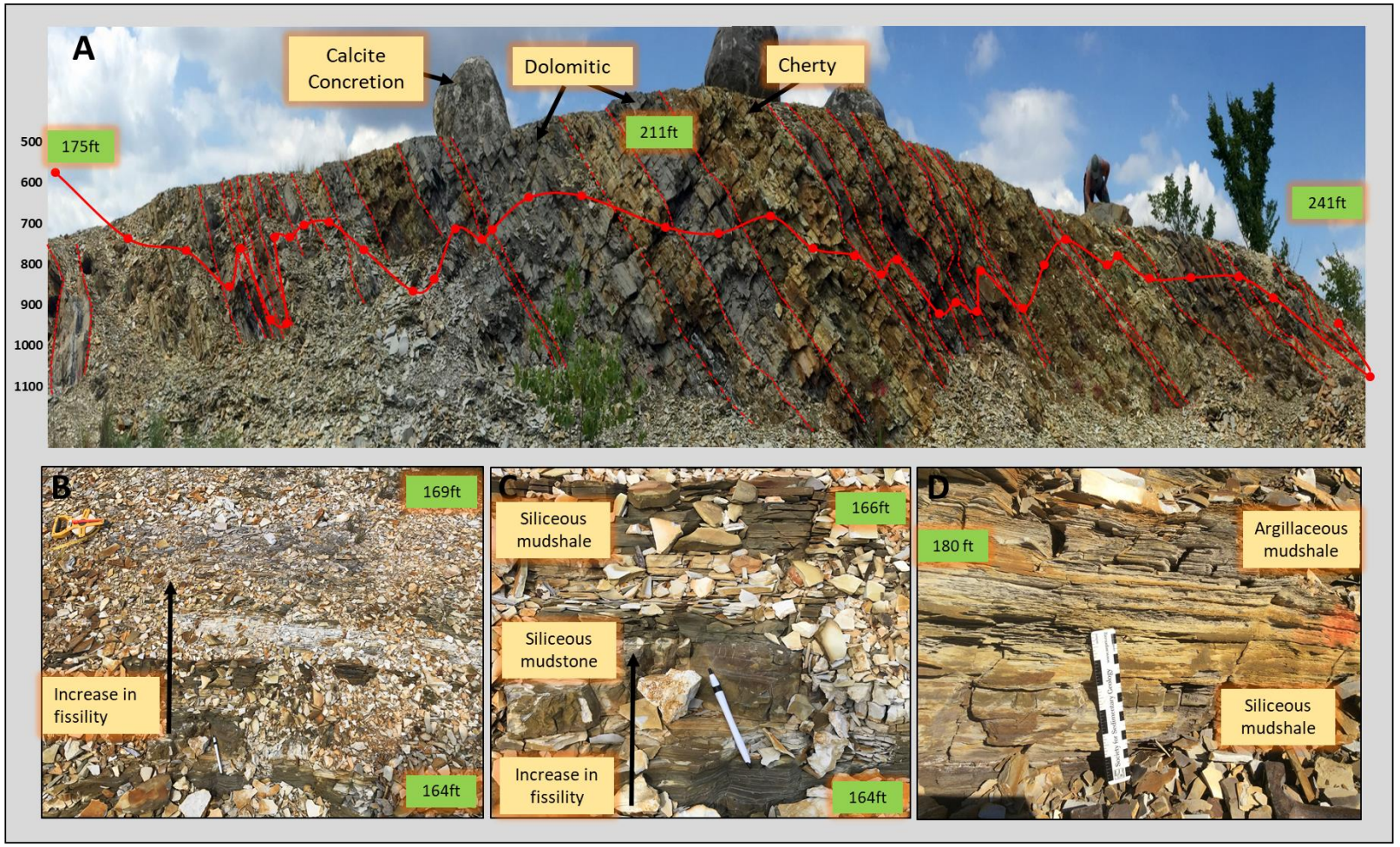

Figure 27. The middle Woodford Shale member. **A**. The uppermost part of the Middle Woodford Shale is dominated by argillaceous shales, with some occurrences of dolomitic mudstones and siliceous mudstones. **B**. Change in lithofacies from resistant mounds (siliceous mudshale – mudstone interbeds) to argillaceous mudshales. **C.** Resistant mounds. **D**. Fissile argillaceous mudshales.

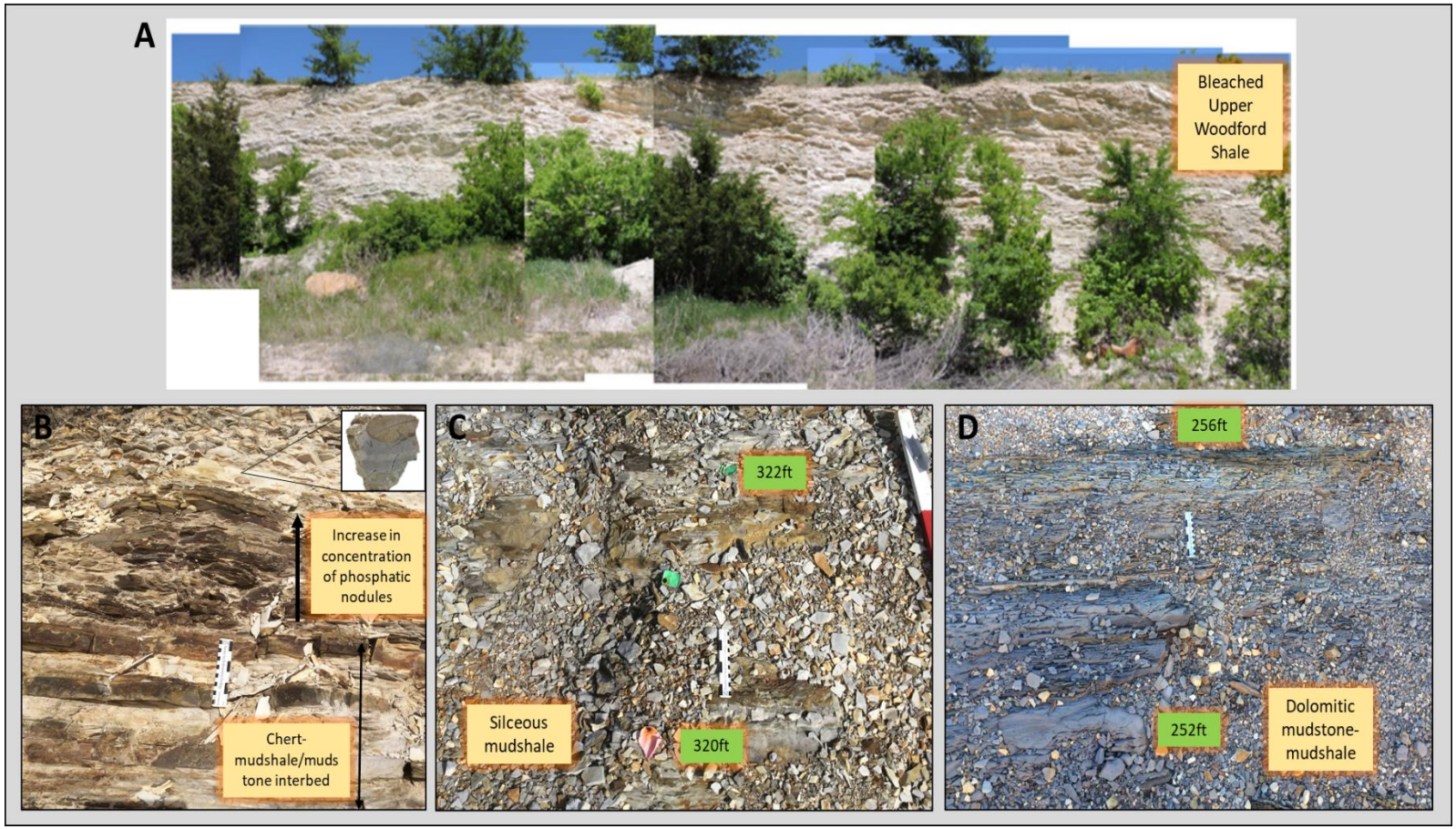

Figure 28. The upper Woodford Shale member. **A**. The bleached uppermost part of the Upper Woodford Shale (modified from Klockow, 2017). **B**. Interbedded Chert and siliceous mudstones/mudshlaes, with phosphatic nodules **C.** Siliceous Mudstones of the Upper Woodford Shale **D**. Dolomitic mudshales of the Upper Woodford Shale.

4. Fissility/Parting

Figure 29, shows the parting types that are observed in the Woodford Shale outcrop, from the thinnest parting (papery) to the thickest (slabby). Notice the variation in color, as it can be inferred that weathering color takes on a darker fabric as parting thickness increases.

Figure 29. Fissility observed in the Woodford Outcrop in the McAlister Quarry.

Figure 30, shows the parting distribution within the informal members, where the thickest parting is observed in the Upper Woodford Shale and the thinnest, in the lower Woodford Shale.

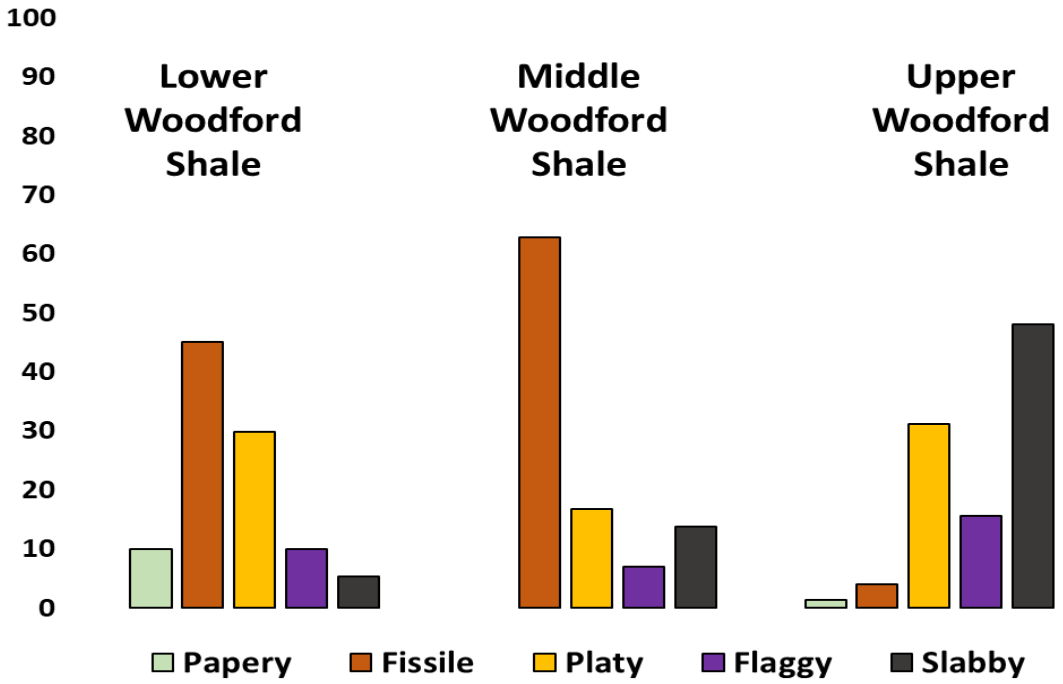

Figure 30. Parting distribution (%) within the informal members of the Woodford Shale, showing the thinnest parting dominating the lower Woodford Shale, and the thickest beds dominating the upper Woodford Shale.

The type of parting a mudrock will display is dependent on the abundance of clays, as well as the quartz content. **Figure 32**, shows a plot of Silicon – Aluminum ratio (Si (ppm)/ Al (ppm)), where the highest Si/Al content corresponds with the thickest beds. That is, bed thickness increases with increasing Si/Al content.

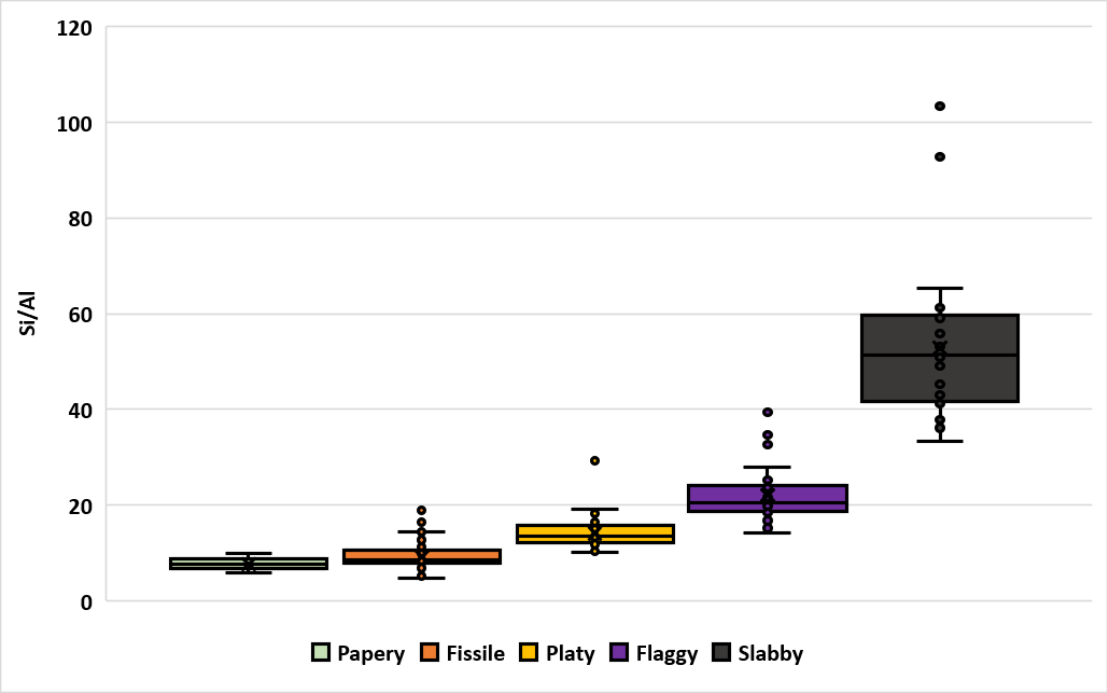

Figure 31. Silicon–Aluminum ratio (Si (ppm)/ Al (ppm)), plotted against parting types. Parting thickness increases with Si/Al ratio.

4.3. Woodford Shale Formational Contacts

Lower Contact (Hunton Group-Lower Woodford Shale)

The Woodford Shale overlies a major regional unconformity that extends across the southern Midcontinent (Ham et al.,1973; Amsden, 1975, 1980). Typically, in the Ardmore Basin, the Woodford Shale overlies eroded strata of the Hunton Group. In some outcrop locations close to the study area, a basal clastic unit (Misener-type Sandstone) is also present. The Misener sandstone represents lag deposits that were eroded from older formations (Amsden and Klapper, 1972; Amsden, 1975;). The Misener Sandstone is absent in the study area.

Seismic studies have demonstrated the paleo-topographical controls on the distribution of the Woodford Shale, owing to the development of karst features and

incised valleys (Gupta et al., 2011; Cardona-Valencia, 2014; Infante-Paez et al., 2016). The Woodford Shale is thinner when underlain by the Hunton Group (Amsden 1975; Blackford, 2007; Althoff 2012; McCullough, 2014). Models created by Infante-Paez et al. (2015); Slatt et al. (2016); Turner (2016) further demonstrates this stratigraphic relationship between the Hunton Group and Lower Woodford Shale. During the Pre-Woodford, sub-areal exposure from a fall in sea level resulted in the erosion and dissolution of the top of the underlying Hunton Group. As sea level began to rise again at the onset of transgression, the Lower Woodford Shale was preferentially deposited within the topographic lows on the unconformity surface until the low was completely filled.

At the study area, the stratigraphic relationship between the Hunton Group and the Lower Woodford Shale is difficult to delineate due to the dip angles of the beds. However, the contact can be recognized by a change in weathered color, from beige (Hunton Group) to light grey (Lower Woodford Shale-Basal) (**Figure 32)**. The Hunton Group exposed at the study area is predominantly crystalline limestone with some cherty and clayey limestones. Limestones are fossiliferous with well-preserved crinoids, brachiopods, and burrows. They appear densely fractured with numerous dissolution features.

Above the Hunton Group, marking the contact between the Hunton Group and the Lower Woodford Shale is the least competent part of the Woodford Shale, dominated by organic poor, low resistivity, interbeds of greenish clayshales and mixed clayshales to mudshales. At the study area, this part of the section forms a low depression owing to

incompetency from clay richness. These low depressions are flooded with rain and snowmelt mainly in the spring, and exposed during the summer **(Figure 32)**.

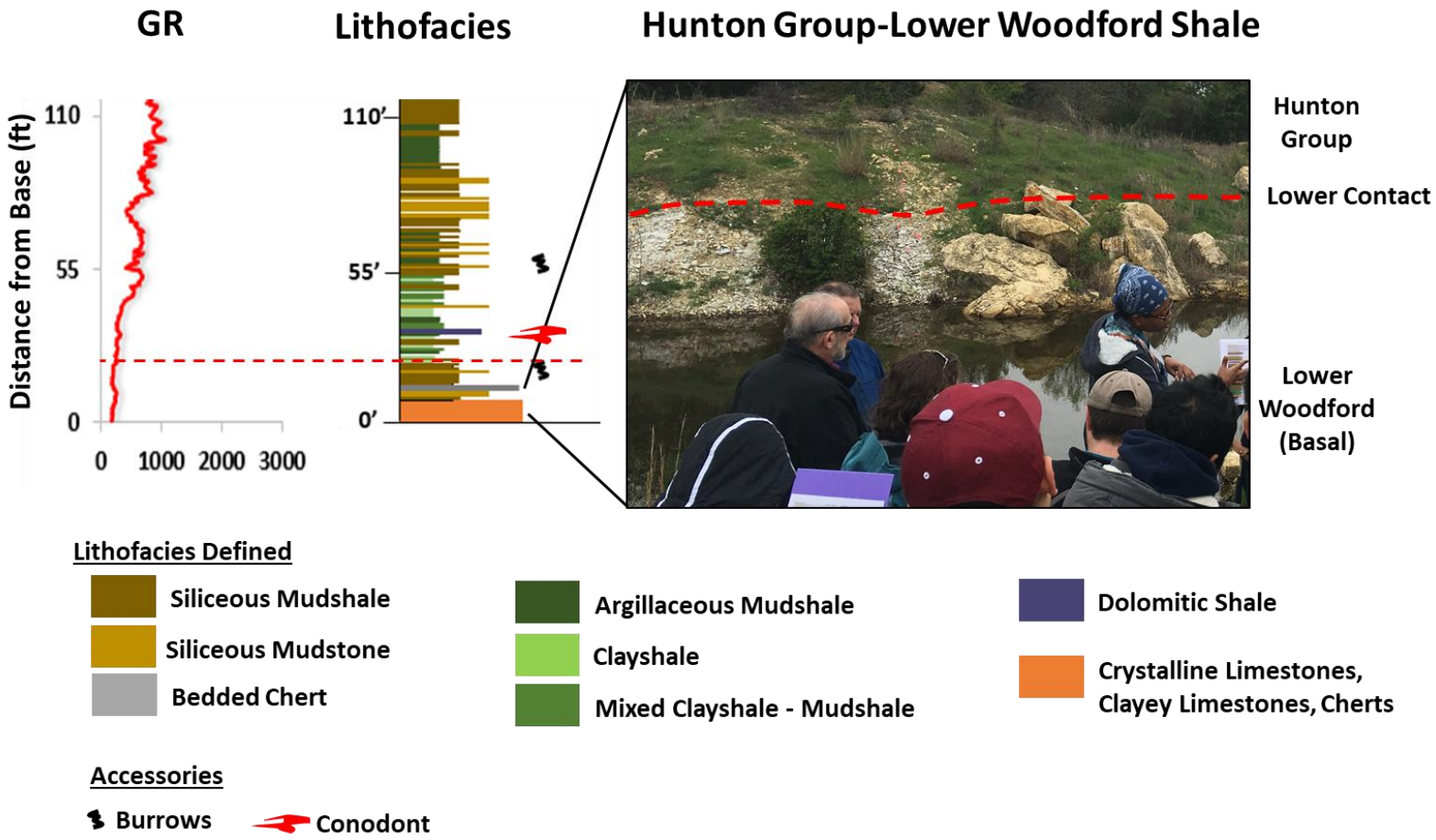

Figure 32. Stratigraphic lower contact between the Hunton Group and the lower Woodford Shale. The Lower Woodford Shale is the least competent part of the Woodford Shale, dominated by organic poor, low resistivity, interbeds of greenish clayshales and mixed clayshales to mudshales. In the outcrop, the Hunton-Lower Woodford contact is marked by a color change from beige to light grey.

Upper Contact (Upper Woodford Shale-Sycamore Formation)

The Woodford Shale is overlain by the Sycamore Formation. The contact is marked by a shift in facies from siliceous mudstones and bedded chert to an interval of transitional green clayshales, and silty limestone. This transitional unit has been described as grey-greenish shales, cherts and limestones (Donovan, 2001; Galvis, 2017; Becerra-Rondon; 2017). At the study area, ~ 8 feet of the green clayshales is present, capped by a 1-foot thick orangish limestone.

The Upper Woodford Shale is mostly bleached, and is composed of interbedded chert and siliceous mudstones and shales. The Sycamore Limestone is characterized by poorly fossiliferous, fine-grained, silty limestone. Galvis (2017) and Bacerra-Rondon (2017) have shown from petrographic and mineralogical analyses that these limestones are hybrid or impure (marlstones?), that consist of silt-angular (~60%) in a micritic to a pseudosparitic matrix (~30%). Closer to the transitional interval, the cherts become clayey, and grade into the green shales. The green clayshales also appear to grade into the overlying limestones. Similar to the clayshale interval at the base of the section, they are incompetent and tend to form low depressions at this part of the section (**Figure 33**).

The stratigraphic relationship between the Woodford Shale and the Sycamore Formation is problematic. Whether the contact is conformable or not is unclear. The terminology 'Pre-Sycamore,' following the works of Galvis (2017) and Becerra-Rondon (2017), was adopted to refer to the green clayshale transitional zone. Biostratigraphic works from Schwartzapfel (1990) and Noble (1995) recognized the post-Woodford Shale deposition (early Mississippian) as a period of slow sedimentation and non-deposition

(hiatus), with deposition resuming over the late Mississippian as limestones and shales of the Sycamore Formation.

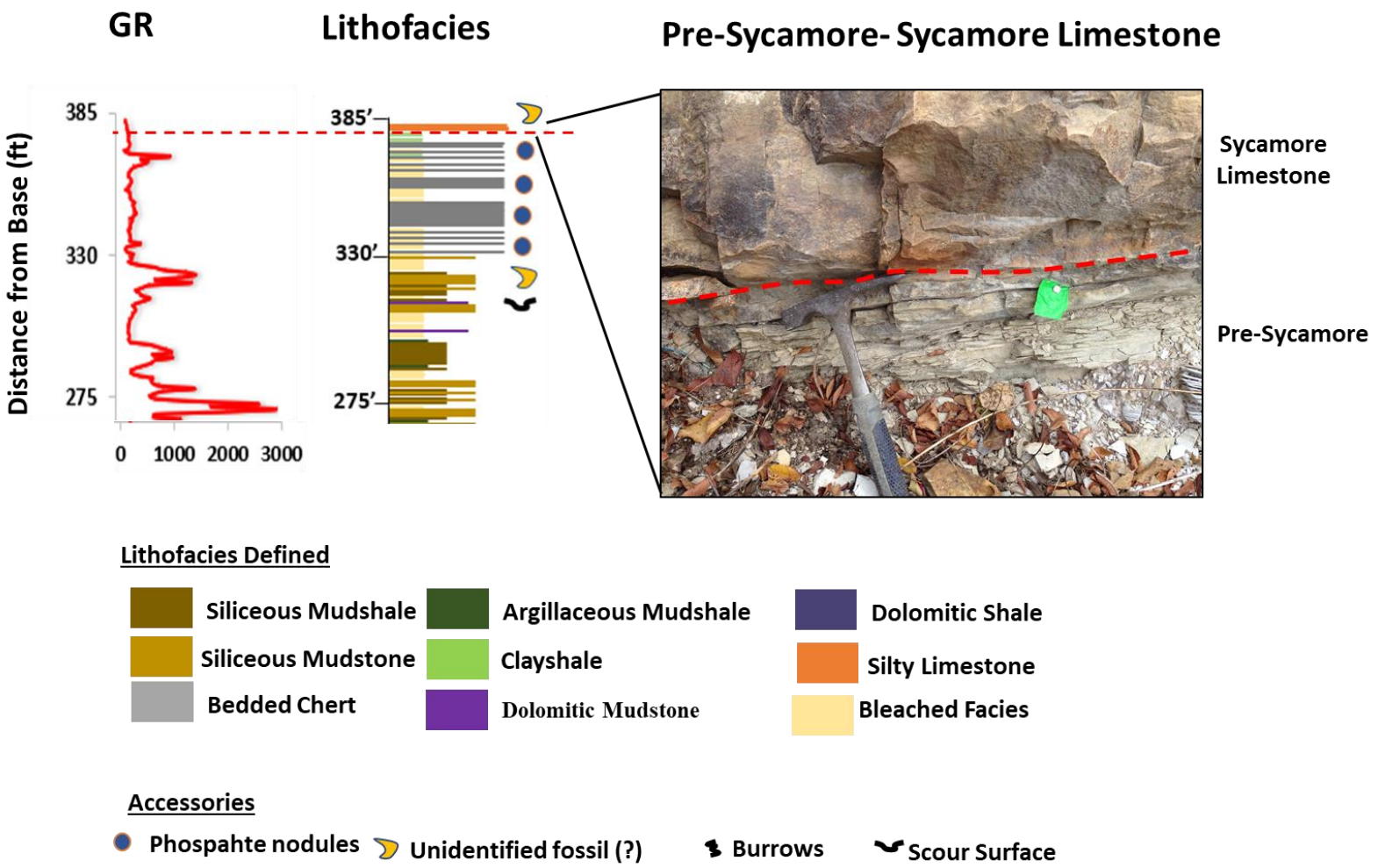

Figure 33. Stratigraphic upper contact between the Woodford Shale and the Sycamore Formation. The contact is marked by a shift in facies from siliceous mudstones and bedded chert to an interval of transitional green clayshales, and silty limestone.

4.4. Defining Woodford Shale Informal Members

The lower-middle Woodford Shale and the middle-upper Woodford Shale boundaries were defined following the work of Paxton et al. (2007). The outcrop GR profile from the McAlister Quarry was correlated to the outcrop GR profile of the Henryhouse Creek section, Carter County, and well log GR from the Amis 1-3 Ramsey well, Murray County (34.42363, -97.07902) (**Figure 34 A-C**). The cross-section is flattened on the boundary between the middle-upper boundary, which has also been established as the regional maximum flooding surface (mfs) of the Woodford Shale.

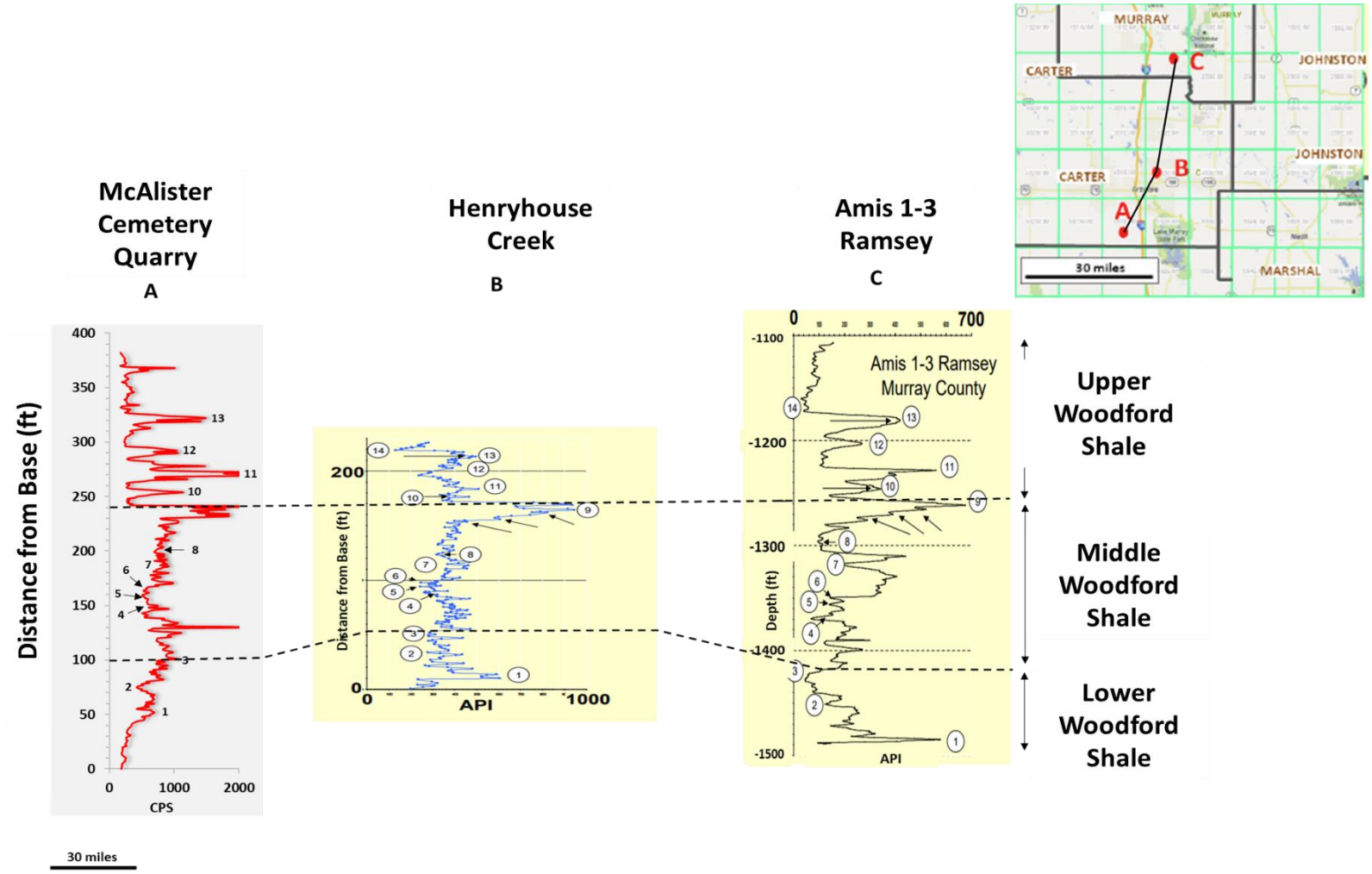

Figure 34 A-C. Regional correlation used to identify the boundaries between the lower-middle Woodford Shale, and the middle-upper Woodford shale. Correlation is flattened on the middle-upper boundary. Modified from Serna-Bernal (2013). Adapted from Paxton et al. (2007).

4.5. XRD Bulk Mineralogy

Results from XRD analysis incorporated into this study was adapted from Serna-Bernal (2013). The bulk XRD analysis results show that the mineralogic composition of the Woodford Shale is dominated by high proportions of quartz (>80%) throughout the section, with the highest concentration in the Upper Woodford Shale. Previous studies (Kirkland et al. 1992; Comer, 2005; and Comer, 2008) on the Woodford Shale have interpreted the majority of the quartz to be biogenically sourced and have been attributed to zones of coastal upwelling or thermal water mass stratification. The analysis also showed the presence of carbonate minerals in a few samples, in the form of dolomites. From thin sections, dolomitic enrichment is low throughout the Woodford Shale. Where they are detected, they occur as discrete beds and are observed to be mostly dominated in the Lower and Middle Woodford, relative to the Upper Woodford Shale.

Also revealed are traces of clay minerals such as illite and kaolinite. A decrease in clay content occurs up section, the Lower Woodford Shale having the highest clay content, followed by the Middle Woodford Shale member. The presence of sodium-rich plagioclase feldspar and orthoclase is also observed, indicating minimal inputs of terrestrial clastic sediments during the Woodford Shale deposition. These terrestrial inputs are most evident in the Lower and the Middle Woodford Shale.

The mineral pyrite, which is a good indicator of anoxic conditions, is common in the entire Woodford Shale, with the highest content in the Middle Woodford Shale. Apatite is also present and is mostly detected in the Upper Woodford Shale in association with phosphate nodules. Traces of gypsum are also present, and this can be attributed to an association with weathering by-products (**Figure 35**).

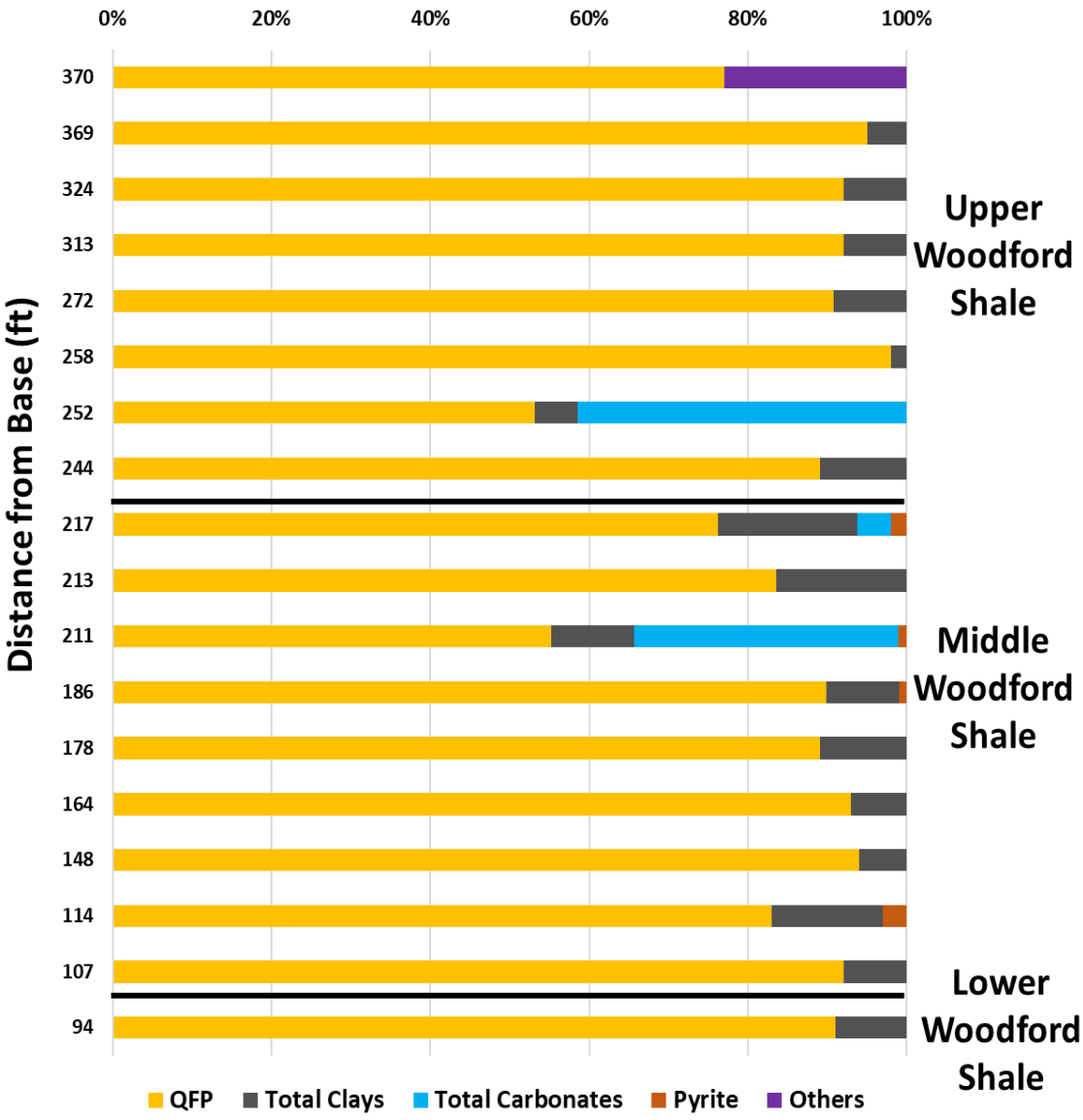

Figure 35: XRF Bulk Mineralogy of the Woodford Shale showing percentile distribution amongst informal members of the Woodford Shale. The Upper Woodford Shale has the highest quartz content, relative to other Woodford Shale members.

CHAPTER V

ORGANIC GEOCHEMISTRY - SOURCE ROCK EVALUATION

Organic-richness, kerogen type, and thermal maturity are important for source rock evaluation, and are assessed in this section using geochemical analysis based on TOC and Rock Eval data. Additional data from Serna-Bernal (2013) was integrated.

5.1. Organic-Richness

TOC values amongst the informal members of the Woodford Shale are displayed in **Figure 36**, which shows TOC variation with depth.

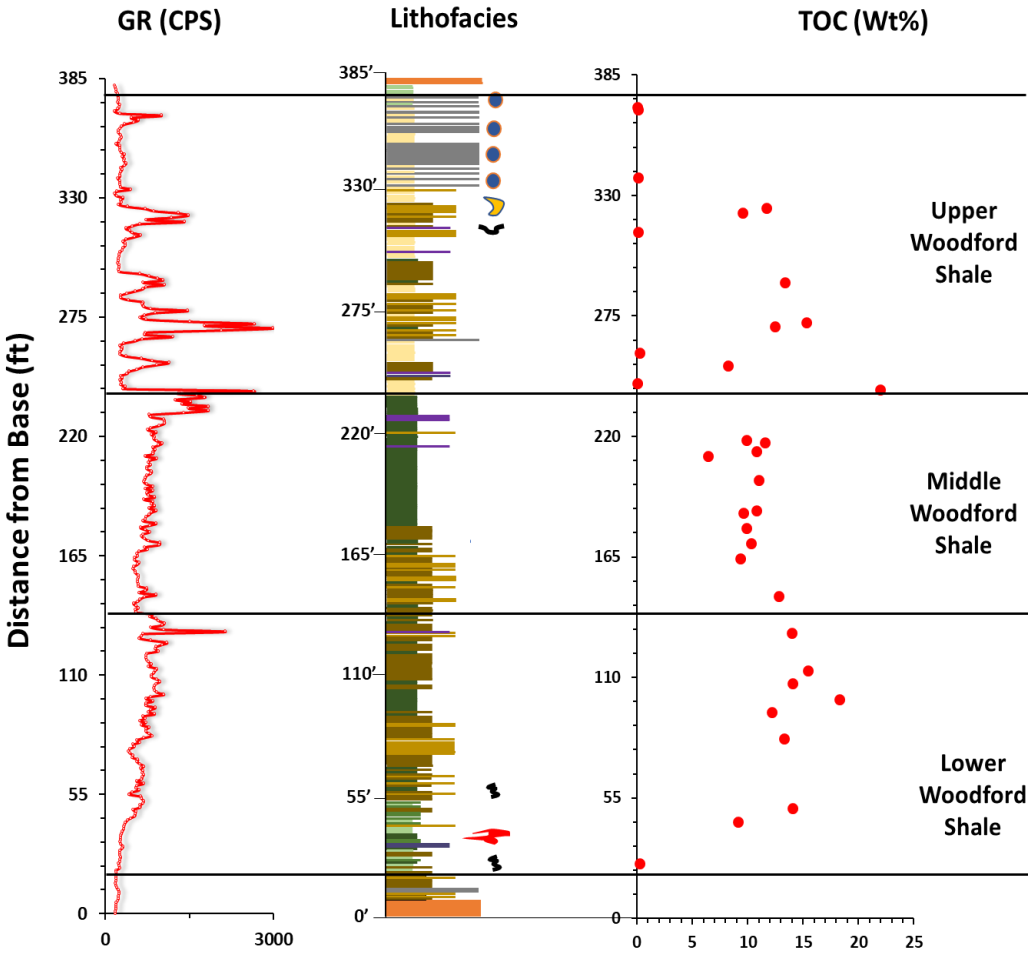

Figure 36. Left to right: GR profile, lithofacies, TOC values distributed along the entire section.

The concentration of total organic carbon (TOC) of the Woodford Shale ranges in values from 0.07 to 22 wt% with an average value of 11 wt%. In terms of conventional source richness (Jarvie, 1991) these values infer excellent source rock potential for this section of the Woodford Shale. This excludes the basal green clayshales, and the bleached facies in the Upper Woodford, both of which have poor TOC values.

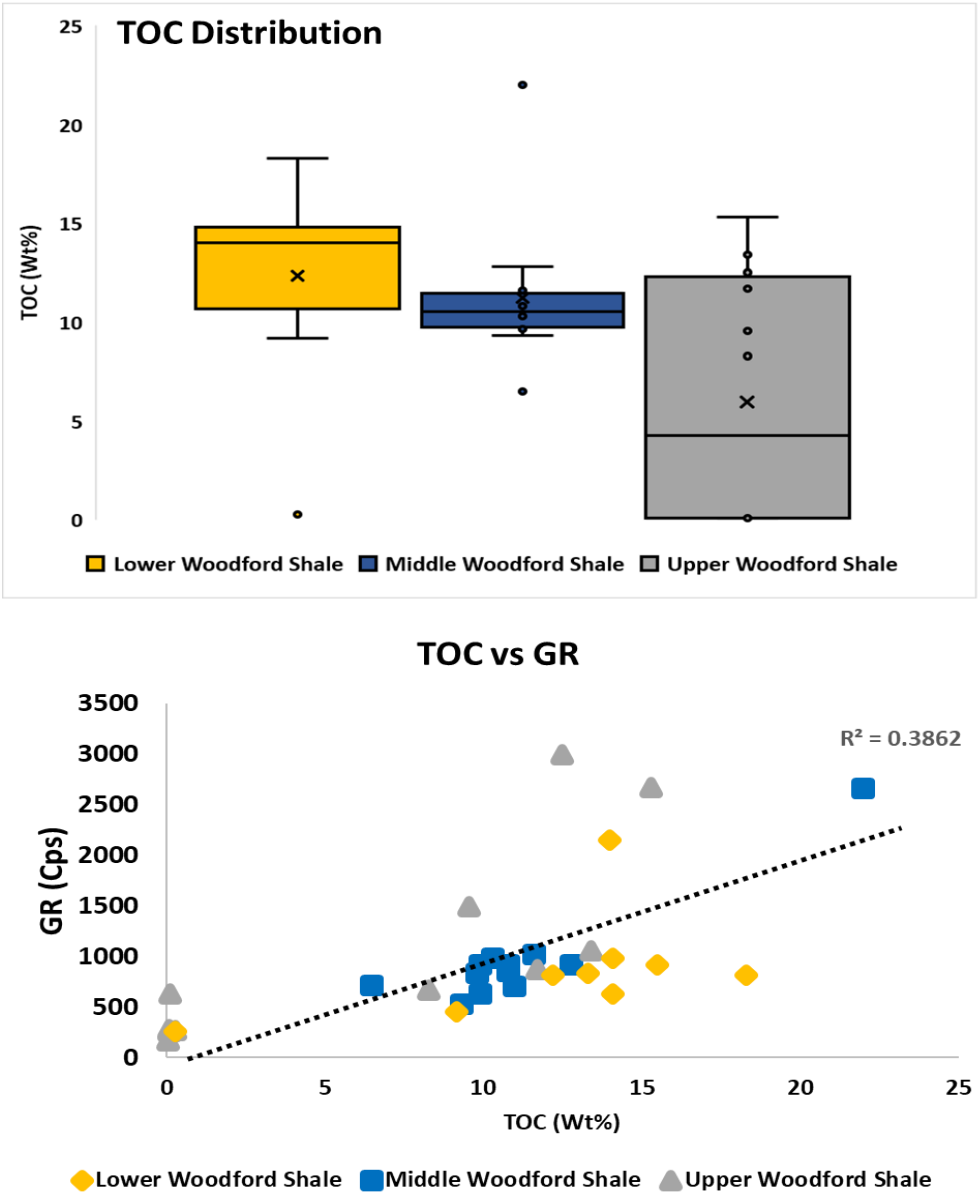

Figure 37. Top: GR distribution among informal members, with the most variation in the lower and upper Woodford Shale, and the least in the middle Woodford Shale. **Bottom**: TOC vs. GR chart of the informal members, showing a good correlation with the middle Woodford representing a better trend.

The Lower Woodford Shale shows TOC values ranging from 0.28 to 18.3 wt% (n=9). The Middle Woodford Shale shows TOC values from 6.48 to 22 w% (n=12). The Upper Woodford Shale shows TOC values from 0.07 to 15.3 wt% (n=12). The Lower, Middle and Upper Woodford Shale possess average TOC values of 12.34 wt%, 11.2 wt%, 5.96 wt%; respectively (**Figure 37**).

The Upper Woodford Shale shows a wide range of variation of TOC (wt%) compared to Lower Woodford, followed by the Middle Woodford which has less variation of TOC values. This TOC variation demonstrates the heterogeneity that characterizes the Woodford Shale. The lesser variation in TOC values observed in the Middle Woodford Shale could be attributed to depositional conditions when the Middle Woodford Shale experienced enhanced stability of the water column during a period of persistent anoxia (euxinia) (Miceli-Romero and Philp, 2012). The variation in the Lower and Upper Woodford Shale TOC values can also be attributed to the paleoenvironmental interpretation of the Woodford Shale by Miceli-Romero and Philip (2012), which postulates that the lower and the Upper Woodford Shale deposition experienced episodic anoxia (euxinia), where oxidative conditions degraded parts of the organic matter.

The notion that the TOC of organic-rich shales can have a direct relationship with radioactivity can be observed here in the Woodford Shale samples. The Woodford Shale radioactivity is driven by the uranium content (Boardman, 2009), and uranium is associated with organic matter. TOC plotted against GR does not show a good relationship due to the heterogeneity that exists in the Woodford Shale. However, it can be observed that the Middle Woodford Shale represents a better trend (**Figure 37**).

5.2. Kerogen Type

Kerogen type and thermal maturity are important factors in determining the hydrocarbon generative potential of a source rock. In others words, the type of kerogen present (Type I-IV) is dependent on the different hydrocarbons produced with increasing thermal maturity.

Figure 38 shows the pseudo Van Krevelen diagram with Hydrogen Index (HI) and Oxygen Index (OI) (Tissot and Welte, 1978) used to differentiate between kerogen types for a sample. A majority of the Woodford Shale informal members plot between type I and II, with high hydrogen index (HI) (>500 mgHC/gTOC), and low oxygen Index (<20 mg CO2/gTOC). The high HI values can be attributed to the predominance of marine algae, which is rich in hydrogen. A few outliers are observed plotting between Type II and Type III Kerogen and could be associated with recent weathering of the samples.

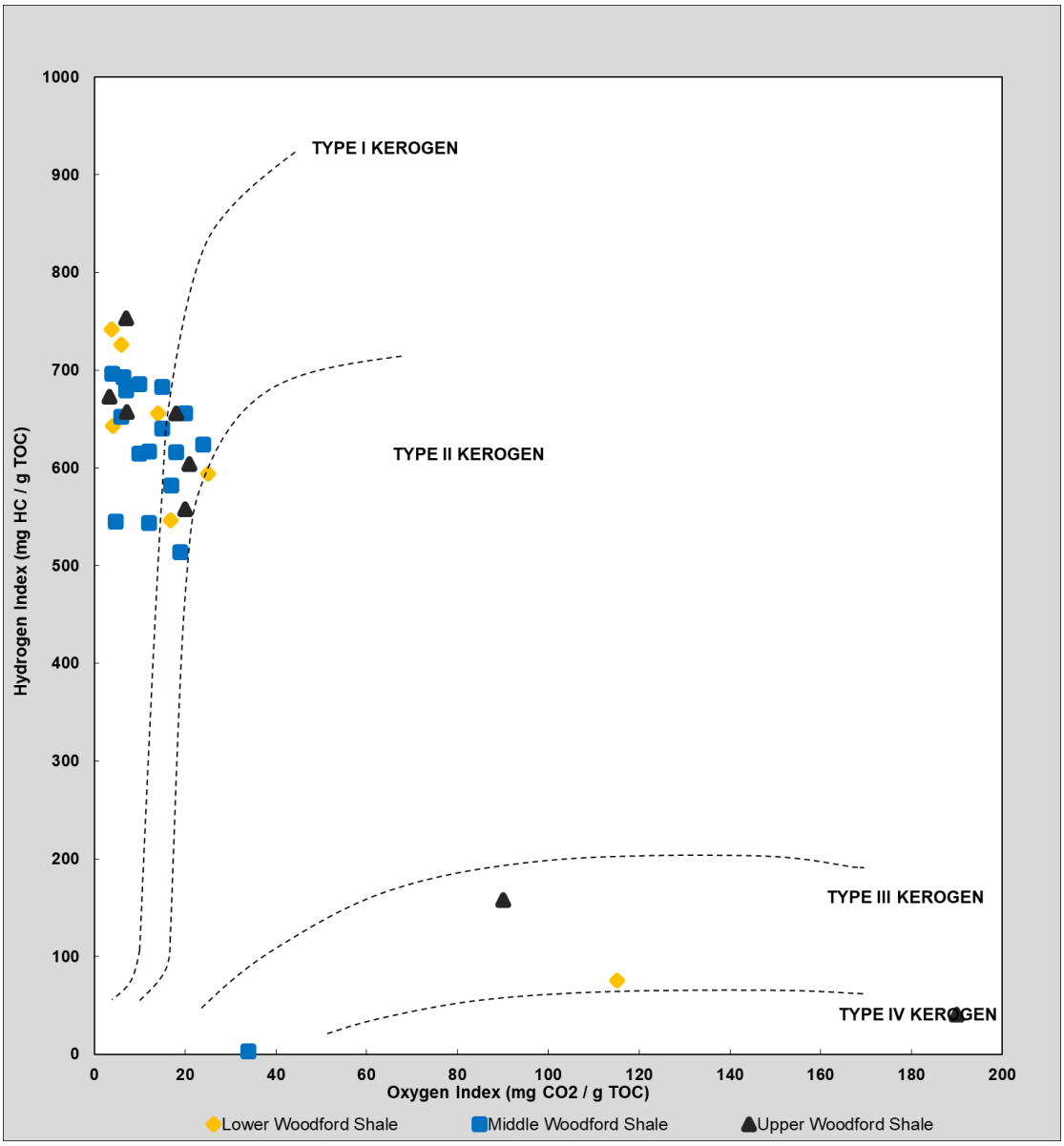

Figure 38. Pseudo Van Krevelen diagram with Hydrogen Index (HI) and Oxygen Index (OI) (Tissot and Welte, 1978) for determining kerogen type. High hydrogen index values indicating the predominance of marine algae.

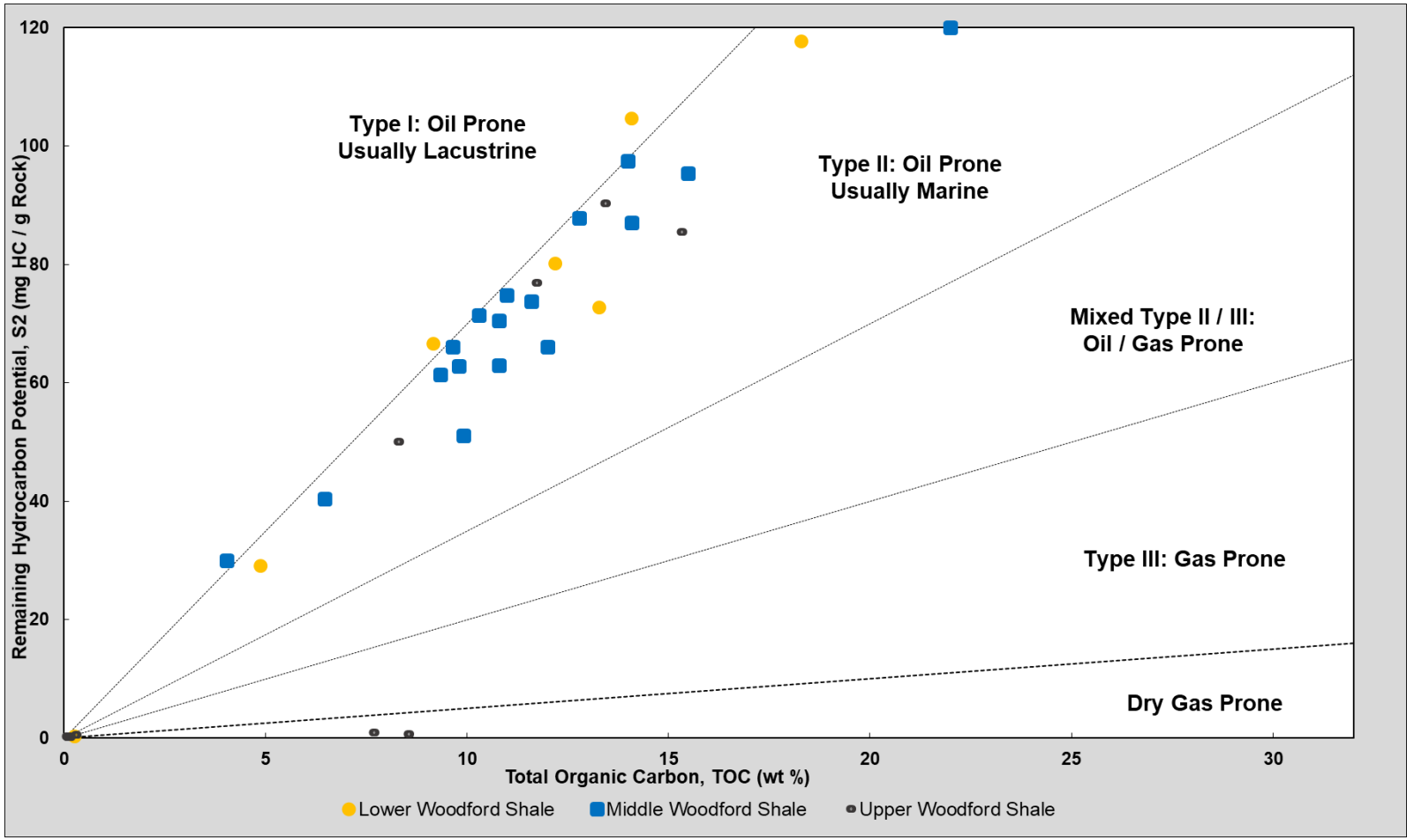

Figure 39. TOC (wt%) and Remaining Hydrogen Potential (S2, mg HC/g Rock) proposed by Cornford et al. (1998) for determining that the Woodford is dominated by kerogen type II (oil-prone, and of marine origin).

Cornford et al. (1998) proposed a technique for a more accurate determination kerogen types using TOC (wt%) and remaining hydrocarbon potential (S2, mg HC/g Rock). All samples are seen to be plotted mostly within Type II kerogen, which is categorized as oil prone, and of marine origin (**Figure 39**). Amongst the informal members, the lower Woodford Shale is predominantly Type II kerogen with a mix of Type I kerogen, which might be an indication for lacustrine type deposition for some parts of the lower Woodford Shale. The middle Woodford Shale is dominated by Type II kerogen. The upper Woodford Shale is also dominated by Type II kerogen, with a few points plotting within the dry gas prone, which is an indication of the presence of vitrinite, a maceral formed from land plant wood.

5.3. Thermal Maturity

As previously mentioned thermal maturity is an important factor in determining the hydrocarbon generative potential of a source rock. Thermal maturity can be determined from measured vitrinite reflectance, and calculated technique of pyrolysis (Tmax, Transformation ratio).

Thermal maturity from pyrolysis uses Tmax (^{o}C) and HI (mh HC/g TOC) to determine the hydrocarbon generative potential. Tmax values range from 413^{o}C to 430 ^{o}C, with an average of 422 ^{o}C, and HI values mostly less than 500. Calculated R_o values range from 0.27 – 0.53 (**Figure 40**).

Although thermal maturity through vitrinite reflectance was not measured for this study, Cardott (2012) from organic petrology based on 41 Woodford Shale sample measurements, determined that the mean random R_o value for the study area is 0.54 R_o,

deduced from a range of 0.49% to 2.45% R_o in the Ardmore Basin. Results from both calculated and measured R_o show that the Woodford Shale has low to moderate thermal maturity in the immature to early oil window. This is an indication that Woodford Shale in this area has not entered the oil window threshold. Hence, any gas present was generated in association with oil (**Figure 41**).

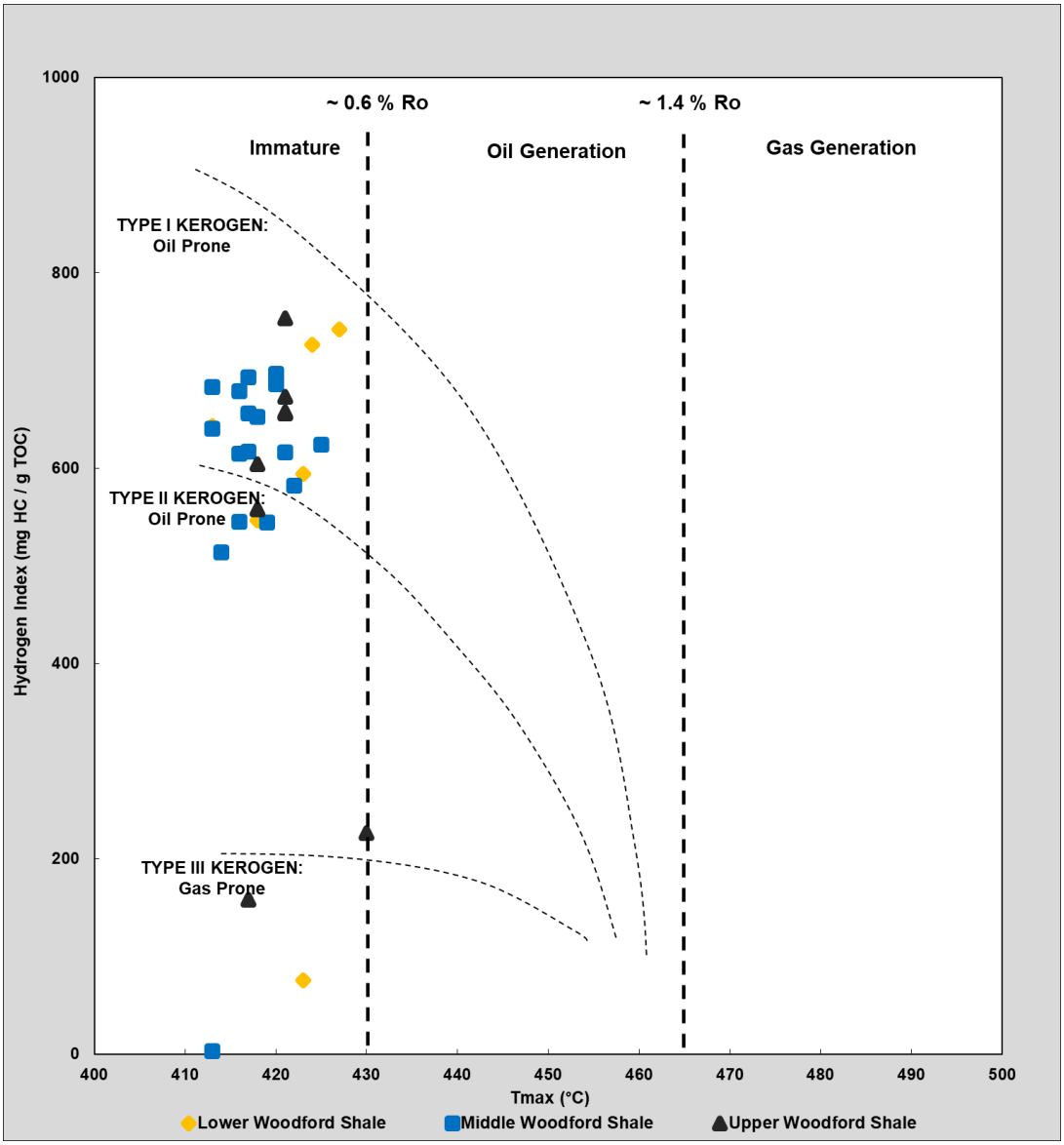

Figure 40. Kerogen type and maturity assessment of the Woodford Shale.

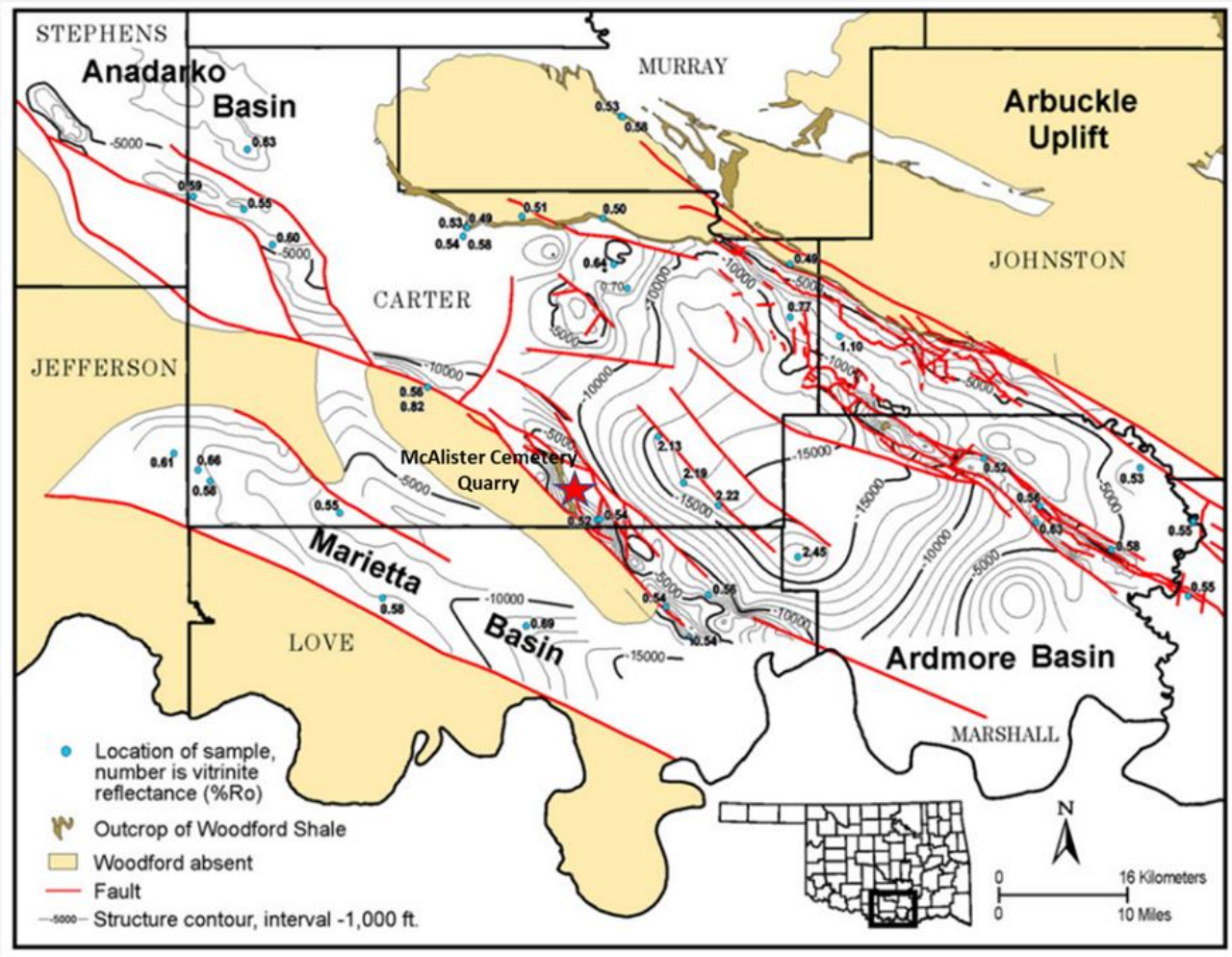

Figure 41. Southern Oklahoma Woodford Shale Vitrine reflectance map (based on 51 locations (Modified from Cardott, 2012). Study area is represented by a red star.

CHAPTER VI

SEQUENCE STRATIGRAPHY

Using lithofacies defined and the criteria from Singh (2008), GR parasequences were defined by "Upward-decreasing"/ "upward-shoaling GR parasequence is characteristic of a gradual fall in sea-level (LST), or late highstand (HST). "Upward-increasing"/ "deepening-upward" GR parasequence represents transgressive deposits during a time of rapid rise in relative sea-level (TST).

The entire Woodford Shale was deposited in 2nd order sea level cycle or as a 2nd order sequence (10-25 Ma) (Slatt et al., 2012), where the Lower and the Middle Woodford Shale were deposited during a TST with identifiable higher order TST and HST cycles, representing a transition into more distal depositional setting (basinward). The transition from TST to HST is capped by an mfs with an associated CS, showing a general increase in GR in association with an increase in organic-rich lithofacies. The Upper Woodford Shale was deposited during an HST showing a relatively cleaner GR in association with a decrease in organic-rich lithofacies, representing deposition in a relatively proximal (landward) depositional setting.

Using interpretation from Slatt et al. (2012), 3rd order regressive-transgressive cycles were identified. Fourteen GR parasequence sets representing fourteen 3rd order regressive-transgressive cycles were interpreted in the entire Woodford Shale section. The Lower Woodford Shale is comprised of five 3rd order cycles. The Middle Woodford Shale is comprised of four 3rd order cycles. The Upper Woodford Shale is comprised of five 3rd order cycles. Generally, the lower and the Middle Woodford shale exhibit thinner regressive cycles/HST packages and thicker transgressive cycles/thicker TST packages,

representing an overall transgression. The Upper Woodford shale exhibits thicker regressive cycles and thin transgressive cycles, representing an overall regression. (**Figure 43**).

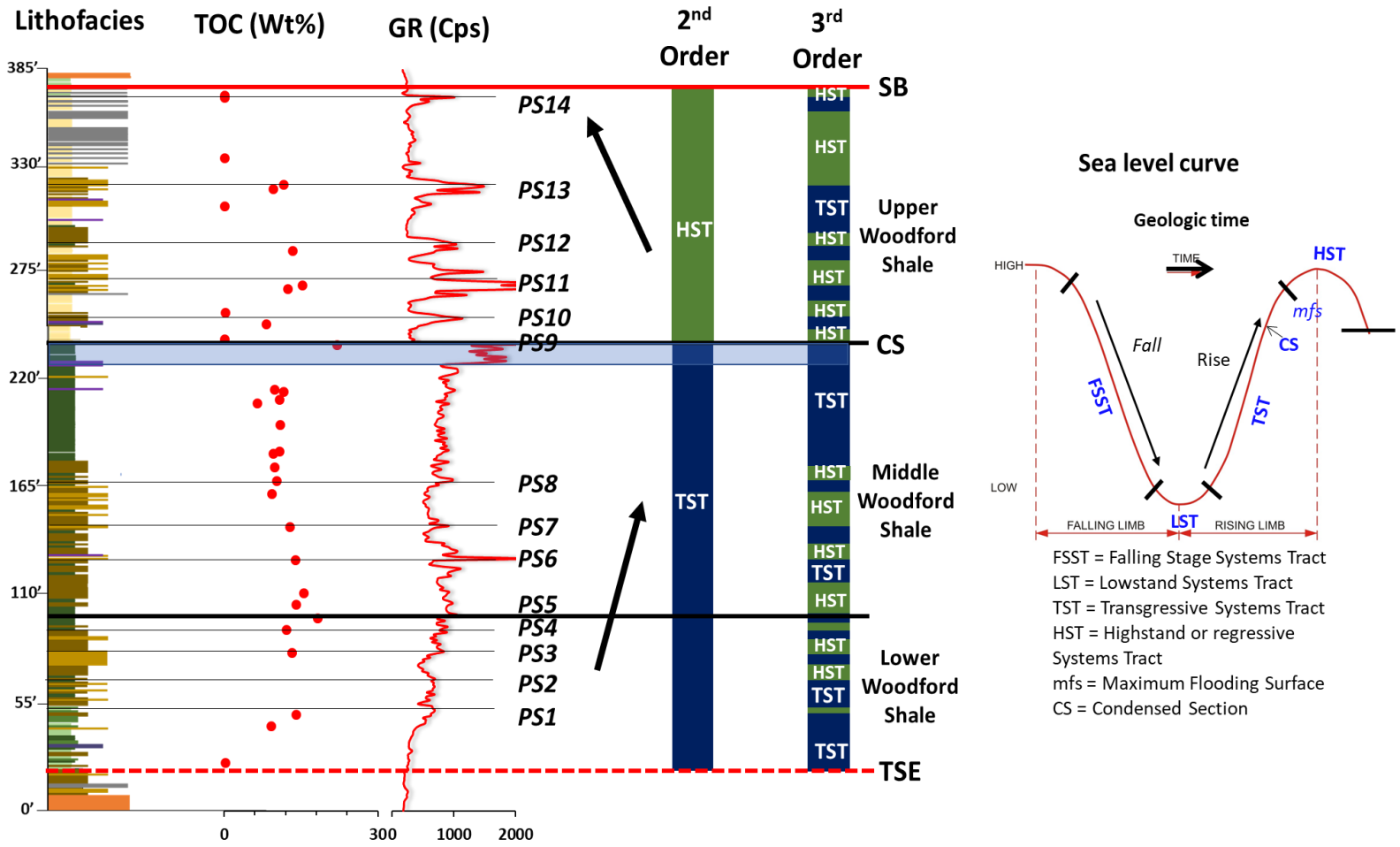

Figure 42. 2nd order cycles, 3rd order cycles, and relative sea level curve defined for the McAlister Cemetery Quarry. TST = Trangressive System Tract, HST = Highstand System Tract, CS = Condensed Section, mfs = maximum flooding surface, SB = sequence boundary, TSE = transgressive surface of erosion.

CHAPTER VII

ELEMNTAL GEOCHEMISTRY

Chemostratigraphy uses major-element and trace-element geochemistry to characterize, subdivide, and correlate strata. The variability in elemental concentrations of sediments can be attributed to source composition, facies, paleoclimate, and diagenesis (Ratcliffe et al., 2007; Hildred et al., 2010). This technique has been used extensively to study several shale plays such as the Niobrara Member of the Mancos Shale (Attar, 2011), the Woodford Shale (Tréanton, 2014; Turner et al., 2015; Turner, 2016), the Haynesville Formation (Sano et al., 2013), and many more. Major elements utilized for interpretation include Aluminum (Al), Potassium (K), Calcium (Ca), Titanium (Ti), Zirconium (Zr), Iron (Fe), Phosphorus (P), Calcium (Ca), Magnesium (Mg), Silicon (Si), and Strontium (Sr). Trace elements utilized are Molybdenum (Mo), Vanadium (V), Nickel (Ni), Copper (Cu), Uranium (U), Cobalt (Co), Chromium (Cr), and Zinc (Zn).

Certain principal elements are used as proxies in developing a chemostratigraphic framework, and for inferring variations in depositional and environmental factors such as sediment source (biogenic vs. detrital), organic paleoproductivity, carbonate productivity, and redox processes. Elements can be divided into three categories of geochemical proxies; detrital proxies, carbonate proxies, and organic and/or redox associations (Vine and Tourtelot, 1970). **Figure 43** summarizes the different mechanisms whereby major and trace elements can be incorporated into the sediments.

7.1. Geochemical Proxies for Detrital, Carbonate, and Phosphate Accumulation

XRD, SEM, and petrographical analysis show significant inputs of detrital materials in the Woodford shale, composed of silty and clay-sized minerals. The silty

fraction is mainly dominated by detrital quartz, and to a lesser degree, k-feldspars, plagioclase, and micas. The clay fraction is mainly composed of kaolinite and illite. Al is commonly utilized as a proxy for fine-grained sediments, because it is a dominant component in aluminosilicate (clay) minerals, and is usually not affected by diagenesis or biological processes (Burmsack, 2006; Tribovillard et al., 2006). To determine which elements are associated with aluminosilicate (clay) content, Pearson's correlation coefficient was used to check the relationship between Al and other elements (See **Table 4**). Zr has a medium association with Al (r = 0.335; Pearson's coefficient), which might suggest that Zr is in the clay fraction, as well as the silt fraction. Ti and K have a strong association with Al, suggesting that Ti and K are mostly in the clay fraction (r = 0.631, 0.705; Pearson's coefficient).

Si can originate from both an extrabasinal (fluvial or eolian derived) or intrabasinal (biogenic opaline quartz). Si is a major component in aluminosilicate (clay) content. The ratio of Si/Al is associated with detrital, and biogenic quartz, putting into consideration its presence in the clay fraction (Sageman, and Lyons, 2004; Tribovillard et al., 2006). A significant increase in Si/Al without an associated increase in Ti or K indicates either a hiatal surface of non-deposition or a planktonic bloom, where longer periods favors a hiatal surface of non-deposition and spike/short episodes indicates a phytoplankton bloom (Turner, 2016)

Ca and Sr are indicators of carbonates (Banner, 2005; Tribovillard et al., 2006). Ca is associated with calcite, and dolomite content. Ca can also be associated with other mineral phases such as clays, feldspars, phosphates, and sulfates. However, observations from the petrographic and XRD analysis indicate that Ca is present mostly in the dolomite

and calcite mineral phases. Sr can substitute for calcium in calcium carbonate mineral structure. Sr is limited in the Upper Woodford shale due to its association with phosphate nodules.

Hence, the lack of correlation observed between Ca and Sr from Pearson's correlation coefficient (r = 0.052; Pearson's coefficient) (**Table 4**). Mg has a medium correlation with Ca (r = 0.309; Pearson's coefficient). As Ca and Mg are present in the dolomite mineral phase. P is indicative of phosphate accumulation (Tribovillard et al., 2006), and may be used as an indicator of upwelling (Turner, 2016) due to its association with upwelling environments. **Table 5** shows the summary for detrital, carbonate, and phosphate indicators with their associated limitation.

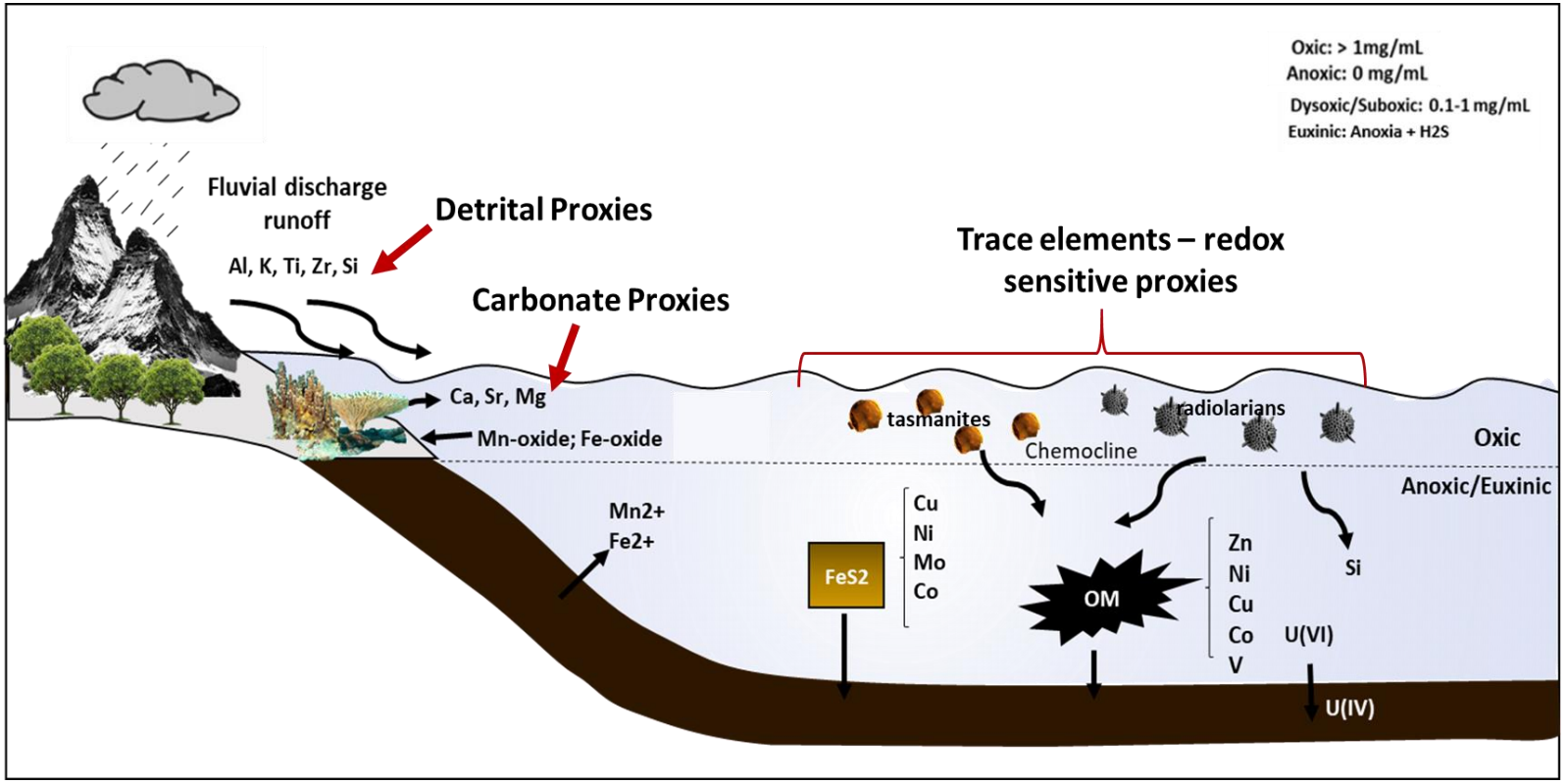

Figure 43. Schematic summarizing the different mechanisms whereby major and trace elements are incorporated into sediments. (Modified from Berryman, 2008: After Cruse, 2010)

Variables	Mg (ppm)	Ca (ppm)	Sr (ppm)	Al (ppm)	K (ppm)	Ti (ppm)	Zr (ppm)	Cr (ppm)	Si (ppm)	Si/Al	P (ppm)	Mo (ppm	V (ppm)	Ni (ppm)	Cu (ppm)	Co (ppm)	Zn (ppm)	S (ppm)	Fe (ppm)	U (ppm)
Mg (ppm)	1	0.349	0.071	0.001	0.000	0.000	0.007	0.144	0.235	0.046	0.000	0.007	0.031	0.004	0.000	0.023	0.009	0.021	0.024	0.011
Ca (ppm)	0.349	1	0.052	0.011	0.003	0.010	0.004	0.306	0.452	0.053	0.004	0.044	0.057	0.008	0.000	0.013	0.039	0.003	0.003	0.002
Sr (ppm)	0.071	0.052	1	0.000	0.000	0.001	0.000	0.052	0.058	0.005	0.007	0.057	0.027	0.004	0.001	0.002	0.065	0.033	0.000	0.000
Al (ppm)	0.001	0.011	0.000	1	0.705	0.631	0.335	0.011	0.020	0.426	0.007	0.031	0.056	0.064	0.010	0.205	0.008	0.181	0.266	0.085
K (ppm)	0.000	0.003	0.000	0.705	1	0.710	0.403	0.007	0.012	0.402	0.002	0.007	0.068	0.017	0.001	0.166	0.003	0.181	0.282	0.058
Ti (ppm)	0.000	0.010	0.001	0.631	0.710	1	0.428	0.002	0.010	0.474	0.006	0.040	0.066	0.032	0.014	0.152	0.012	0.151	0.225	0.058
Zr (ppm)	0.007	0.004	0.000	0.335	0.403	0.428	1	0.000	0.003	0.163	0.004	0.020	0.131	0.000	0.007	0.030	0.007	0.017	0.067	0.006
Cr (ppm)	0.144	0.306	0.052	0.011	0.007	0.002	0.000	1	0.488	0.112	0.002	0.009	0.000	0.051	0.002	0.056	0.072	0.003	0.008	0.015
Si (ppm)	0.235	0.452	0.058	0.020	0.012	0.010	0.003	0.488	1	0.235	0.007	0.001	0.080	0.090	0.001	0.157	0.071	0.014	0.102	0.019
Si/Al	0.046	0.053	0.005	0.426	0.402	0.474	0.163	0.112	0.235	1	0.006	0.036	0.046	0.091	0.017	0.226	0.031	0.165	0.243	0.080
P (ppm)	0.000	0.004	0.007	0.007	0.002	0.006	0.004	0.002	0.007	0.006	1	0.000	0.004	0.000	0.000	0.000	0.000	0.000	0.000	0.001
Mo (ppm)	0.007	0.044	0.057	0.031	0.007	0.040	0.020	0.009	0.001	0.036	0.000	1	0.000	0.121	0.005	0.137	0.003	0.270	0.132	0.132
V (ppm)	0.031	0.057	0.027	0.056	0.068	0.066	0.131	0.000	0.080	0.046	0.004	0.000	1	0.007	0.013	0.079	0.033	0.089	0.108	0.000
Ni (ppm)	0.004	0.008	0.004	0.064	0.017	0.032	0.000	0.051	0.090	0.091	0.000	0.121	0.007	1	0.055	0.670	0.168	0.096	0.271	0.071
Cu (ppm)	0.000	0.000	0.001	0.010	0.001	0.014	0.007	0.002	0.001	0.017	0.000	0.005	0.013	0.055	1	0.022	0.090	0.001	0.003	0.004
Co (ppm)	0.023	0.013	0.002	0.205	0.166	0.152	0.030	0.056	0.157	0.226	0.000	0.137	0.079	0.670	0.022	1	0.130	0.362	0.766	0.125
Zn (ppm)	0.009	0.039	0.065	0.008	0.003	0.012	0.007	0.072	0.071	0.031	0.000	0.003	0.033	0.168	0.090	0.130	1	0.011	0.041	0.000
S (ppm)	0.021	0.003	0.033	0.181	0.181	0.151	0.017	0.003	0.014	0.165	0.000	0.270	0.089	0.096	0.001	0.362	0.011	1	0.519	0.210
Fe (ppm)	0.024	0.003	0.000	0.266	0.282	0.225	0.067	0.008	0.102	0.243	0.000	0.132	0.108	0.271	0.003	0.766	0.041	0.519	1	0.126
U (ppm)	0.011	0.002	0.000	0.085	0.058	0.058	0.006	0.015	0.019	0.080	0.001	0.132	0.000	0.071	0.004	0.125	0.000	0.210	0.126	1

Table 4. Pearson's coefficient correlation for all geochemical proxies. Green highlight represents elements with large correlation. The orange highlight stands for elements with medium correlation. The Red highlights stand for elements with small correlation

Element	Indication	Limitation	References
Titanium (Ti), Zirconium (Zr)	Indicator of continentally derived sediments	Ti is associated with dust fractions	Sageman and Lyons, 2004; Tribovillard et al., 2006
Aluminum (Al), Potassium (K)	Primarily associated with clay minerals.	Could be associated with feldpars	Sageman and Lyons, 2004; Tribovillard et al., 2006
Silicon/Aluminum (Si/Al)	Indicator of detrital, and biogenic quartz.	Dual origin (either detrital, authigenic or biogenic)	Pearce and Jarvis, 1992; Pearce et al, 1999; Tribovillard et al., 2006.
Phosphorus (P)	Phosphate accumulation	Present in phosphate nodules and skeletal vertebrate	Tribovillard et al., 2006
Calcium (Ca)	Indicator of carbonates.	Present in phosphates, feldspars, and sulfates Also present in clay minerals (Sr, Ca, & Mg)	Banner, 2005
Magnesium (Mg)	Indicator of carbonates. Primarily associated with dolomite.	Also present in clay minerals.	
Strontium (Sr)	Indicator of carbonates.	Present in phosphates, feldspars, and sulfates. Also present in clay minerals.	Banner, 1995; Tribovillard et al., 2006.

Table 5. A list of detrital, carbonate and phosphate proxies showing their indicative role and limitation. Modified from Pearce and Jarvis, 1992; Pearce et al, 1999; Banner, 2005; Sageman and Lyons, 2004; Tribovillard et al., 2006.

7.2. Chemostratigraphy and Sequence Stratigraphy

Detrital proxies show a general decline trend up section. The Lower Woodford Shale was deposited on a regional unconformity that formed from the subaerial exposure of the Hunton Limestone. According to this scenario, high sedimentation rates would be expected associated with LST deposits indicating progradation, and this should be identifiable from the elemental geochemistry (Turner, 2016). Instead, we observe retrogradation which implies transgression. The absence of LST deposits suggests an event of sediment bypassed to distal basins or non-deposition. The Lower Woodford Shale shows several high-frequency cycles of increase and a decline in detrital proxies, where the highest detrital influx corresponds to the basal green clayshale and mixed clayshale-mudshale of the Lower Woodford Shale, which marks the onset of transgression (**Figure 44**).

The Middle Woodford shale demonstrates a relatively aggradational increase in the concertation of detrital proxies with associated depletion in Si/Al ratio in the uppermost part. This significant increase in detrital proxies, evident from the dominance of argillaceous mudshales, suggests a transition to a more distal depositional environment relative to the sediment source. This supports the distal depositional environment for the Middle Woodford reported in Cardott (2005) and Slatt et al. (2012) (**Figure 44)**.

Above the mfs preserves a progradational sequence of an HST, which characterizes the Upper Woodford Shale. The Upper Woodford Shale shows a decline in detrital proxies, as it is mainly dominated by bedded cherts and siliceous mudshales/mudstones. Spikes in the Si/Al ratio throughout the section is related to non-riverine inputs of Si due to biogenic processes (planktonic bloom), along with periods of

low sedimentation. This elevated Si/Al ratio is associated with the appearance of biogenic quartz-rich lithofacies. Petrographic and SEM analysis indicate the presence of recrystallized radiolarians and sponge spicules, as well as diagenetic infill of *tasmanites* which dominates mostly the matrix of the Upper Woodford shale bedded cherts and siliceous mudstones. It is important to note the likely distortion in the geochemical signals by the bleaching effect in the Upper Woodford shale. For example, the bleaching effect underestimates the Si/Al ratio in most parts of the Upper Woodford shale (**Figure 44)**.

Relative to the Lower and Middle Woodford Shale, the Upper Woodford is depleted in detrital elements and enriched in Si/Al (biogenic quartz). This is a significant observation because the Upper Woodford Shale we interpret as a 2nd order HST deposit. Therefore, it would be expected that more detrital sediments would have been deposited into the basin. If this scenario is true, then the detrital influence should be identifiable in the Upper Woodford Shale. Ruppel (2016) has attributed this observation to facies/systems tract offset (from proximal to distal). Typically, marine mudrocks are at the tail of the slug model, and they often do not carry the signatures of the activities that occur on the platform. Hence, parasequences will be better identified in proximal than distal settings. These distal facies are dominated by pelagic biogenic sediment. Because the flux of biogenic quartz is not controlled by sea level change or water depth, but rather by nutrient supply and productivity, thus distal facies will likely not be influenced by sediment supply/ changes in sea level occurring in the proximal deposition (**Figure 45**). Furthermore, changes in organic matter (OM) abundances, redox process, fauna, or oxygenation may not necessarily be related to changes in water depth. This explains why the detrital proxies in the Upper Woodford Shale are depleted as opposed to an

enrichment associate with progradation. Instead what we observe are blooms of biogenic productivity that alternate with slower deposition of clay minerals (Ruppel, 2016).

The proxies (Ca, Sr, Mg) associated with carbonate accumulation shows sporadic occurrences throughout the section, where the spikes are associated with dolomitic mudshales and mudstones. Other elevated concentrations observed are associated with the basal clayshale and mixed clayshale-mudshale of the Lower Woodford Shale, which can be explained by increased bioturbation in these lithofacies (Maynard, 2016). Elevated concertation is also observed in the Middle Woodford shale in association with argillaceous mudshales which from the petrographic analysis can be explained by the presence of dolomitic aggregates. The increased Sr in the Upper Woodford Shale is associated with the emergence of phosphatic nodules, and not with dolomitic phase, except where dolomitic mudshales or mudstones occur. The phosphate accumulation proxy, P, is associated with the occurrence of phosphate nodules, and are usually indicative of upwelling conditions. It is important to note that spikes in the P occur only when phosphate nodules are analyzed.

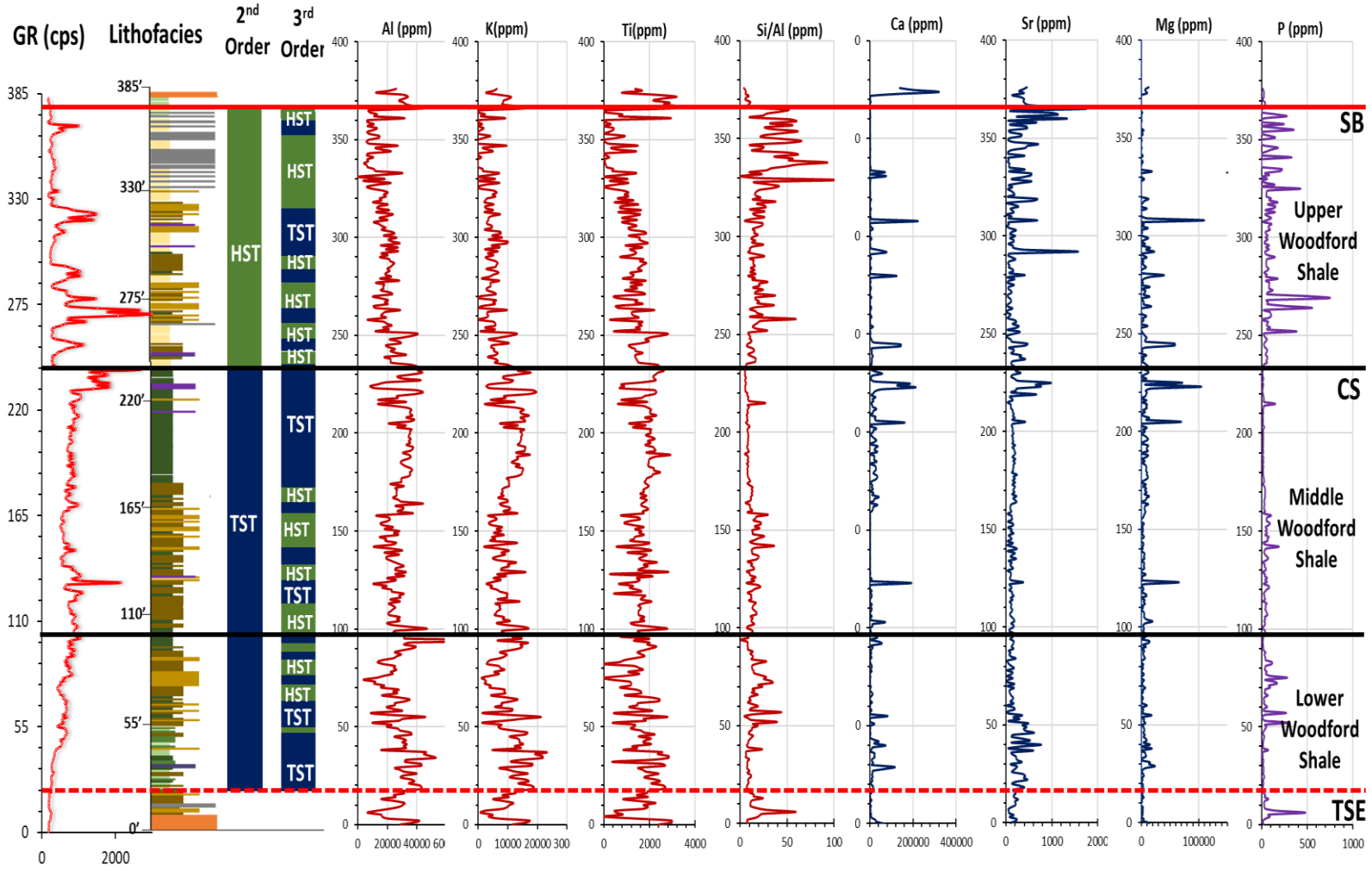

Figure 44. Chemostratigraphic profile of the McAlister Quarry for principle elements (detrital, carbonate, and phosphate). Profile shows Gr profile (cps), and the interpreted sequence-stratigraphic framework (2nd and 3rd order cycles).

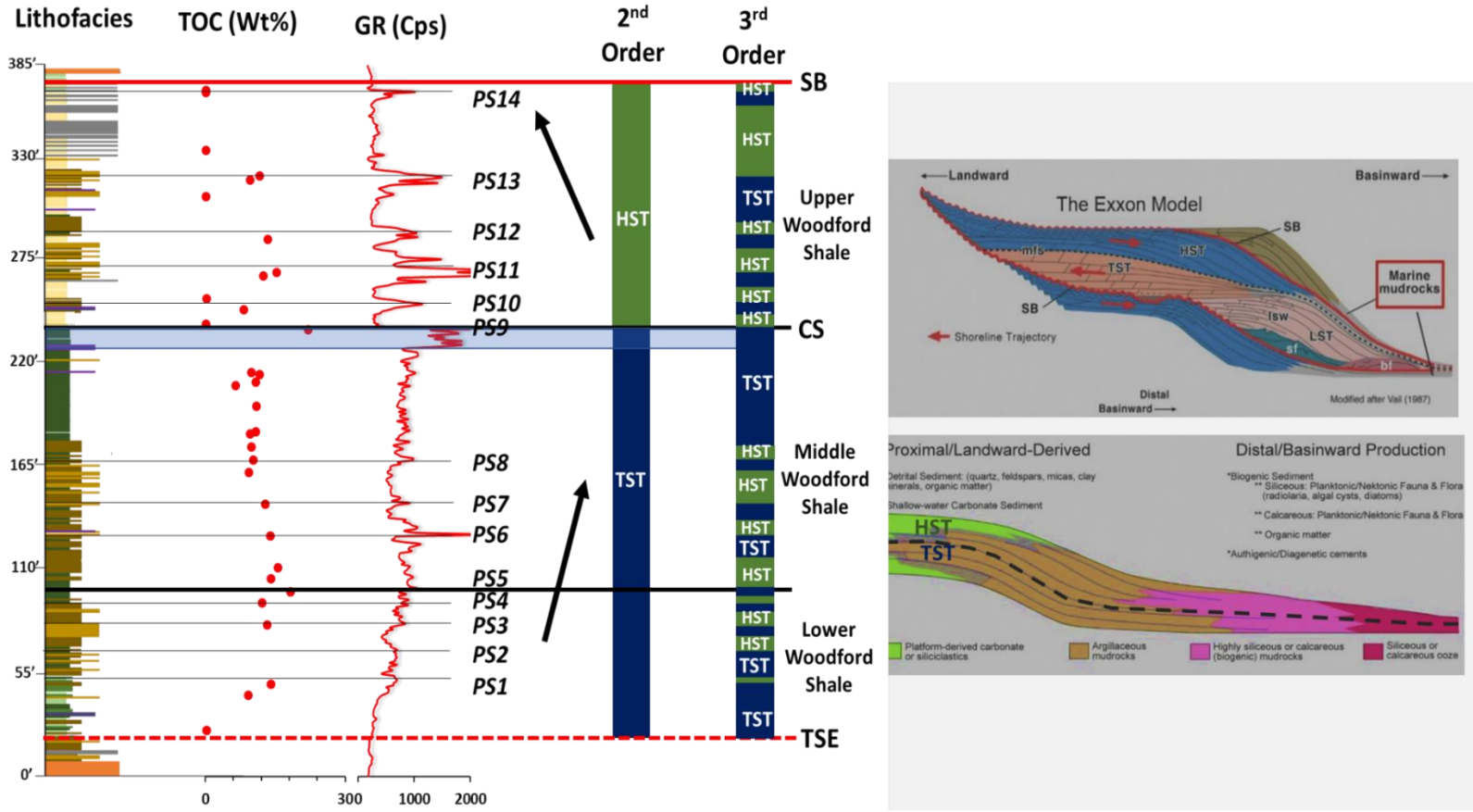

Figure 45. Facies/systems tract offset concept. Shows the lithofacies, GR (cps), and the sequence stratigraphic framework, and its relative position in the slug model from proximal to a distal depositional setting. Modified from Ruppel, 2016. (Exxon Model adapted from Vail, 1987).

7.3. Redox-Sensitive Geochemical Proxies

Certain trace elements in inorganic shales have been used as proxies for delineating paleoredox conditions in a given depositional system (Sageman and Lyons, 2004; Algeo and Lyons, 2006; Algeo and Rowe, 2012; Gilleaudeau and Kah, 2015; Tribovillard, 2016; among others). During oxidative weathering of the continental crust, redox-sensitive trace metals are released and delivered to the oceans by fluvial systems, where they are more soluble under oxidizing conditions, and less soluble under reducing conditions. This results in the sequestration of reduced metals through abiotic processes in oxygen-depleted sediments, making them useful paleoredox proxies (Gilleaudeau and Kah, 2015; Tribovillard, 2016).

Trace elements can be sequestered in sediments along with organic carbon, diagenetic and syngenetic pyrite (both referred to as sedimentary pyrite, henceforth) (Huerta-Diaz and Morse, 1992; Tribovillard et al., 2006; Gregory et al., 2015), clay minerals (Large et al., 2011), and in other cases forming its own sulfide (i.e. CuS, ZnS, etc.). The uptake of trace elements is also possible through biotic processes, where they can serve as minor or micronutrients for phytoplankton (Tribovillard et al., 2006). To conduct paleoenvironmental analysis, it is important to determine which phase the trace element is sequestered, whether in association with organic matter, sedimentary pyrite, sulfidic mineral, and/or detrital flux.

1. Redox-sensitive elements

The precipitation of sedimentary pyrite can occur within the water column under euxinic bottom water conditions or within the pore waters of sediments (Lyons et al., 1997, 2003). Trace elements can be incorporated into pyrite during diagenesis of anoxic

sediments by precipitation or coprecipitation. Some of these redox-sensitive elements (e.g., Cu, Ni, Zn) can be delivered into the sediments in association with organic matter (OM) and retained in the sediments in association with pyrite (Tribovillard et al., 2006).Trace elements (examples refer only to trace elements used for this study) that can get incorporated into pyrite can be grouped as heavy metals (e.g. Cu, Ni, Co), oxyanionic elements (e.g. Mo), elements that occur as Zn-sulfide inclusions (e.g. Zn), and elements that occur as silicates or organic inclusions (e.g. V) (Gregory et al., 2015).

Maslennikov and Bull (2015) from the analysis of sedimentary pyrite in 45 carbonaceous shale and unconsolidated sulfidic sediment samples from Paleoarchean age to present day has shown that Ni, Cu, and Co are part of the group of the most abundant trace elements incorporated into the structure of pyrite. Co, they have shown to be mostly incorporated into the structure of pyrite or as evenly distributed nanoinclusions (Gregory et al., 2015). Tribovillard et al. (2006) raised concerns about using Co as a reliable redox proxy due to strong detrital influence. Observations made from Pearson's correlation coefficient (**Table 4**) shows that Co has a large association with iron (Fe) ($r = 0.66$; Pearson's coefficient), and a medium association with sulfur (S) ($r = 0.362$; Pearson's coefficient). Assuming that Fe and S are in the pyrite phase, this may suggest that Co is also in the pyrite phase. Co shows a small correlation with detrital proxies ($r < 0.205$; Pearson's coefficient), suggesting that Co is weakly tied to the abundance of clastic material.

Ni can also be incorporated into the structure of pyrite or as evenly distributed nanoinclusions. Ni tends to be enriched in most diagenetic pyrite, and is not strongly affected by metamorphism or hydrothermal overprints (Gregory et al., 2015). Ni may be

released from OM decay to pore waters, and under euxinic conditions, it may be incorporated into pyrite (Tribovillard et al., 2006). Pearson's correlation coefficient (**Table 4**) shows Ni and Co, have a large association (r = 0.67; Pearson's coefficient). This suggests that Ni, as Co, is also associated with pyrite.

Cu(II) is reduced to Cu(I) at reducing conditions (euxinic), and is incorporated similarly as Ni and Co at low concentrations, however, at high concentrations, the occurrence of Cu-bearing sulfides is typical (Gregory et al., 2015; Tribovillard et al., 2006). Cu can also be released from OM decay into the pore waters, adsorbed onto particulate Fe-Mn-oxyhydroxides, and/or diagenetically fixed by authigenic nontronite or smectite minerals. Pearson's correlation coefficient (**Table 4**) shows no association of Cu with any elements. This could suggest that Cu was either depleted during deposition or concentrations are below the detection limit. For this reason, Cu might not be a reliable redox proxy for the Woodford Shale section.

Zn can also be released from OM decay into the pore waters, and/or adsorbed onto particulate Fe-Mn-oxyhydroxides. Zn may also be incorporated as sphalerite (ZnS) inclusions in pyrite or, form its own sulfides, sphalerite ([Zn, Fe]S) (Huerta-Diaz and Morse, 1992; Tribovillard et al., 2006). Pearson's correlation coefficient (**Table 4**) shows small association of Zn with Ni and Co (may suggest slight inclusions in pyrite), and no association with other elements. This could suggest that Zn was either depleted in the water column during deposition or concentrations are below the detection limit. For this reason, Zn like Cu might not be a reliable redox proxy for the Woodford Shale section.

Cr is reduced from Cr(IV) to Cr(III) under anoxic conditions, which can be incorporated or adsorbed by Fe-Mn-oxyhydroxides, upon OM mineralization, Cr does

not stay trapped in the sediments in the form of a sulfide because Cr is not readily taken up by Fe-sulfides. Hence, Cr becomes immobile, and can be lost through diffusion to the water column. Cr also has a strong detrital influence as it can be incorporated into clay minerals, and ferromagnesian minerals (Tribovillard et al., 2006). Pearson's correlation coefficient (**Table 4**) shows a moderate correlation with Si and Ca (r = 0.45; r = 0. 306; Pearson's coefficient), and small correlation with Mn and Mg (r = 0.187; r = 0.144; Pearson's coefficient). The preferential incorporation of Cr into silicates and carbonate limits the usefulness of Cr as a redox proxy for the Woodford Shale section.

V is reduced from V(V) to V(IV) under mildly reducing conditions, forming vanadyl ions. V(IV) is removed to the sediments through adsorption unto OM. Under euxinic conditions, V is further reduced to V(II), and can be taken up by geoporphyrins or precipitated as solid oxide V_2O_3 or hydroxide $V(OH)_3$ phase. V may be removed from the pore waters by Fe-Mn-oxyhydroxides, and is not readily incorporated into Fe-sulfides. V (III) can also be incorporated into clay minerals, as it can substitute for Al in the clay mineral structure. Additionally, V can be incorporated into phosphate nodules. In fact, it has been identified in Turner (2016), as well as this work that an enrichment in V in the Upper Woodford coincides with the occurrence of phosphate nodules. For this reason, V might not be a reliable redox proxy, at least not for the Upper Woodford Shale section.

U is reduced from U(VI) to U(IV) in anoxic conditions. The authigenic enrichment of U takes place in the sediments, and not the water column, which may indicate an influence of sedimentation rate and oxygen penetration depth, as slower sedimentation rate allows for efficient diffusion from the water column to the sediments. U usually shows a good correlation with carbon rain rate and with organic carbon content

in anoxic (non-sulfidic) facies (Algeo and Maynard, 2004; Tribovillard et al., 2006). An increase in oxygen penetration depth can cause remobilizing of U within the sediments, thereby causing the migration of the initial U peak to another location (Tribovillard et al., 2006).

ELEMENT	INDICATION	LIMITATION	REFERENCES
Molybdenum (Mo)	Mo is associated with anoxic conditions.	sequestration mechanism.	Sageman and Lyons, 2004; Tribovillard et al., 2006; Algeo and Lyons, 2006; Algeo and Rowe, 2012
Vanadium (V)	Redox-sensitive element Associated with suboxic to anoxic conditions.	Possibly a bionutrient. Can be associated with clay minerals (kaolinite).	Tribovillard et al., 2006; Algeo and Rowe, 2012.
Uranium (U)	Redox-sensitive element	Can be incorporated into phosphates. Can be remobilized Dissolution during intermittent oxic periods.	Tribovillard et al., 2006
Nickel (Ni)	Redox-sensitive element	Behaves as a micronutrient in oxic environments	Tribovillard et al., 2006
Cobalt (Co)	Redox-sensitive element	Detrital influence	Tribovillard et al., 2006
Copper (Cu)	Redox-sensitive element	Behaves partially as a micronutrient in oxic environments.	Calvert and Pedersen, 1993;

		Can be incorporated into clays (smectite minerals).	Tribovillard et al., 2006
Chromium (Cr)	Redox-sensitive element	Detrital influence	Tribovillard et al., 2006
Zinc (Zn)	Redox-sensitive element	Can behave partially as a micronutrient in oxic environments. Can be incorporated into phosphorites.	Tribovillard et al., 2006

Table 6: **Redox-sensitive geochemical proxies** showing their indicative role and limitation. Modified from Calvert and Pedersen, 1993; Sageman and Lyons, 2004; Algeo and Lyons, 2006; Algeo and Rowe, 2012; Tribovillard et al., 2006.

Mo is in the solution as molybdate (MoO_4^{2-}) in oxic conditions. Authigenic Mo is enriched in euxinic conditions in the presence of free hydrogen sulfide (H_2S), where dissolved sulfides convert molybdate (MoO_4^{2-}) to thiomolybdates. Mo is scavenged by organic detritus into the sediments and may be enhanced by metal-oxyhydroxide (MnOOH, FeOOH) particulate shuttles in the water column (Tribovillard et al., 2006; Algeo and Tribovillard, 2009; Tribovillard et al., 2012). Mo has been used in analyzing the degree of water mass restriction in anoxic marine environments and has been demonstrated by Algeo and Lyons (2006), Algeo and Rowe (2012), Tribovillard et al. (2012). **Table 6** shows a summary of the trace elements, their indicative roles, and possible limitations.

Table 6 shows the Pearson's coefficient correlation for redox-sensitive elements versus TOC. TOC values from Serna-Bernal (2013) were excluded to have a better control on the data. Strong correlations are observed between TOC and the elements Mo

and Co. Medium correlation between TOC and the elements Ni, Fe, and S, and small correlation with the other elements.

Yu et al. (2015) in their analysis has shown the close relationship between TOC and pyrite in deep water reducing depositional environments. In strong reducing environments, Fe^{3+} is reduced to Fe^{2+}. Hydrogen sulfide (H_2S) produced from the reduction of sulfate during the decomposition of organic matter by sulfur reducing bacteria, reacts with Fe^{2+} to form pyrite that eventually gets incorporated into the sediments. Organic matter is a factor that controls the formation of pyrite, and the relationship between organic carbon and sulfur in the pyrite is good (Berner, 1985; Yu et al., 2015). This may explain the medium association between TOC, and the elements Fe and S (if we assume that they are both in the pyrite phase), as well as elements associated with pyrite (Co and Ni).

Figure 46 shows the geochemical profile for the redox-sensitive elements. A marked increase is observed at ~48ft. This represents the onset of anoxia/euxinia, and also coincides with an increase of GR and TOC. **Figure 46** confirms observations deduced from **Table 4** and **Table 7**. Ni and Co are medium to largely associated with Fe and S (assuming incorporation into pyrite), evident from the similar profile trend. The highest concentration of Ni, Co, Fe, and S is observed in the uppermost part of the Middle Woodford Shale, with depletion occurring in the uppermost Upper Woodford Shale. Iron appears to be the limiting agent of pyrite formation in the Upper Woodford Shale. Zn at least in the Upper and some parts of the Lower Woodford Shale is associated with pyrite forming elements (Ni, Co, Fe, S), suggesting incorporation as ZnS, or forming its own sulfides (i.e., sphalerite).

Zn, as well as Cu, is depleted mostly in the Middle Woodford Shale. As suggested previously, Zn and Cu may be below detection limits, at least in the Middle Woodford Shale part of the section. Cr has no association with any of the other trace elements as previously mentioned. Mo and TOC have a similar trend, confirming the strong association seen in **Table 7**. U and TOC show no correlation. A good correlation may be inhibited by the presence of phosphate, by a high carbonate, by loss during intermittent oxic periods, and by diagenetic remobilization (Luening and Kolonic, 2003; Tribovillard et al., 2006). Vanadium is most enriched in the Upper Woodford Shale, coinciding with the onset of the presence of phosphate nodules.

Variables	Cr (ppm)	Mo (ppm)	V (ppm)	Ni (ppm)	Cu (ppm)	Co (ppm)	Zn (ppm)	S (ppm)	Fe (ppm)	U (ppm)	TOC
Cr (ppm)	1	0.015	0.000	0.220	0.163	0.125	0.035	0.000	0.028	0.239	0.163
Mo (ppm)	0.015	1	0.072	0.513	0.190	0.448	0.037	0.325	0.368	0.001	0.607
V (ppm)	0.000	0.072	1	0.165	0.089	0.351	0.009	0.169	0.286	0.470	0.108
Ni (ppm)	0.220	0.513	0.165	1	0.532	0.611	0.147	0.153	0.359	0.006	0.376
Cu (ppm)	0.163	0.190	0.089	0.532	1	0.167	0.109	0.002	0.023	0.000	0.182
Co (ppm)	0.125	0.448	0.351	0.611	0.167	1	0.060	0.668	0.896	0.000	0.525
Zn (ppm)	0.035	0.037	0.009	0.147	0.109	0.060	1	0.003	0.027	0.000	0.024
S (ppm)	0.000	0.325	0.169	0.153	0.002	0.668	0.003	1	0.805	0.000	0.358
Fe (ppm)	0.028	0.368	0.286	0.359	0.023	0.896	0.027	0.805	1	0.000	0.420
U (ppm)	0.239	0.001	0.470	0.006	0.000	0.000	0.000	0.000	0.000	1	0.039
TOC	0.163	0.607	0.108	0.376	0.182	0.525	0.024	0.358	0.420	0.039	1

Table 7. Pearson's correlation coefficient for TOC and redox-sensitive elements. Green highlight represents elements with large correlation. The orange highlight stands for elements with medium correlation. The Red highlights stand for elements with small correlation. TOC values from Serna-Bernal (2013) were excluded from this analysis.

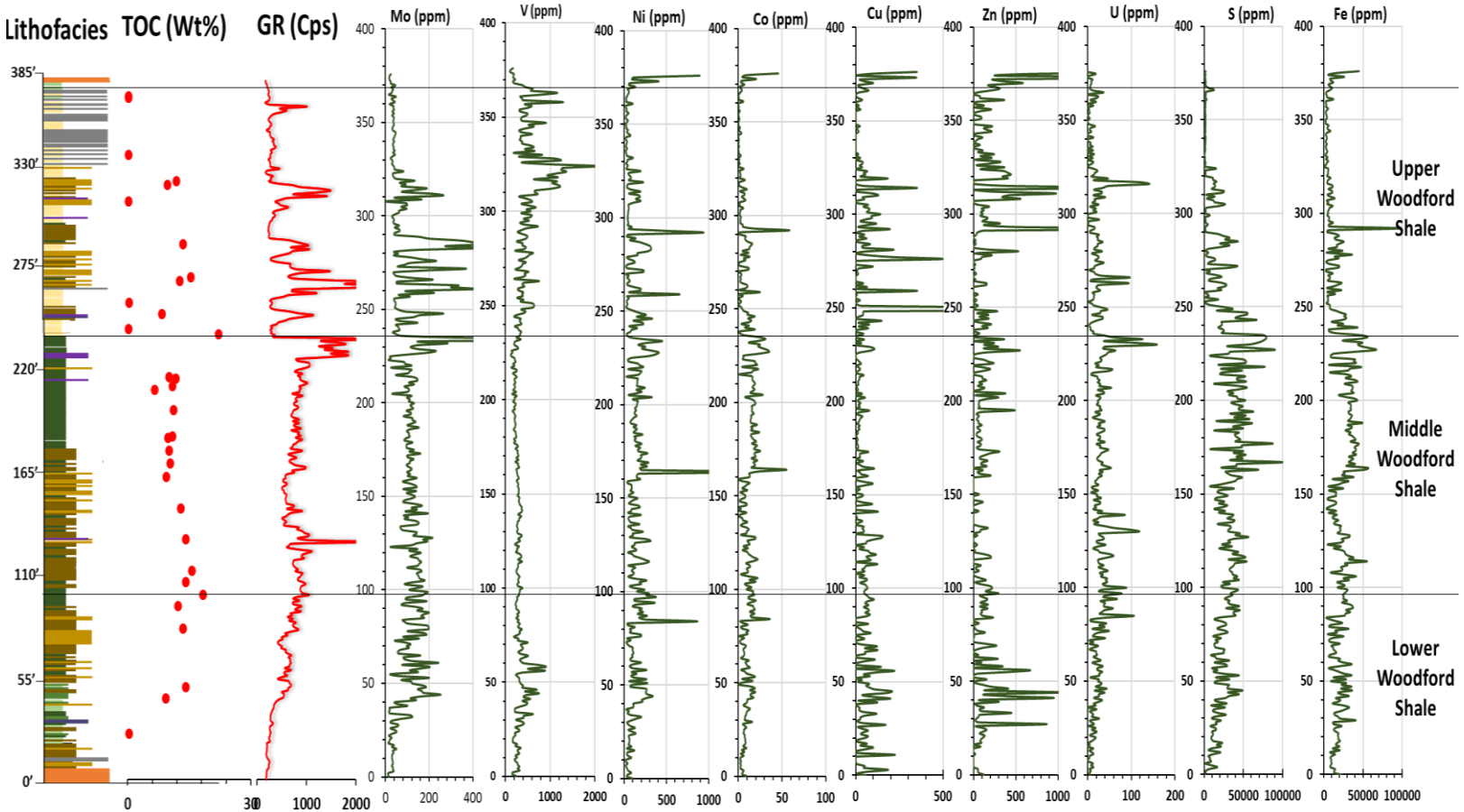

Figure 46. Lithofacies, GR (cps), TOC (wt%), and stratigraphic distribution of redox-sensitive elements. The onset of anoxia/euxinia is observed at ~48ft, which also coincides with an increase of GR and TOC.

7.4. Redox-Sensitive Geochemical Proxies and their Application to Paleoenvironmental Reconstruction

Redox-sensitive elements, and/or sulfide-forming elements are used for analyzing paleoenvironmental conditions: bottom water redox conditions, the process of metal-oxyhydroxide particulate shuttles in the water column and the degree of water mass restriction. The analysis of paleoenvironmental conditions was used to confirm the current interpretations of redox conditions of the Woodford Shale, and also provides new insights on the process of particulate shuttle in the water column, and water mass restriction. Analysis adapted followed the works developed by Algeo and Tribovillard (2009) and Tribovillard et al. (2012). Their ideas are extended to the analysis of the paleoenvironmental conditions to the Woodford Shale.

1. Previous Interpretations of Bottom Water Redox Conditions of the Woodford Shale Informal Members

Using the presence of aryl isoprenoids, Miceli-Romero and Philp (2012) determined that the Lower and Upper Woodford Shale members were deposited under dysoxic to suboxic conditions and episodic periods of photic zone euxinia (PZE) whereas the middle member was deposited under anoxic conditions and persistent PZE. Connock (2015), proposed that the Lower Woodford shale was deposited in anoxic waters, with intermittently stratified isolated periods of photic zone euxinia observed from elevated concentrations of C_{40} aromatic carotenoids. Relative to the lower member, he proposed that the upper member may have experienced minimal H_2S invasion rather than episodic as Miceli-Romero and Philp (2012) suggested. Turner (2016) and Jones (2017) in their

interpretations of the Upper Woodford Shale demonstrated sporadic horizons of anoxia and marine restriction, within generally well-circulated bottom water conditions.

2. Using Ni/Co Geochemical Index to Interpret Bottom Water Redox Conditions

In Jones and Manning (1994), Ni/Co geochemical index can be used an indicator of bottom water redox conditions. It was proposed that mudstones deposited during oxic conditions the Ni/Co ratio is usually <5, with 5-7 depicting dysoxic water column, and > 7 values for suboxic to anoxic conditions.

Figure 47 shows that the Lower Woodford Shale was deposited in mostly suboxic to anoxic conditions, agreeing with interpretations from Connock (2015). Episodes of oxic–dysoxic conditions, especially within the basal green clayshales and mixed clayshale-mudshale samples. The Middle Woodford Shale is mostly suboxic to anoxic. However, Miceli-Romero and Philp (2012) and Connock (2015) have shown that the Middle Woodford Shale is more anoxic (euxinic) than suboxic conditions. Additionally, few samples show oxic to dysoxic conditions. For the Upper Woodford Shale, all bleached lithofacies were not included. Samples are mostly suboxic to anoxic (mostly siliceous mudshales and mudstones). Pure chert samples towards the top of the section plot within oxic conditions. This confirms the interpretation of Turner (2016) and Jones (2017) for the Upper Woodford where sporadic horizons of anoxia and marine restriction, within generally well-circulated bottom water conditions have been identified.

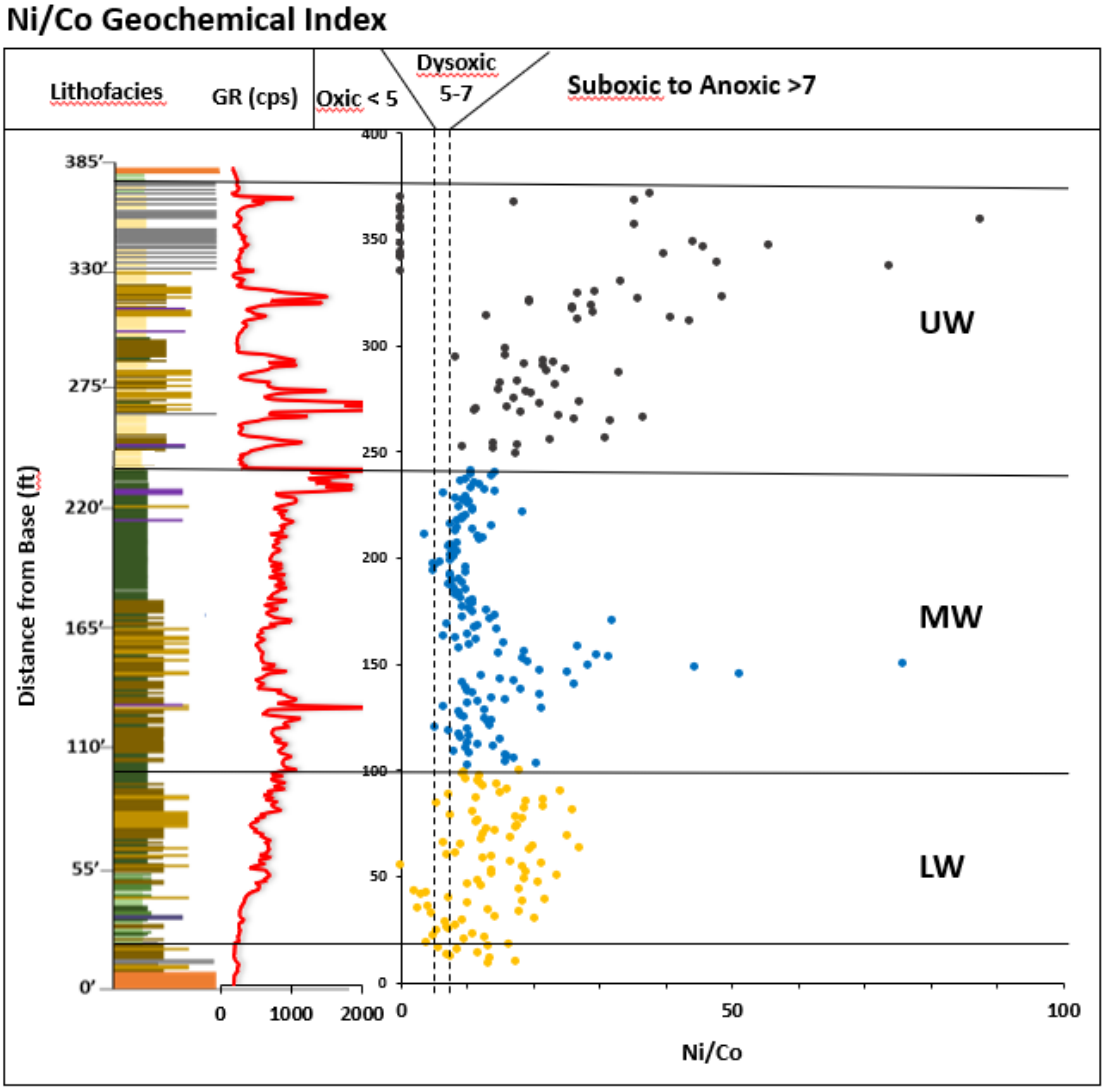

Figure 47. Stratigraphic distribution of Ni/Co geochemical index. The lowermost Lower Woodford Shale was deposited in mostly oxic to dysoxic conditions. The uppermost Lower Woodford Shale was deposited in mostly suboxic to anoxic conditions with episodes of dysoxia. The Middle Woodford Shale was deposited in mostly suboxic to anoxic conditions with episodes of dysoxic conditions. The lowermost Upper Woodford shale was deposited in mostly suboxic to anoxic conditions. The uppermost Upper Woodford was deposited in mostly oxic conditions.

3. Application of U-Mo Covariation to Bottom Water Redox Conditions and Metal-Oxyhydroxide Particulate Shuttle Process

The application of U-Mo covariation provides more information regarding bottom water redox conditions and seeks to distinguish between suboxic and anoxic (euxinic) conditions.

Molybdenum and uranium enrichment factors

Enrichment factors (EFs) have been used for several studies to compare respective enrichments of trace elements in shales (Tribovillard et al., 2006; Algeo and Tribovillard, 2009; Tribovillard et al., 2012; and others). The enrichment factor, X_{EF} is defined by $[(X/Al)_{sample}/(X/Al)_{PAAS}]$, where X and Al represent the weight concentrations of a trace element and aluminum, respectively. To compare authigenic Mo and U, Algeo and Tribovillard (2009) normalized all samples using PAAS (post-Archean average shale compositions of Taylor and McLennan (1985). Algeo and Tribovillard (2009) have pointed out the usefulness of enrichment factors for rapid assessment of the authigenic enrichments of Mo and U, despite the potential pitfalls of the normalization by Al.

U-Mo covariation

The trace elements, U and Mo, are used as paleoenvironmental proxies due to their differential geochemical behavior: (1) authigenic U is taken up by marine sediments at the Fe (II) – Fe (III) redox boundary (i.e., suboxic conditions), authigenic Mo is enriched in euxinic conditions in the presence of free hydrogen sulfide (H_2S), and (2) the transfer of aqueous Mo to the sediments may be enhanced by metal-oxyhydroxide (MnOOH, FeOOH) particulate shuttles in the water column, U is not affected by this

process (Algeo and Tribovillard, 2009; Tribovillard et al., 2012). For example, particulate Mn-oxides can play a role as a shuttle that transports molybdate oxyanions through the water column. These particles are reductively dissolved, releasing the anions that either diffuse back to the water column or are retained in the sediments through other processes.

Algeo and Tribovillard (2009) and Tribovillard et al. (2012) in their papers used the differences in geochemical behavior of U and Mo to show how the covariation of U and Mo can provide information about redox conditions during deposition. Using different modern marine settings (eastern tropical Pacific, Cariaco Basin, and the Black Sea), three patterns of U-Mo covariation were identified. The eastern tropical Pacific sediments, exhibited a greater relative authigenic U, where Mo: U ratios are ~ 0.1 to 0.3 x SW at low EFs, indicating suboxic conditions. Another trend with greater relative authigenic Mo, where Mo: U ratios are ~ 1 x SW at high EFs, indicating a shift from suboxic to weakly anoxic conditions. In the sediments of the Cariaco basin, the U-Mo covariation shows a distinct trend, where there is a strong enrichment in Mo relative to U at all EFs. This has been indicated to represent the process of metal-oxyhydroxide particulate shuttle that aids the transport of aqueous Mo to the sediment. Mo: U ratios are 3 to 10 x SW. The third pattern represents that of the Black Sea, where decreasing Mo: U ratios follows increasing EFs (**Figure 48A**).

Interpretations from U-Mo covariation

In **Figure 48B**, a majority of the data plots in the restricted marine region. The Lower Woodford Shale shows a widespread relative to the middle and upper members. The Lower Woodford Shale falls in the range from suboxic to strongly anoxic (euxinic) conditions, dominating the zones of weakly anoxic to strongly anoxic (euxinic)

conditions. Additionally, few samples (all plot off scale) show minor enrichments in U and Mo (i.e., U EFs < 1), which might be indicative of episodes of oxidizing conditions. These episodes of oxidizing conditions are better demonstrated in the Ni/Co plots (**Figure 47**), where episodes of oxic to dysoxic conditions are observed in the lowermost Lower Woodford Shale. Interpretations for the Lower Woodford Shale confirms the interpretation from Connock (2015) that suggests that the Lower Woodford Shale was deposited in mostly anoxic conditions, with intermittently stratified isolated periods of PZE. However, U-Mo covariation has identified episodes of oxic to suboxic conditions typical of the lowermost Lower Woodford Shale (mostly the green clay shales and mixed clayshale – mudshale lithofacies). Also observed is the particulate shuttle effect, which indicates transport of Mo through the water column by metal-oxyhydroxides.

The Middle Woodford Shale has less spread, and ranges from weakly anoxic to predominantly strongly anoxic (euxinic) conditions, showing maximum authigenic U and Mo enrichments. Few samples show episodes of suboxic conditions. This confirms the interpretations of the Middle Woodford Shale from Romero and Philp (2012) and Connock (2015), who suggests that the Middle Woodford Shale was deposited under anoxic conditions, with persistent PZE. No shuttle effect is observed in the samples of the Middle Woodford Shale, which suggests that the transport of Mo was not aided by particulate metal-oxyhydroxides during the deposition of the Middle Woodford Shale.

The distribution in the U-Mo chart for the Upper Woodford Shale is not entirely representative of this part of the section, as all bleached facies were excluded due to alterations that might obscure interpretations. Thirteen samples (uppermost clean chert of the Upper Woodford Shale) show minor enrichments in U and Mo (i.e., U EFs < 1), which

might be indicative of episodes of oxidizing conditions/ well circulated bottom water conditions (data points plot off scale). The data points represented for the Upper Woodford Shale are composed mostly of the mudshale and mudstone lithofacies and were deposited in predominantly weakly anoxic to strongly anoxic (euxinic) conditions. This confirms the interpretations of Tuner (2016) and Jones (2017), which indicates that though the Upper Woodford Shale was deposited generally in a well-circulated marine condition, especially the uppermost Upper Woodford Shale (dominated by pure cherts), sporadic high levels of marine restriction are also observed (also confirmed in the Ni/Co plot, **Figure 48**). These high levels of marine restriction observed are correlative to the mudshales and mudstones present in the Upper Woodford Shale. The particulate shuttle effect that affects Mo, is observed in a few samples.

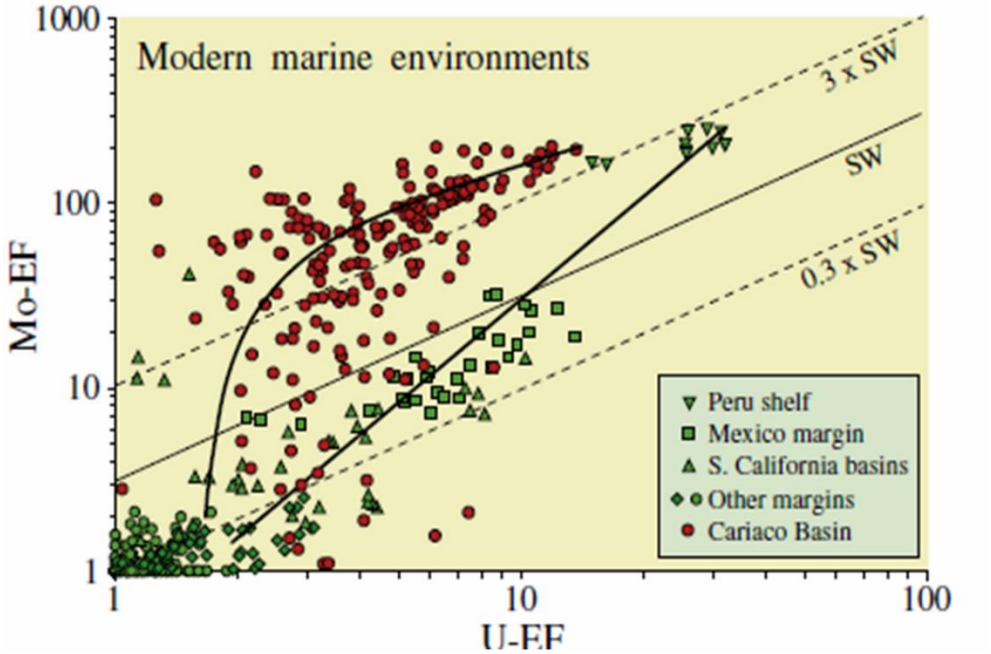

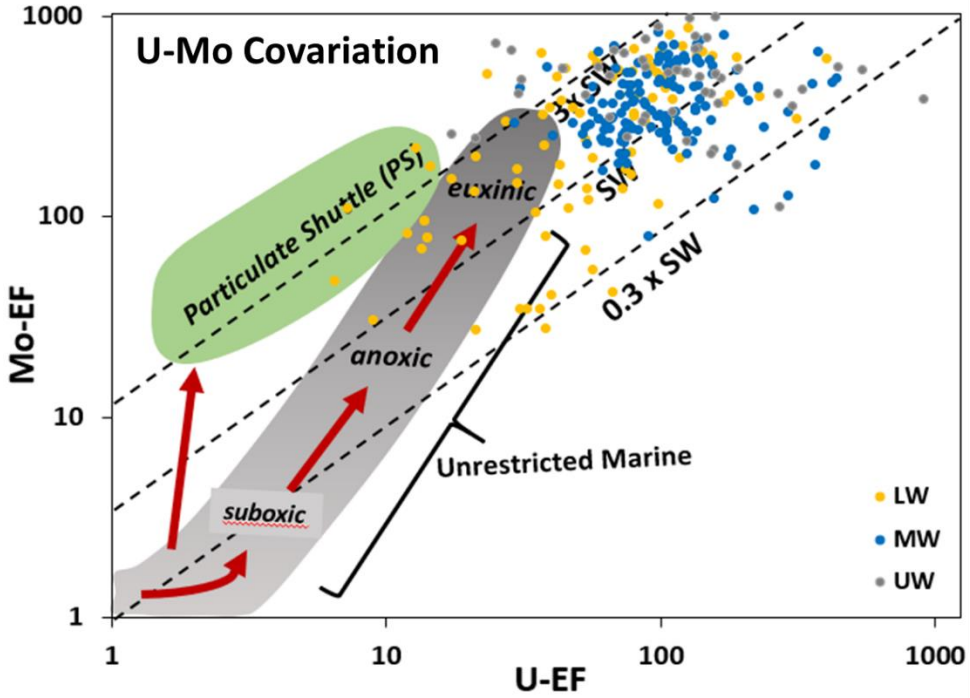

Figure 48 A-B. A. U-EF vs. Mo-EF for modern marine environments. Green symbols represent samples form unrestricted marine facies of the eastern tropical Pacific. Red symbols represent samples from the restricted Cariaco Basin. The solid line represents the trend or patterns for the restricted and unrestricted depositional environments. The eastern tropical Pacific sediments show a trend with a greater relative authigenic U, where Mo: U ratios are ~ 0.1 to 0.3 x SW at low EFs, indicating suboxic conditions. Also, with a greater relative authigenic Mo, where Mo: U ratios are ~ 1 x SW at high EFs, which

indicates a shift from suboxic to weakly anoxic conditions. The Cariaco basin shows a distinct trend, where there is a strong enrichment in Mo relative to U at all EFs. This indicates the process of metal-oxyhydroxide particulate shuttle that aids the transport of aqueous Mo to the sediment. Mo:U ratios for this trend are 3 to 10 x SW. **B.** Shows the general patterns of U–EF vs. Mo–EF covariation in modern marine environments. The gray field represents the general trend of the eastern tropical Pacific, and the green field represents the "particulate shuttle" (PS) trend for the Cariaco Basin. The Lower Woodford plots from suboxic to strongly anoxic (euxinic) conditions, with a few plotting in the particulate shuttle region. Green clay shales and mixed clayshale – mudshale lithofacies of the lowermost Lower Woodford plots off the scale, suggesting the presence of oxidative conditions. The Middle Woodford plots in the weakly anoxic to strongly anoxic (euxinic) conditions. The Upper Woodford Shale is predominantly weakly anoxic to strongly anoxic (euxinic) (all bleached samples were excluded. Pure cherts of the uppermost Upper Woodford Shale plot off scale, suggesting oxidative conditions. (Concept Modified form Tribovillard, 2012. Adapted from Algeo and Tribovillard, 2009).

4. Application of Mo-TOC Covariation to Understanding the Degree of Water Mass Restriction

Mo/TOC ratios in modern marine systems

The use of trace-metal-TOC ratios in understanding the degree of water mass restriction to anoxic marine environments has been demonstrated by Algeo and Lyons (2006), Algeo and Rowe (2012), Tribovillard et al. (2012), and others. More recently, this same idea has been applied to the Woodford Shale in the Arkoma Basin by Turner (2016). These studies have shown the positive relationship between the drawdown of aqueous Mo into the sediments and TOC. Thus, the validity of this positive relationship was confirmed in **Figure 49**, where Mo is observed to have the strongest positive correlation with TOC, in relation to other trace elements.

Algeo and Lyons (2006) analyzed a spectrum of aqueous chemical conditions represented by different modern anoxic silled marine basins such as the Black Sea,

Framvaren Fjord, Cariaco Basin, and the Saanich Inlet. Each basin has different degrees of basin restriction and connection with oceanic circulation patterns, and comparing the Mo-TOC covariation between these modern silled basins to that of the Woodford Shale can aid in making inferences on the depositional conditions of the Woodford Shale.

Interpretations

Mo-TOC cross-plots, with resulting regression lines (representing varying degrees of mass restriction with time) for the lower, middle, and Upper Woodford Shale members shows that the Woodford Shale falls between the Cariaco basin, and the Framvaren Fjord (**Figure 49**), which suggests varying basin restrictions during the deposition of the Woodford Shale. These results are in line with the interpretations of the depositional conditions of the Woodford Shale in the Arkoma Basin in Turner (2016).

The Lower Woodford Shale is the most similar to the degree of mass water restriction to the modern basin, Framvaren Fjord of Norway (**Figure 49**). The Framvaren Fjord is a relatively shallow anoxic basin, allowing organic material to reach the sediments with minimal mineralization. The Framvaren Fjord and the Woodford Shale both represent long-term 2^{nd} order transgressive deposits, superimposed by 3^{rd}–4^{th} order higher frequency regression and transgression. The Framvaren Fjord represents transgressive deposits within an incised valley (similar to the shale in the Arkoma Basin (Turner, 2016)), and the Woodford Shale in the Ardmore Basin represents in fill within the karst features of the underling Hunton Group.

The Framvaren Fjord at the end of the last glaciation period was cut-off from the open sea, forming a meromictic lake, replacing marine organisms with fresh water organisms. In 1850, to once again connect the lake to the open ocean, a channel was

constructed, and as a result, sea water replaced freshwater (Roos, 2001). This event led to a water mass renewal, and marked the onset of anoxia in the basin. In Skei (1983, 1986), Algeo and Lyons (2006), Turner (2016), and others, there is a reference of the results of this 1850 event, which is characterized by the interface that separates laminated black marine muds from underlying bioturbated greenish lake muds (organic poor). From the outcrop characteristics of the Woodford Shale, there is a similarity in depositional cyclicity, where green clayshale (organic poor) and mixed clayshale-mudshale lithofacies (as defined in this study) are typically observed at the base of the Woodford Shale as an indication of the onset of transgression.

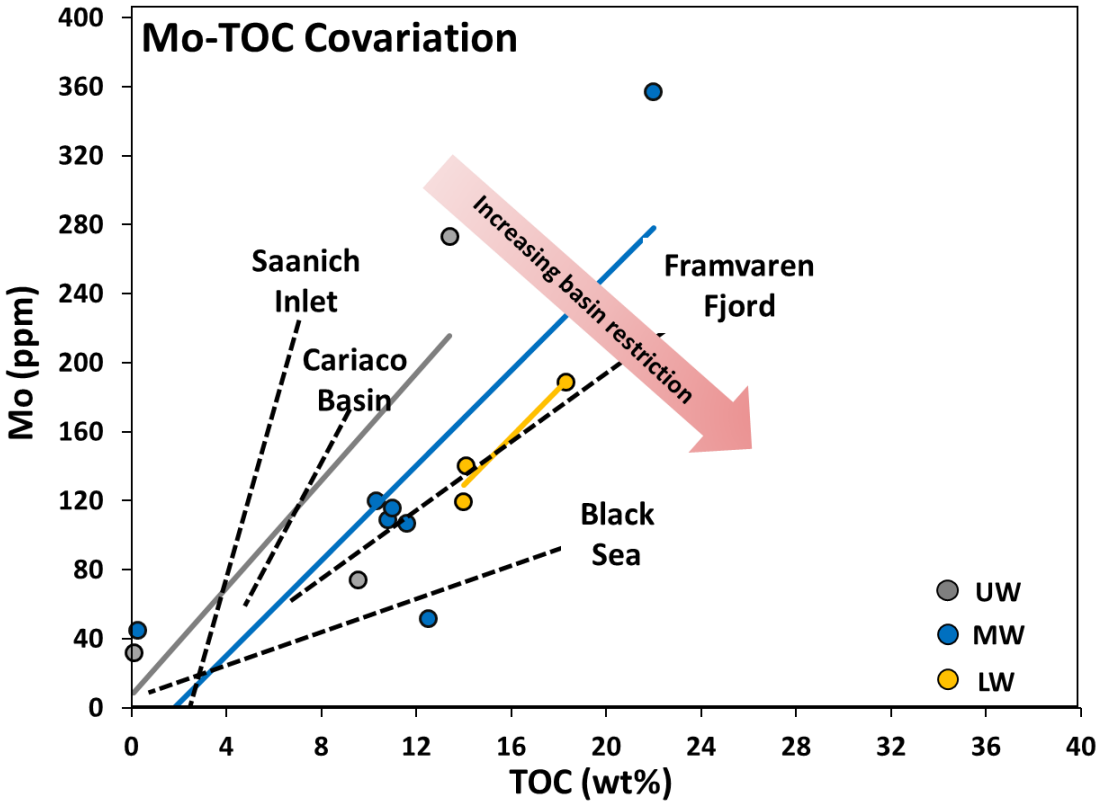

Figure 49. Mo/TOC ratios in modern marine systems. The dashes black lines represent the regressions lines of four modern marine systems: Saanich inlet, Cariaco Basin, Framvaren Fjord, and the Black Sea. Solid lines represent regressions lines for the informal members of the Woodford Shale. Modified from Tinnin and Darmaoen

(2016). Adapted from Algeo and Lyons (2006). An upward increasing circulation is observed, where the Lower Woodford Shale plots closer to the Framvaren Fjord, and the Upper Woodford Shale plots closer to the Cariaco Basin. The Middle Woodford Shale plots in between.

The Middle Woodford Shale is most similar to the degree of mass water restriction to the Cariaco Basin of Venezuela (**Figure 49**). The Cariaco Basin is a small, deep, east-west trending anoxic basin, characterized by two subbasins separated by a central saddle, and isolated from the Caribbean Sea by several shallow sills. The Cariaco Basin is not as restricted as the Framvaren Fjord, and in fact, the nature of the basin allows for both seasonal trade wind-induced upwelling, and recognizable dry and wet seasons (Peterson et al., 1991), yet still preserving periods of bottom water anoxia.

Peterson et al. (1991) recognized the implication of seasonal contrast on the phytoplankton abundance in the Cariaco Basin. It was recognized that during the summer-fall rainy season, run-off periods when coastal upwelling is reduced or absent, water column stability is high, and primary productivity is relatively low, green algae and dinoflagellates tend to dominate over diatoms. In contrast, during the dry season, strong upwelling results in the rise of cold nutrient-rich water to the surface, causing high productivity, with diatoms dominating as primary producers. Although the phytoplankton mentioned above are absent in the Woodford Shale, this idea might shed some light on the general characteristics of the Middle Woodford Shale, at least in this particular stratigraphic section. The Middle Woodford is characterized by siliceous facies (siliceous mudshales and mudstones) at the lowermost part and clay-rich facies (argillaceous mudshales) at the uppermost part. This might be indicative of seasonal contrast recognized by Peterson et al. (1991), where the clay-rich lithofacies are dominated by *tasmanites cysts,* indicating periods of runoff, and the siliceous lithofacies are dominated

by radiolaria, indicating periods of upwelling, perhaps not as intense or strong as observed in the Upper Woodford Shale.

The Upper Woodford shale has a steeper Mo-TOC slope and is also similar to the Cariaco Basin. The Upper Woodford shows slightly weaker water mass restriction than the lower and the middle, which is coincidental with an overall decreasing trace metal enrichment, and TOC (especially within the bedded cherts), although it has been established that the Upper Woodford Shale preserves sporadic periods of marine restriction (especially in the mudstones and mudshales) (Turner, 2016; Jones, 2017; see **Figures 47 and 49**). The invalidity of this approach for determining the water mass restriction for the Upper Woodford Shale was addressed in Turner (2016), where it was proposed that this approach is no longer applicable. It has been suggested that the occurrence of phosphate nodules in the Upper Woodford Shale is as a result of active upwelling during the time of deposition (Miceli-Romero and Philp, 2012; Slatt et al., 2012; Turner et al., 2015; Turner 2016). Algeo and Lyons (2006) emphasized the limitation of this approach to upwelling systems where hydrographic restriction is limited or nonexistent.

7.5 Chemofacies Definition and the Implication on the Stratigraphic Subdivision and Paleodepositional Conditions of the Woodford Shale

Using hierarchical clustering analysis (HCA), chemofacies were defined to highlight geochemical variability within the stratigraphic section. Defining chemofacies might reveal information that was not evident when viewing elemental profiles separately (Nance and Rowe, 2015; Turner et al. 2015; Tuner, 2016). Therefore, defining

chemofacies presents an opportunity to better understand the paleodepositional conditions of the Woodford Shale, and to investigate the ability to go beyond the informal subdivision of the Woodford Shale sequence.

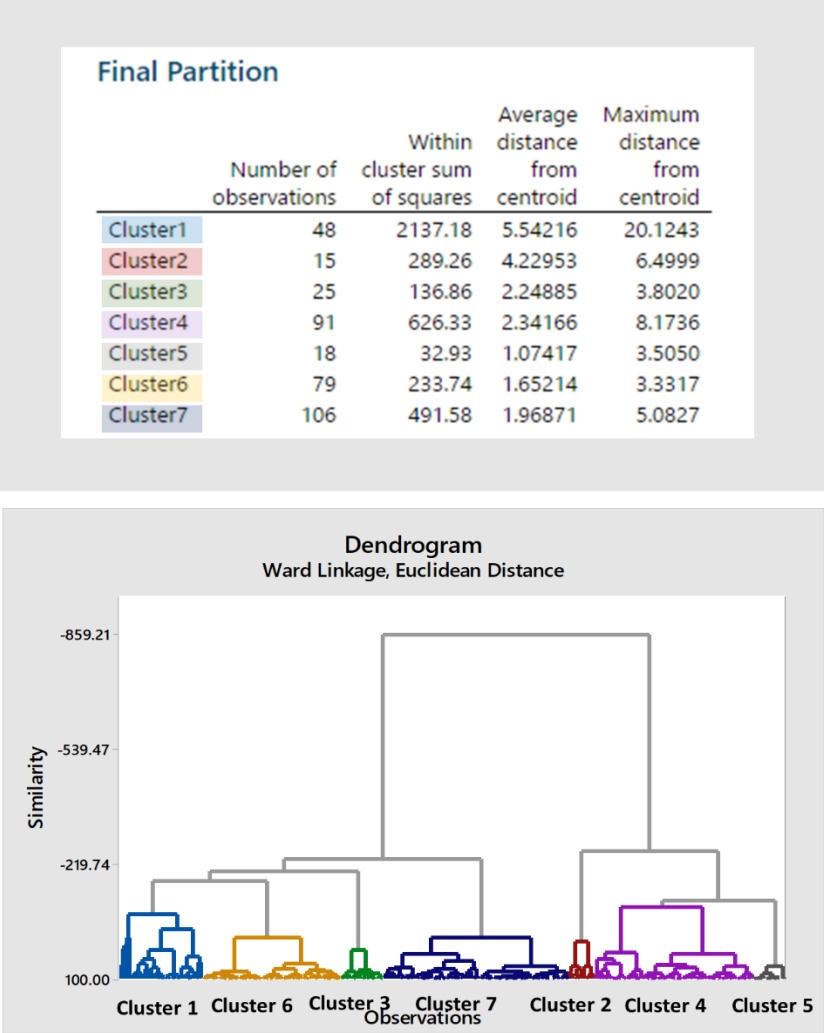

Final Partition

	Number of observations	Within cluster sum of squares	Average distance from centroid	Maximum distance from centroid
Cluster1	48	2137.18	5.54216	20.1243
Cluster2	15	289.26	4.22953	6.4999
Cluster3	25	136.86	2.24885	3.8020
Cluster4	91	626.33	2.34166	8.1736
Cluster5	18	32.93	1.07417	3.5050
Cluster6	79	233.74	1.65214	3.3317
Cluster7	106	491.58	1.96871	5.0827

Figure 50: Final partition and dendrogram from hierarchical clustering analysis (HCA). Final partition provides information about the number of observations within each cluster, within cluster sum of squares, the average distance from the centroid, and distance from the centroid. The vertical axis of the dendrogram represents similarity between clusters, and the horizontal axis represents the objects and clusters.

A total of seven clusters/chemofacies were defined. **Figure 50** shows the final partition which includes information about the number of observation within each cluster,

within cluster sum of squares, the average distance from the centroid, and distance from the centroid. Also shown is the dendrogram which illustrates the similarity between each cluster. Chemofacies 1 defines zones with high redox-sensitive elements (Mo, V, Ni, Cu, Co, Zn, U). Chemofacies 2 defines zones with high carbonate elements (Ca, Sr, Mg). Chemofacies 3 defines zones with very high detrital elements (Al, K, Ti, Zr), high Sr, and low redox-sensitive elements. Chemofacies 4 defines zones with high Si/Al ratio, high V and Sr. Chemofacies 5 defines zones with very high Si/Al ratio, low detrital elements, and low redox sensitive element. Chemofacies 6 defines zones with overall low-redox-sensitive elements. Chemofacies 7 represents zones with high-very high detrital elements (Al, K, Ti, Zr), elements associated with sulfides (Fe, S, Co, Ni), and high Mo and U (**Table 8**).

Chemofacies Defined	
1	High redox-sensitive elements (Mo, V, Ni, Cu, Co, Zn, U)
2	High carbonate elements (Ca, Sr, Mg)
3	Very high detrital elements (Al, K, Ti, Zr), High Sr, low redox-sensitive elements.
4	High Si/Al Ratio, high V and Sr
5	Very high Si/Al ratio, low detrital elements, low redox sensitive elements
6	Low redox-sensitive elements
7	Very high-high detrital elements (Al, K, Ti, Zr) & elements associated with sulfides (Fe, S, Co, NI), high Mo and U

Table 8. Chemofacies defined for the Woodford Shale section.

Based on chemofacies trends observed, the Woodford Shale was subdivided into six geochemical units; Woodford Shale A, B, C, D, E, and F. These subdivisions were defined irrespective of the already defined informal members of the Woodford Shale. The Lower Woodford Shale includes Woodford Shale A and B units. The Middle Woodford consists of parts of Woodford Shale C and D units. The Upper Woodford Shale consists of the Woodford E and F units.

Woodford Shale A unit is dominated by chemofacies 3 and 6, with minor occurrences chemofacies 4. Woodford Shale B unit is dominated by chemofacies 4, 6, and 7, with minor occurrences of chemofacies 1. Woodford C unit is dominated by chemofacies 6 and 7, with minor occurrences of chemofacies 4. Woodford D unit is dominated by chemofacies 7 with minor occurrences of chemofacies 1 and 2. Woodford E unit is predominantly by chemofacies 1 and 4, with minor occurrences chemofacies 6. Woodford F unit is predominantly by chemofacies 4 and 5. From this subdivision, inferences on the paleodepositional conditions of the Woodford Shale were made.

Woodford Shale A unit represents deposition in dominating well-oxygenated conditions. Low trace element concentrations (dominated by chemofacies 3 & 6) suggest a well-oxygenated water column, deposition above the chemocline. Lithofacies (green clayshales), marked by low GR and TOC were deposited during the early transgressive phase of the Woodford Shale deposition, pre-initiation of anoxia. The mixture of terrestrial and autochthonous marine organic fractions, observed from kerogen type suggests a nearshore environment, an interplay between the nearshore sedimentary processes and open shelf sedimentation (**Figure 51**).

The boundary between A and B marks the onset of anoxia (euxinia). Chemofacies 7 is characterized by enrichment in sulfide forming elements, and thus represents periods of euxinic conditions. The lowermost Woodford Shale B unit is dominated by chemofacies 7, and transitions into an uppermost part dominated by chemofacies 4 and 6. Woodford Shale B unit is dominated by siliceous mudshale lithofacies and averages the highest TOC (**Figure 51**).

The fluctuations observed in Woodford Shale C units, characterized by chemofacies 7, represents periodic occurrences of euxinia. Lithologically, siliceous mudshale dominated this unit, averaging the second highest TOC (**Figure 51**).

Woodford Shale D unit is dominated by chemofacies 7, which suggests deposition in mostly sulfidic conditions (persistent euxinia). Lithofacies are dominantly clay-rich (argillaceous mudshales) in relation to other units, suggesting deposition in a distal setting relative to sediment source. Average TOC is 11.3 wt%, lower than Woodford Shale unit B and C due to dilution from detrital materials (**Figure 51**).

Woodford Shale E unit is dominated by chemofacies 1 and 4. Anoxic (euxinic?) zones are recognized, but not as episodic as in the Woodford Shale B or C unit, suggesting minimal invasion of the photic zone. Thus, a deposition during the cessation of H_2S as circulation increased. These anoxic zones correspond to the high TOC values observed in the Upper Woodford Shale. Woodford Shale E is dominated by siliceous mudstone lithofacies with an average TOC of 7.8 wt% (**Figure 51**).

Woodford Shale F unit is dominated by chemofacies 4 and 5, characterized by pure chert lithofacies, with an average TOC of 0.1wt%. This suggests deposition in an open marine setting. (**Figure 51**).

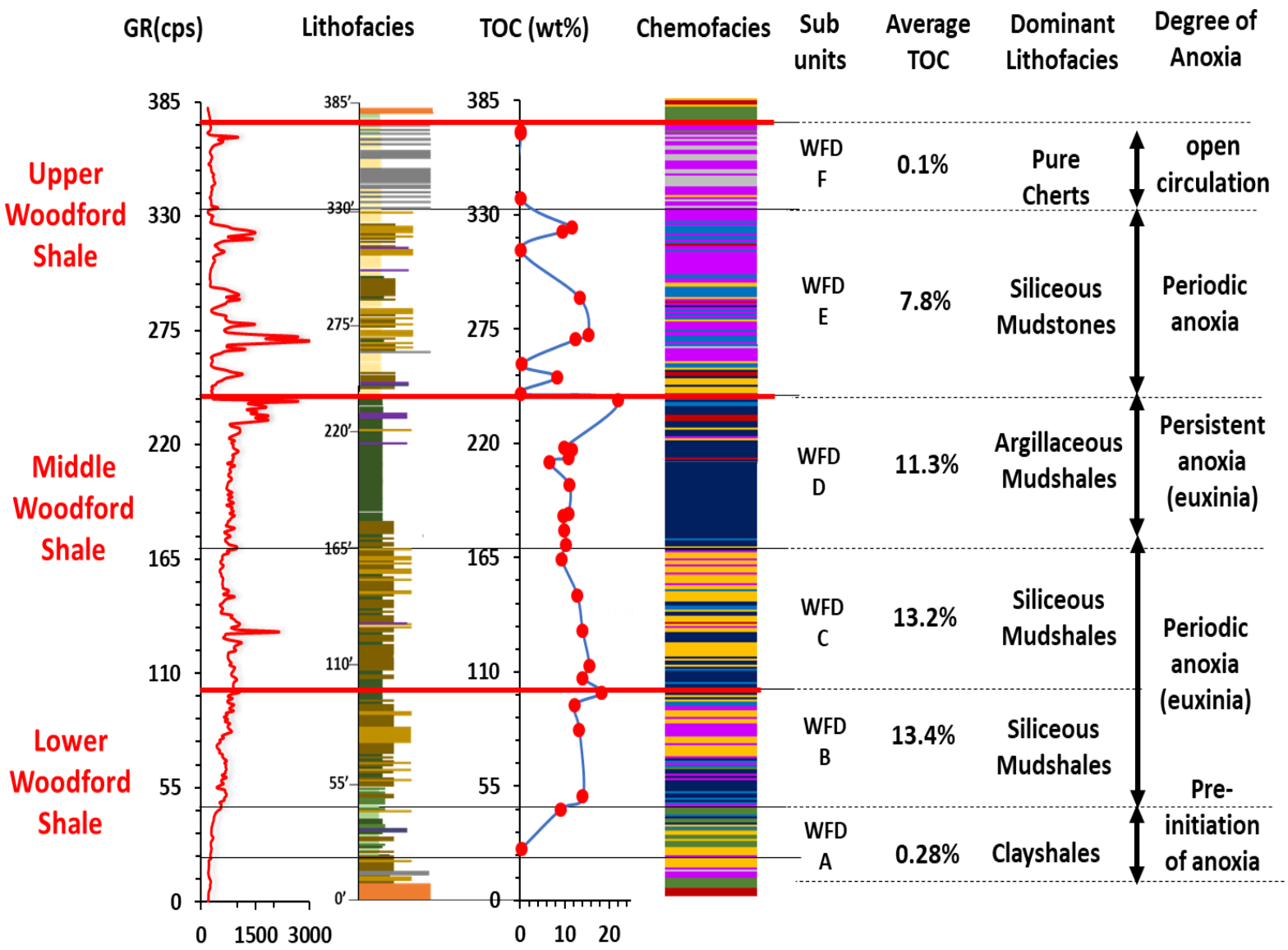
GR(cps)
Lithofacies
TOC (wt%)
Chemofacies
Sub units
Average TOC
Dominant Lithofacies
Degree of Anoxia
Upper Woodford Shale
Middle Woodford Shale
Lower Woodford Shale
385
330
275
220
165
110
55
0
385′
330′
275′
220′
165′
110′
55′
0′
0
1500
3000
0
10
20
WFD F
0.1%
Pure Cherts
open circulation
WFD E
7.8%
Siliceous Mudstones
Periodic anoxia
WFD D
11.3%
Argillaceous Mudshales
Persistent anoxia (euxinia)
WFD C
13.2%
Siliceous Mudshales
Periodic anoxia (euxinia)
WFD B
13.4%
Siliceous Mudshales
WFD A
0.28%
Clayshales
Pre-initiation of anoxia

Figure 51. GR (cps), lithofacies, TOC (wt%), sequence stratigraphic framework, chemofacies and Woodford Shale subdivision defined, and interpreted degree of photic zone euxinia (Modified from Connock 2015). Woodford Shale A unit is interpreted as deposition before the onset of anoxia. Woodford Shale B and C unit is interpreted as deposition during intermittent euxinic conditions (deep chemocline). Woodford D unit represents deposition during persistent euxinic condtions (shallow chemocline). Woodford Shale E unit represents deposition during the cessation of H_2 S. Woodford Shale F unit represents deposition during open circulation.

CHAPTER VII

DISCUSSION

Basin restriction and relation to the depositional model of the Woodford Shale

Results from this study support the depositional model for the Woodford Shale in Infante et al. (2016), Slatt et al., 2016, and Turner (2016) (**Figure 52**). Their model begins with a sub-areal exposure, representing a regional unconformity from a fall in sea level resulting from the erosion and dissolution of the top of the underlying Hunton Group or in some areas, the Sylvan Shale. These erosional processes result in the development of variable topographic relief on the unconformity surface due to incised valleys, sinkholes, and karst topography (Cardona-Valencia, 2014; McCullough, 2014; Slatt et al., 2016, Turner, 2016). The result would be the formation of numerous karsted sub-basins on the underlying Hunton Group that receive variable degrees of basin oceanic circulation (Turner, 2016) (Figure 52).

During early stage sea-level rise, the onset of transgression, the Lower Woodford Shale was preferentially deposited within the sub-basins on the unconformity surface until the lows were completely filled. During this time, the sub-basins were cut off from the open ocean circulation, causing oxygen-deficient waters to form due to restricted conditions, perhaps conducive for the preservation of organic matter (Cardona-Valencia, 2014; Slatt, 2015, Slatt et al., 2016) (**Figure 52**). The occurrence of high TOC intervals in the Lower Woodford Shale support this hypothesis**. Figure 49** also supports this hypothesis as it shows that the Lower Woodford Shale has the strongest basin restriction amongst all three members. Slatt (2015) and Slatt et al. (2016) attributed the strata in the

vicinity of these TOC-rich zones as potential 'sweet spot areas' for drilling. These 'sweet spots' are going to be discontinuous regionally due to the topographical influence.

The low TOC basal green shales underlying the TOC-rich zones in the Lower Woodford Shale is attributed to deposition before the onset of intense degrees of basin restriction, characterized by a mixture of terrestrial and autochthonous marine organic fractions. The mixed clayshale-mudshale were probably deposited during a period of alternating oxic and anoxic conditions, though the anoxic conditions occurred for shorter periods of time. The continued sea-level rise will result in an increase in basin circulation, depositing the Middle Woodford Shale. During the highstand of sea-level, there is improved circulation and oxygenation in the basin, resulting in the overall deposition of organic poor sediments. The presence of oxygenated waters will cause the oxidation of any land-or-marine-derived organic matter that might have been present (Infante et al., 2016; Slatt et al., 2016). **Figure 49** supports this hypothesis, showing decreasing basin restriction from the Lower to the Upper Woodford Shale.

Implication of seasonal contrast on productivity levels and phosphate accumulation

An upwelling model was proposed by Comer (2012), attributing upwelling as a result of aridity and high evaporation rates within the shallow epicontinental seaway that existed across the southern U.S. The implication of seasonal contrast on the phytoplankton abundance in the Cariaco Basin was recognized by Peterson et al. (1991). During the summer-fall rainy season, run-off periods when coastal upwelling is reduced or absent, green algae and dinoflagellates dominate over diatoms. During this period, the water column stability is high, and primary productivity is relatively low. In contrast,

during the dry season, diatoms dominate as primary producers. Strong upwelling results in the rise of cold nutrient-rich water to the surface, causing plankton blooms of high productivity.

As previously mentioned, the idea of seasonal contrast might have an implication on the general characteristics of the Woodford Shale, at least in this particular stratigraphic section. The Middle Woodford is characterized by siliceous lithofacies (siliceous mudshales and mudstones) at the lowermost part and clay-rich lithofacies (argillaceous mudshales) at the uppermost part. This lithofacies shift might be an indication of the seasonal contrast recognized by Peterson et al. (1991), where the clay-rich lithofacies of the upper Middle Woodford Shale may be enriched by *tasmanites cysts*, indicating periods of runoff. The siliceous facies of the lower Middle Woodford Shale (radiolaria-rich) indicates periods of upwelling, perhaps not as intense or strong as observed in the Upper Woodford Shale.

The implication of this hypothesis on the accumulation of phosphate nodules can be explained by applying the phosphogenic model proposed in She et al. (2014). It is possible that run-off sediments as a result of summer-fall rainy season during the deposition of the Woodford Shale (specifically the middle member) resulted in the influx of P from the continent. P gets scavenged by blooming algae followed by "organic rain" to the sea floor with P still bound to organic matter (OM). P is then liberated through microbial decomposition (e.g., microbial sulfate reduction due to increased sulfate availability) (She et al., 2014). Since the water column is stable due to the absence of upwelling/vertical mixing in the water column, P builds up in the deeper waters.

After a period of stagnant conditions, the occurrence of upwelling currents may have permitted the influx of cold nutrient-rich deep waters into the photic zone, leading to the development of a productivity bloom, allowing phosphate nodules to precipitate during the deposition of the Upper Woodford Shale (Beier and Hayes, 1989; She et al., 2014). This hypothesis could explain why phosphate nodules are observed mainly in the Upper Woodford Shale, and only rarely within the rest of the section. How frequent the seasonal contrast occurred during the deposition of the Woodford is uncertain, and is up for further investigation.

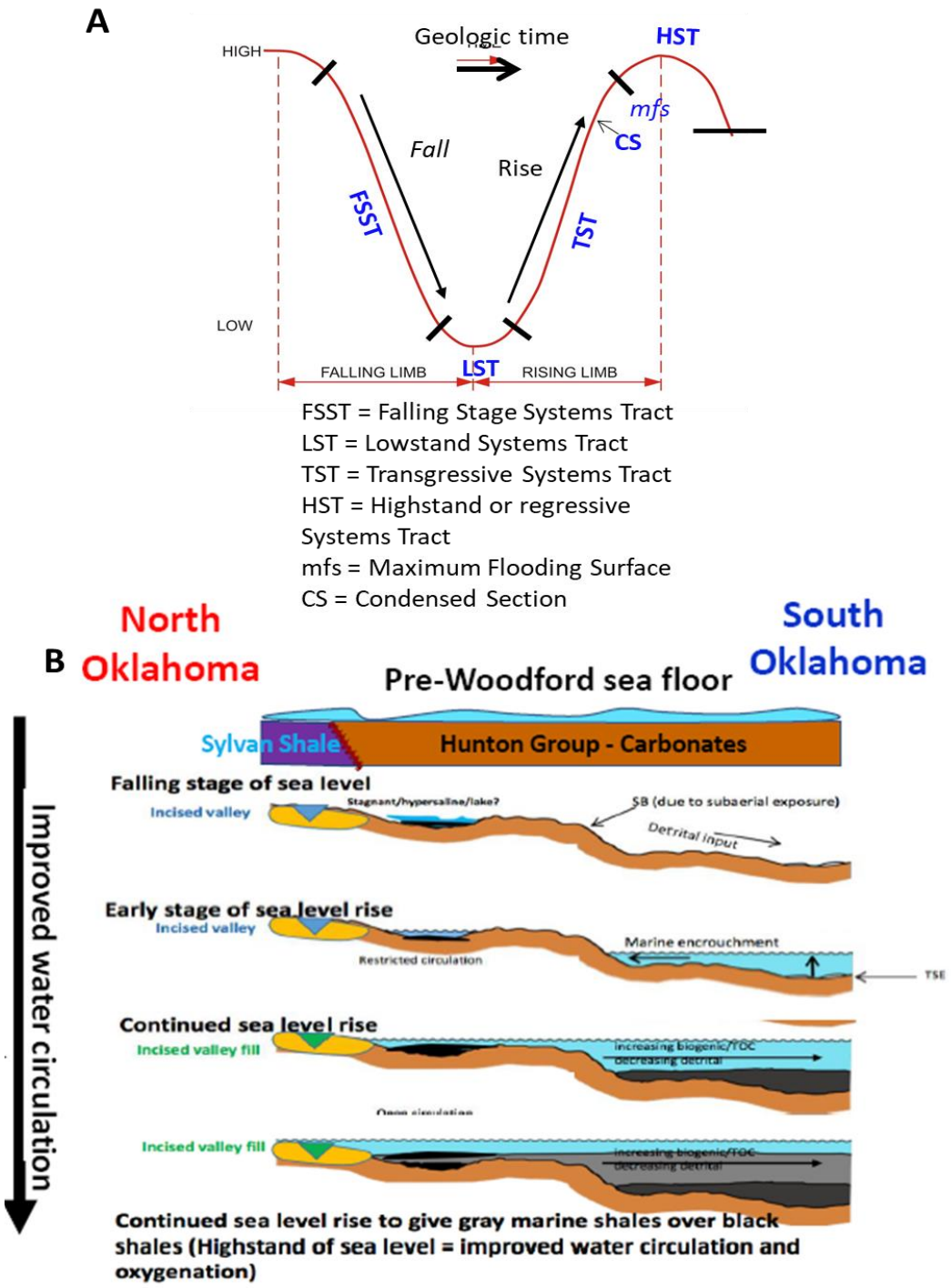

Figure 52 A-B. Depositional model for the Woodford Shale through one seal-level cycle. **A.** Sea-level curve (Slatt, 2013). B. The depositional of the Woodford Shale as a function of sea-level, and paleotopography (Slatt, 2017).

CHAPTER VIII

CONCLUSIONS

By utilizing results from rock description (physical textures) XRD, XRF, and petrographic analysis, eight lithofacies were defined for the Woodford Shale section, starting from most clay-rich to most siliceous, and decreasing degree of fissility: clayshales, mixed clayshale – mudshale, argillaceous mudshales, siliceous mudshales, siliceous mudstones, and radiolarian chert. Calcareous lithofacies defined include dolomitic mudstones and dolomitic mudshales. A bleached lithofacies from the Upper Woodford Shale was also defined. Siliceous mudshales, followed by siliceous mudstones are the most abundant lithofacies throughout the section. Clayshales, mixed clayshale – mudshale (organic poor lithofacies) dominate the basal Lower Woodford. Argillaceous mudshales dominate the Middle Woodford. Interbedding of bedded cherts (organic poor facies) and mudstones/mudshales dominate the Upper Woodford Shale.

Organic-richness, kerogen type, and thermal maturity were assessed for source rock evaluation. The lower and the Upper Woodford Shale showed variations in TOC values, with the Middle Woodford showing the least variation. In general, the Lower Woodford Shale averages the highest TOC values, with the Upper Woodford Shale averaging the least. The variations in TOC values demonstrate the heterogeneity that characterizes the Woodford Shale. Kerogen type assessment shows that the Woodford Shale is dominated by Type II kerogen (oil-prone, and of marine origin), with a mix of Type I kerogen in the Lower Woodford Shale, and dry gas prone in the Upper Woodford Shale. Thermal Maturity assessment shows that the Woodford Shale is of low to

moderate thermal maturity, and falls within the immature to early oil window, indicating the area has not entered the oil window threshold.

From sequence stratigraphic interpretations fourteen GR parasequence sets representing fourteen 3rd order regressive-transgressive cycles were identified. In the Lower Woodford Shale, five 3rd order cycles were identified. Four 3rd order cycles were defined in the Middle Woodford Shale. Five 3rd order cycles were defined in the Upper Woodford Shale. The Lower and Middle Woodford Shale were deposited during a 2nd order TST showing an upward-increasing GR representing deposition toward a distal (basinward) depositional setting. The Upper Woodford Shale was deposited during a 2nd order HST showing a relatively upward-decreasing GR in association with a decrease in organic-rich lithofacies, representing deposition in a relatively proximal (landward) depositional setting.

Based on elemental geochemistry, the depositional environment of the Woodford Shale can be interpreted as one with a successive change in redox conditions, with increasingly oxidizing conditions towards the Upper Woodford Shale. It was found that the lower and upper members were characterized by episodic euxinic conditions, with the Middle Woodford Shale (mainly the uppermost part) subjected to persistent euxinic conditions. The Lower Woodford accumulated under the most variable conditions, followed by the Upper Woodford. The Middle Woodford Shale was deposited under the most stable conditions. Overall, the redox-sensitive elements (U-Mo covariation) suggest similar environments to those inferred by trace element indices (especially Ni/Co).

Chemostratigraphy paired with hierarchical clustering analysis (HCA) present the opportunity to better understand the paleodepositional conditions and to investigate the

possibility for the subdivision of the Woodford Shale. Seven chemofacies were defined and were eventually used to subdivide the Woodford Shale into six units. Results show stratigraphic geochemical variation in the section, where Woodford Shale A unit is characterized by low redox-sensitive elements associated with very high detrital content. Woodford Shale B and C units are characterized by periodic euxinic conditions. Woodford Shale D unit shows persistent euxinic conditions associated with very high - high detrital content. Woodford E unit is dominated by high quartz content with few intervals of high redox-sensitive elements, suggesting periods of basin restriction. Woodford F unit is dominated by high quartz content with low redox-sensitive elements, suggesting deposition during open circulation.

Basin restriction model from Mo-TOC covariation shows increasing basin circulation upwards, from the lower to the Upper Woodford Shale corroborating with the depositional model proposed in Infante et al., (2016), Slatt et al., 2016, and Turner (2016). The Lower Woodford shale shows the most restricted conditions associated with high TOC intervals, with the Upper Woodford deposited as circulation increased upward, although preserving several intervals of restricted conditions (high TOC zones in the Upper Woodford Shale).

FUTURE WORK/RECOMMENDATION

Several questions have been raised about the bleached Upper Woodford Shale at the McAlister Quarry. Questions include; under what conditions did the bleaching occur? Why is the bleaching restricted to just the Upper Woodford Shale? In the subsurface, would the bleaching characteristics be observed? So far in other locations, bleaching has not been reported in the subsurface. To answer these questions, an outcrop core needs to be drilled at the McAlister Quarry as done at the Wyche Farm Quarry (Portas, 2009; Molinares, 2013). I recommend the core be drilled from the top of the resistant Upper Woodford Shale. I also recommend a study to understand the chert and mudstone/mudshale interbedding that characterizes the Upper Woodford Shale. Adapting an age dating technique may help in understanding how long it took for each chert or mudstone/mudshale bed to be deposited.

REFERENCES

Algeo, T.J., and Lyons, T. W., 2006, Mo–total organic carbon covariation in modern anoxic marine environments: Implications for analysis of paleoredox and paleohydrographic conditions: Paleoceanography, v. 21, p. 1-23.

Algeo, T.J., and Maynard, J.B., 2004, Trace-element behavior and redox facies in core shales of Upper Pennsylvanian Kansas-type cyclothems: Chemical Geology, v. 206, p. 289-318.

Algeo, T.J. and Rowe, H., 2012, Paleoceanographic applications of trace-metal concentration data: Chemical Geology, v. 324-325, p. 6-18.

Algeo, T.J., and Tribovillard, N., 2009, Environmental analysis of paleoceanographic Systems based on molybdenum–uranium covariation: Chemical Geology, v. 268, p. 211-225.

Althoff, C.D., 2012, Characterization of depositional megacycles in the Woodford trough of central Oklahoma: M.S. thesis, University of Oklahoma, 99 p.

Amorocho Sanchez, J.D., 2013, Sequence stratigraphy and seismic interpretation of the Upper Devonian-Lower Mississippian Woodford Shale in the Cherokee Platform; a characterization approach for unconventional resources: M.S. thesis, University of Oklahoma, 109 p.

Amsden, T.W., 1975, Hunton Group (Late Ordovician, Silurian, and Early Devonian) in the Anadarko basin of Oklahoma. OGS Bulletin, v. 121, 214 p.

Amsden, T.W. & Klapper, G., 1972, Misener Sandstone (Middle-Upper Devonian), north-central Oklahoma: AAPG Bulletin, v. 56, p. 2323-2334.

Anderson, J.R., 2013, A regional stratigraphic synthesis of the Woodford Shale between the Arkoma and Anadarko basins with an emphasis on sediment transport and deposition across the Nemaha Ridge: M.S. thesis, Utah Valley University, 63 p.

Ataman, O., 2008, Natural fracture systems in the Woodford Shale, Arbuckle Mountains, Oklahoma: M.S. thesis, Oklahoma State University, 139 p.

Aufill, M.G., 2007, Outcrop-based correlation of magnetic susceptibility with spectral gamma- ray spectrometry in the Woodford Shale: MS thesis, Oklahoma State University, 210p.

Banner, J.L. 1995. Application of the trace element and isotope geochemistry of strontium to studies of carbonate diagenesis: Sedimentology, 42, 805-824.

Becerra-Rondon, D.M., 2017, Comprehensive characterization of the Woodford Shale at

the I-35 outcrop, Arbuckles Mountains Area, Oklahoma: M.S. thesis, University of Oklahoma, 187p.

Beier, J.A., and Hayes, J.M., 1989, Geochemical and isotope evidence for paleoredox conditions during deposition of the Devonian-Mississippian New Albany Shale, southern Indiana: Geological Society of America Bulletin, v. 101, p. 774-782.

Berner, R. A., 1985, Sulphate reduction, organic matter decomposition and pyrite formation, Phil. Trans. R. Soc. Lond., 1985, A 315, 25–38.

Berryman, R.R., 2008, Constraints on development of anoxia through geochemical facies mapping of Devonian black shales in the Midcontinent: M.S. Thesis, Oklahoma State University, 57p.

Bixler, W. G., 1993, Structural analysis of the central Arbuckle Anticline, Southern Oklahoma: M.S. Thesis, Baylor University.

Blackford, M.A., 2007, Electrostratigraphy, thickness, and petrophysical evaluation of The Woodford Shale, Arkoma Basin, Oklahoma: MS Thesis, Oklahoma State University, 84p.

Boardman, 2009, Preliminary analysis of phosphate nodules in the Woodford Shale, Late Devonian-Early Mississippian, southern Oklahoma: MS thesis Oklahoma State University, 77p.

Brito, R.J., Slatt, R.M, Ekwunife**,** I.C., Turner, B.W., 2017, The Woodford Shale in the Marietta Basin (Oklahoma and Texas): Abstract presented at 2017 AAPG Mid-Continent Section Continent Section Meeting, Oklahoma City, Oklahoma, September 30-October 3.

Brumsack, H.J., 2006. The trace metal content of recent organic carbon-rich sediments: implications for Cretaceous black shale formation. Palaeogeography, Palaeoclimatology, Palaeoecology, v. 232, p. 344-361.

Calvert, S.E., Pedersen, T.F., 1993. Geochemistry of recent oxic and anoxic sediments: Implications for the geological record: Marine Geology, v. 113, p.67–88.

Cardona-Valencia, L.F., 2014, Integrated characterization of the Woodford Shale in the Southern Cherokee Platform, Oklahoma: Norman, Oklahoma, M.S. thesis, University of Oklahoma, 98 p.

Cardott, B.J., W.J. Metcalf, and J.L. Ahern, 1990, Thermal maturation by vitrinite reflectance of Woodford Shale near Washita Valley fault, Arbuckle Mountains, Oklahoma, in: V.F.Nuccio and C.E. Barker, eds., Applications of thermal maturity studies to energy exploration: SEPM, Rocky Mountain Section, p.139-146.

Cardott, B.J., 2005. Overview of unconventional energy resources of Oklahoma. In: Cardott, B.J. (Ed.), Unconventional Energy Resources in the Southern Midcontinent, 2004 Symposium: Oklahoma Geological Survey Circular110, p.7-18.

Cardott, B.J., 2012, Thermal maturity of Woodford Shale gas and oil plays, Oklahoma, USA: International Journal of Coal Geology, v.103, p.109-119.

Comer, J.B., 2005, Facies distribution and hydrocarbon production potential of Woodford Shale in the southern Midcontinent, in: B.J. Cardott, ed., Unconventional energy resources in the southern Midcontinent, Oklahoma Geological Survey Circular 110, p.51-62.

Comer, J.B., 2008, Woodford Shale in southern Midcontinent, USA-Transgressive system tract marine source rocks on an arid passive continental margin with persistent oceanic upwelling: AAPG Annual Convention, San Antonio, TX, poster, 3 panels.

Comer, J.B., 2012, Woodford Shale and the evaporate connection – the significance of aridity and hypersalinity in organic matter productivity and preservation: of Geological Society America Abstracts with Programs, v. 44(5), p. 6.

Connock, G.T., 2015, Paleoenvironmental interpretation of the Woodford Shale, Wyche Farm shale pit, Pontotoc County, Arkoma Basin, Oklahoma with primary focus on water column structure: M.S. thesis, University of Oklahoma, 253 p.

Cornford, C., Gardner, P. & Burgess, C., 1998, Geochemical truths in large data sets. Part I: Geochemical screening data. Organic Geochemistry, v. 29, p. 519-530.

Cruse, A, 2010, Schematic Figures, Personal Correspondence. In Berryman, R.R., 2008, Constraints on development of anoxia through geochemical facies mapping of Devonian black shales in the Midcontinent: M.S. Thesis, Oklahoma State University.

DeGarmo, C.D., 2015, Geochemical characterization of the Woodford Shale (Devonian-Mississippian), McAlister Cemetery Quarry, Criner Hills Uplift, Ardmore Basin, Oklahoma: M.S. Thesis, University of Oklahoma, unpublished, 198 p.

Demaison, G. J., and Moore, G. T., 1980. Anoxic environments and oil source bed genesis: Organic Geochemistry, v. 2, p. 9-31.

Donovan, R.N., 2001, Field study of the Sycamore Formation on Interstate Highway 35 in the Arbuckle Mountains, Oklahoma, in K.S. Johnson, ed., Silurian, Devonian, and Mississippian geology and petroleum in the southern Midcontinent, 1999 symposium, Oklahoma Geological Survey Circular 105, p. 139-149.

Ekwunife, I.C., Turner, B.W., Slatt, R.M, Chemostratigraphy of the Woodford Shale, McAlister Cemetery Quarry, Ardmore Basin, Oklahoma: Abstract from 2016 AAPG Annual Convention and Exhibition, Calgary, Alberta, June 19-22.

Ekwunife, I.C., and Slatt, R.M, High-Resolution Chemostratigraphy of the Woodford Shale in the McAlister Quarry, Ardmore Basin, Oklahoma: Implications for depositional conditions and stratigraphic subdivision: Abstract from 2017 AAPG International Convention and Exhibition, London, England, October 15-16.

Ellis, R., 2013, Analysis of the cyclostratigraphy at The Devonian-Carboniferous boundary in south-central Oklahoma: MS thesis, Louisiana State University, 45p.

Fishman, N.S., G.S. Ellis, A.R. Boehlke, S.T. Paxton, and S.O. Egenhoff, 2013, Gas storage in the Upper Devonian-Lower Mississippian Woodford Shale, Arbuckle Mountains, Oklahoma: How much of a role do chert beds play?, in: J.Y. Chatellier and D.M. Jarvie, eds., Critical assessment of shale resource plays: AAPG Memoir 103, p.81-107.

Galvis, H.A., 2017. Detailed Lithostratigraphic Characterization and Sequence Stratigraphy of a complete Woodford Shale Outcrop Section in Southern Oklahoma: M.S. thesis, University of Oklahoma, 142p.

Gupta, N., Sarkar, S., and Marfurt, K. J., 2011, Seismic characterization of the Woodford Shale in the Anadarko basin: SEG Technical Program Expanded Abstracts, v. 30, p. 1083-1087.

Grayson, R., 1985, Tectonism and Sedimentation in the Arbuckle Mountain region, Southern Oklahoma Aulacogen: Baylor Geological Society, AAPG Student Chapter, 43p.

Grotzinger, J. G., and T. H. Jordan, 2010, *Understanding earth* (6th ed.): W. H. Freeman.

Ghosh, S., 2017a, Integrated Studies on the Woodford Shale natural fracture attributes, origin, and their relation to hydraulic fracturing: Doctoral thesis, University of Oklahoma, p. 264.

Ghosh, S., 2017b. High-resolution stratigraphic characterization of natural fracture attributes in the Woodford Shale, Arbuckle Wilderness and US-77D Outcrops, Murray County, Oklahoma. Interpretation v. 6(1), p.1-64.

Gilleaudeau, G.J., Kah, L.C., 2013b. Oceanic molybdenum drawdown by epeiric sea expansion in the Mesoproterozoic. Chemical Geolology, v.356, p. 21-23.

Gregory, D.D., Large, R.R., Halpin, J.A., Baturina, E.L., Lyons, T.W., Wu, S., Danyushevsky, L., Sack, P.J., Chappaz, A., Maslennikov, V.V., and Bull, S.W.,

2015, Trace element content of sedimentary pyrite in black shales: Economic Geology, v. 110, p. 1389-1410.

Güler, C., Thyne, G.D., McCray, J.E., & Turner, A.K. 2002. Evaluation of graphical and multivariate statistical methods for classification of water chemistry data. Hydrogeology Journal, v.10, p. 455-474.

Gupta, N., Sarkar, S., & Marfurt, K.J., 2011, Seismic characterization of the Woodford Shale in the Anadarko Basin: SEG Annual Meeting, p. 1083-1087.

Ham, W.E., and Amsden, T.W., 1973, Regional geology of the Arbuckle Mountains, Oklahoma: Oklahoma Geological Survey Special Publication 73-3, 61p.

Hardie, W.E., 1990, Subsurface structural study of the buried Ouachita thrust front, southeastern Oklahoma: Oklahoma City Geological Society, Shale Shaker, v. 41, p. 32-55.

Hester, T.C., J.W. Schmoker, and H.L. Sahl., 1990, Log-derived regional source-rock characteristics of the Woodford Shale, Anadarko basin, Oklahoma: U.S. Geological Survey Bulletin 1866-D, 38p.

Hildred, G.V., Ratcliffe, K.T., Wright, A.M., Zaitlin, B.A., and David, S.W., 2010, Chemostratigraphic applications to low-accommodation fluvial incised-valley settings: an example from the lower Mannville Formation of Alberta, Canada: Journal of Sedimentary Research, v. 80, 1032-1045.

Hoffman, P., J.F. Dewey, and K. Burke, 1974, Aulacogens and their genetic relation to geosynclines, with a proterozoic example from Great Slave Lake, Canada, in Modern and ancient geosynclinal sedimentation: SEPM Special Publication No.19, p.38-55.

Huerta-Diaz, M.A., Morse, J.W., 1990. A quantitative method for determination of trace metal concentrations in sedimentary pyrite. Marine Chemistry. 29, 119-144.

Infante-Paez, L., Cardona, L. F., McCullough, B., & Slatt, R., 2016, Seismic analysis of paleotopography and stratigraphic controls on total organic carbon: Rich sweet spot distribution in the Woodford Shale, Oklahoma, USA. Interpretation, v.5-1, p. 33-47.

Ingram, R.L., 1953, Fissility of Mudrocks: GSA Bulletin, v. 64 (8), p. 869-878.

Jarvie, D. M., 1991, Source and Migration Processes and Evaluation Techniques, chapter 11, p. 113-118.

Jones, L., 2017, An integrated analysis of sequence stratigraphy, petroleum geochemistry, and Devonian mass extinction events in the Woodford Shale, Southern Oklahoma: M.S. thesis, University of Oklahoma.

Jones, B., & Manning, D. (1994). Comparison of geochemical indices used for the interpretation of paleoredox conditions in ancient mudstones. Chemical Geology, 111-129.

Kaushik, N., 2009, Clustering Analysis: Technological Institute of Textile & Sciences, Adapted from LinkedIn SlideShare.

Kirkland, D.W., R.E. Denison, D.M. Summers, and J.R. Gormly, 1992, Geology and organic geochemistry of the Woodford Shale in the Criner Hills and western Arbuckle Mountains, in: K.S. Johnson and B.J. Cardott, eds., Source rocks in the southern Midcontinent symposium: Oklahoma Geological Survey, Circular 93, p.38-69.

Klockow, C.M., 2017, Structural survey of the Woodford Shale at McAlister Cemetery, Quarry Carter County, Oklahoma: M.S. thesis, University of Oklahoma, 40 p.

Krystyniak, A.M., 2005, Outcrop-based gamma-ray characterization of the Woodford Shale of south-central Oklahoma: MS thesis, Oklahoma State University, 145p.

Lambert, M.W., 1993, Internal stratigraphy and organic facies of the Devonian-Mississippian Chattanooga (Woodford) Shale in Oklahoma and Kansas, in B.J. Katz and L.M. Pratt, eds., Source rocks in a sequence stratigraphic framework: AAPG Studies in Geology 37, p. 163-176.

Landis, E.R., 1962, Uranium and other trace elements in Devonian and Mississippian black shales in the central midcontinent area: U.S. Geological Survey Bulletin 1107-E, p.289-336.

Large, R.R., Bull, S.W., and Maslennikov, V.V., 2011, A carbonaceous sedimentary source-rock model for Carlin-type and orogenic gold deposits: Economic Geology, v. 106, p. 331-358.

Lewan, M., 1978, Laboratory Classification of Very Fine Grained Sedimentary Rocks: Geology, v. 6, p. 745-748.

Luening, S., and Kolonic, S., 2003, Uranium spectral gamma-ray response as a proxy for organic richness in black shales; applicability and limitations: Journal of Petroleum Geology, v. 26, no. 2, p. 153–174.

Lyons, T.W., 1997, Sulfur isotopic trends and pathways for iron sulfide formation in upper Holocene sediments of the anoxic Black Sea: Geochimica et Cosmochimica Acta, 61, 3367–3382.

Lyons, T.W., Werne, J.P., Hollander, D.J., Murray, R.W., 2003, Contrasting sulfur geochemistry and Fe/Al and Mo/Al ratios across the last oxic-to-anoxic transition in the Cariaco Basin,Venezuela: Chemical Geololgy, 195, 131–157.

Molinares-Blanco, C.E., 2013, Stratigraphy and palynomorphs composition of the Woodford Shale in the Wyche Farm Shale Pit, Pontotoc County, Oklahoma. M.S. thesis, University of Oklahoma, 90 p.

McCreight, K., 2014, Geochemical analysis of the Woodford Shale, Anadarko Basin, Oklahoma: MS thesis, University of Texas Arlington, p. 10-40.

McCullough, B.J., 2014, Sequence stratigraphic framework and characterization of the Woodford Shale on the southern Cherokee Platform of central Oklahoma. University of Oklahoma, MS thesis, 211p.

Milliken, K.L., Choh, S.-J., Papazis, P., Schieber, J., 2007. "Cherty" stringers in the Barnett Shale are agglutinated foraminifera. Sedimentary Geology 198, 221–232.

Nance, H.S. & Rowe, H. 2015. Eustatic controls on stratigraphy, chemostratigraphy, and water mass evolution preserved in a Lower Permian mudrock succession, west Delaware Basin, Texas, USA: Interpretation, 3, SH11-SH25.

Noble, P.J., 1995, Regional sedimentation patterns associated with the passive- to active-margin transition, Ouachita Orogeny, southern Midcontinent, U.S.A., in K.S. 152.

Maynard, S., 2016, SCorrelation of bioturbated facies, chemostratigraphy, total organic carbon, and sequence stratigraphy in the Woodford Shale of south central Oklahoma: M.S. Thesis, University of Oklahoma, 119p.

Miceli-Romero, A., 2008. Geochemical characterization of the Woodford Shale, Central and Southeastern Oklahoma: M.S. Thesis, University of Oklahoma.

Miceli-Romero, A., and R.P. Philp, 2012, Organic geochemistry of the Woodford Shale, southeastern Oklahoma: How variable can shales be?: AAPG Bulletin, v. 96, p. 493-517.

Molinares-Blanco, C.E., 2013, Stratigraphy and palynomorphs composition of the Shale Woodford in the Wyche farm shale pit, Pontotoc County, Oklahoma, University of Oklahoma, MS thesis, 90p.

Parrish, 1982, J. T., Upwelling and Petroleum Source Beds, With Reference to Paleozoic: AAPG Bulletin, v. 66, No. 6, p. 750-774.

Paxton, S. T., A. Cruse, and A. Krystyniak, 2007, Fingerprints of global sea level change revealed in hydrocarbon source rock?: http://www.searchanddiscovery.com/documents/2006/06095paxton/images/

paxton.pdf (accessed February 5, 2013).

Paxton, S.T., and B.J. Cardott, 2008, Oklahoma gas shales field trip, October 21-23, 2008, Oklahoma Geological Survey Open File Report 2-2008, 110p.

Pearce, T.J., Besly, B.M., Wray, D.S., & Wright, D.K. 1999. Chemostratigraphy: a method to improve interwell correlation in barren sequences – a case study using onshore Duckmantian/Stephanian sequences (West Midlands, U.K.): Sedimentary Geology, v. 124, p. 197-220.

Pearce, T.J. & Jarvis, I. 1992. Applications of geochemical data to modelling sediment dispersal patterns in distal turbidites: Late Quaternary of the Madeira Abyssal Sedimentary Petrology, v. 62, p. 1112-1129.

Pearson's Correlation Coefficient, statistics.leard.com. https://statistics.laerd.com/statistical-guides/pearson-correlation-coefficient-statistical-guide.php (accessed December 1, 2017).

Peterson, L.C., Overpeck, J.T., Kipp, N.G., Imbrie, J., High-resolution late quaternary upwelling record from the anoxic Cariaco Basin, Venezuela: paleoceanography, vol. 6(1), p. 99-119.

Pike, J., Kemp, A.E.S., 1996. Silt aggregates in laminated marine sediment produced by agglutinated Foraminifera. Journal of Sedimentary Research 66, 625–631.

Portas, A.R.M., 2009, Characterization and origin of fracture patterns in the Woodford Shale in Eastern Oklahoma for applications to exploration and development: M.S. Thesis, University of Oklahoma.

Potter, P.E., Maynard, J.B., and Pryor, W.A, 2013, Sedimentology of shale: study guide and reference source: Springer Science & Business Media, 300p.

Ratcliffe, K.T., Morton, A.C., Ritcey, D.H., Evenchick, C.A., 2007, Whole-rock geochemistry and heavy mineral analysis as petroleum exploration tools in the Bowser and Sustut Basins, British Columbia, Canada: Bulletin of Canadian Petroleum Geology v. 55(4), p. 320-336.

Roos, P., 2001, Studies of anoxic conditions in Framvaren fjord, Gullmaren fjord and Byfjorden and of mixing between seawater and freshwater at the Kalix river and estuary: Palsson. S.E., v. 33(5), p. 3-28

Rowe, H., Hughes N., Robinson, K., 2012, The quantification and application of handheld energy-dispersive x-ray fluorescence (ED-XRF) in mudrock chemostratigraphy and geochemistry: Chemical Geology, p. 122-131.

Rowe, H. D., R. G. Loucks, S. C. Ruppel, and S. M. Rimmer, 2008, Mississippian Barnett Formation, Fort Worth Basin, Texas: Bulk geochemical inferences and Mo-TOC constraints on the severity of hydrographic restriction: Chemical Geology, v. 257, p. 16-25.

Ruppel, S.C., 2016, Can sequence stratigraphic concepts be applied in mudrock systems? AAPG Search and Discovery Article #51380, Adapted from oral presentation given at AAPG Annual Convention & Exhibition, Houston, Texas, April 2-5, 2017.

Sageman, B. B., and Lyons, T. W., 2004, Geochemistry of fine-grained sediments and sedimentary rocks: *In*: Mackenzie, F., 2004, Sediments, diagenesis, and sedimentary rocks: Treatise on Geochemistry, vol. 7, p. 115-158.

Sano, J.F., Ratcliffe, K.T., and Spain, D.R., 2013, Chemostratigraphy of the Haynesville Shale: AAPG Memoir 105, p. 137-154.

Schieber, J., 1996, Early diagenetic silica deposition in algal cysts and spores: a source of sand in black shales?: Journal of Sedimentary Research, v. 66, p. 175-183.

Schieber, J., 2009, Discovery of agglutinated benthic foraminifera in Devonian black shales and their relevance for the redox state of ancient seas: Palaeogeography, Palaeoclimatology, Palaeoecology v. 271, p. 292-300.

Schwartzapfel, J.A., 1990, Biostratigraphic investigations of late Paleozoic (Upper Devonian to Mississippian) Radiolaria within the Arbuckle Mountains and Ardmore basin of south-central Oklahoma: Ph.D. dissertation, University of Texas, 475 p.

Serna-Bernal, A., 2013, Geological Characterization of the Woodford Shale McAlister Cemetery Quarry, Criner Hills, Ardmore Basin, Oklahoma: M.S. thesis, University of Oklahoma, 85p.

She, Z., Strother, Paul., Papineau, D., (2014), Terminal Proterozoic cyanobacterial blooms and phosphogenesis documented by the Doushantuo granular phosphorites II: microbial diversity and C isotopes: Precambrian Research, v. 251, p. 62-79.

Singh, P., 2008, Lithofacies and sequence stratigraphic framework of the Barnett Shale, northeast Texas: Ph.D. dissertation, University of Oklahoma, 199 p.

Skei, J. (1983). Geochemical and sedimentological considerations of a permanently anoxic fjord- Framvaren, south Norway: Sedimentary Geology, v. 36 131-145.

Skei, J. (1986). The Biogeochemistry of Framvaren. Data report 1931-1985. NIVA). ISBN 82-Framvaren, south Norway: Sedimentary Geology, v. 36, p. 131-145.

Slatt, R.M., 2013a, Stratigraphic Reservoir Characterization for Petroleum Geologists, Geophysicists, and Engineers: Science, 688p.

Slatt, R.M., 2013b, Sequence stratigraphy of the Woodford Shale and application to drilling and production: AAPG Search and Discovery Article #50792, Adapted from oral presentation, 2013 AAPG Woodford Shale Forum, Oklahoma City, Oklahoma, April 11.

Slatt, R.M., 2017, Outcrop and subsurface geology applied to drilling, sweet spot and target zone detection of resource shales: the Woodford example: SPE Luncheon, Oral presentation, November, 2017.

Slatt, R.M., Buckner, N., Abousleiman, Y., Sierra, R., Philp, P., Micelli-Romero, A., Portas, R., O'Brien, N., Tran, M., Davis, R., & Wawrzyniec, T., 2012, Outcrop-behind outcrop (quarry): multiscale characterization of the Woodford gas shale, Oklahoma, in J. Breyer, ed., Shale reservoirs-giant resources for the 21st century, AAPG Memoir 97, p. 382-402.

Slatt, R.M., Jordan, D.W., D'Agostino, A.E., & Gillespie, R.H. 1992. Outcrop gamma-ray logging to improve understanding of subsurface well log correlations. In: Hurst, A., Griffths, C.M., & Worthington, P.F. (eds.) Geological Applications of Wireline Logs II: Geological Society of London Special Publication, 65, 3-19.

Slatt, R.M., McCullough, B.J., Molinares-Blanco, C.E., & Baruch, E.T., 2016, Paleotopographic and Depositional Environmental Control on "Sweet Spot" locations in Some Unconventional Resource Shales. The Houston Geological Society Bulletin, v. 58 (8), p. 37-39.

Slatt, R.M. and N.D. Rodriguez., 2012, Comparative sequence stratigraphy and organic geochemistry of gas shales: Commonality or coincidence? Journal of Natural Gas Science and Engineering, v.8, p.68-84.

Suneson, H., 1996, The geology of the Ardmore Basin in the Lake Murray State Park Area,Oklahoma: Field Trip, Oklahoma Geological Survey, 32p.

Taff, J.A., 1902, Description of the Atoka quadrangle: U.S. Geological Survey Geologic Atlas Folio 79, scale 1:125,000, 8 p.

Taylor, S.R., McLennan, S.M., 1985, The Continental Crust: Its Composition and Evolution. Blackwell Scientific Publication,, 312 p.

Tinnin, B.M., and Darmaoen, S.T.R., 2016, Chemostratigraphic variability of the eagle ford shale, south texas: insights into paleoredox and sedimentary facies changes. in J. A Breyer, ed., The Eagle Ford Shale: A renaissance in U.S. oil production: AAPG Memoir 110, p. 259–283.

Tissot, B.P., Welte; D.H., 1978, Petroleum Formation and Occurrence, Berlin; New York: Springer-Verlag, 538 p.

Tréanton, J., 2014, Outcrop-derived chemostratigraphy of the Woodford Shale, Murray County, Oklahoma: Norman, University of Oklahoma, unpublished M.S. thesis 65 p.

Turner, A.K. & Closs, L.G. 2009. Cluster Analysis. GEGN 532: Geological Data Analysis. Colorado School of Mines Lecture, April 14, 2009.

Turner, B.W., C.E., Molinares, and R.M., Slatt, 2015. Chemostratigraphic, palynostratigraphic, and sequence stratigraphic analysis of the Woodford Shale, Wyche Farm Quarry, Pontotoc County, Oklahoma: Journal Interpretation, v.3-1, p.1-9.

Turner, B. W., 2016, Utilization of chemostratigraphic proxies for generating and refining sequence stratigraphic frameworks in mudrocks and shales: Doctoral thesis, University of Oklahoma, Norman, 119p.

Turner, B.W., J.A. Tréanton, and R.M. Slatt, 2016, The use of chemostratigraphy to refine ambiguous sequence stratigraphic correlations in marine mudrocks. An example from the Woodford Shale, Oklahoma, USA: London, Journal of the Geological Society, v.173 (5), p. 854-868.

Tribovillard, N., Algeo, T. J., Lyons, T., and Riboullean, A., 2006, Trace metals as paleoredox and paleoproductivity proxies: an update: Chemical Geology, v. 232, p. 12-32.

Tribovillard, N., Algeo, T.J., Baudin, F., Riboulleau, A., 2012, Analysis of marine Environmental paleoceanography: Chemical Geology, 324-325, p. 46–58.

Vail, P.R., 1987, Seismic stratigraphy interpretation using sequence stratigraphy. Part I: Seismic stratigraphy interpretation procedure. In Atlas of Seismic Stratigraphy, ed. AW Bally, p. 1-10. Am. Assoc. Petrol. Geol. Stud. Geol. no. 27, v.1, 125 p.

Vine, J. D., and Tourtelot, E. B., 1970, Geochemistry of black shale deposits, a summary report, Economic Geology, vol. 65(3), p. 253-272.

Walper, J., 1977, Paleozoic tectonics of the Southern Margin in North America: Gulf Coast Association of Geological Societies, v. 27, p.230-241.

Ward, J.H. 1963. Hierarchical grouping to optimize an objective function. Journal of the American Statistical Association, 69, 236-244.

Wickham, J., 1978, The Southern Oklahoma Aulacogen: School of Geology & Geophysics, University of Oklahoma, 41p.

Witzke, B. J., and Heckel,P. H.,1989,Paleoclimatic indicators and inferred Devonian Paleolatitudes of Euramerica,in McMillan,N. J.,Embry,A. F.,and Glass,D. J.,eds.,Devonian of the world: Calgary, Canadian Society of Petroleum Geologists,Memoir 14 ,v. 1, p. 49-63.

Yu, G., Hu, W., He, Z., Kui, X., Hu, H., He, L., Wang, T., Li, P., 2015, Complex resistivitycharacteristics of high TOC marine shale core samples and its applications: SEG Technical Program Expanded Abstracts 2014: p. 2964-2968.

APPENDIX I: HARDNESS

Hardness tests were performed on all 382 samples using an Equotip Bambino 2® hardness tester, provided by the Institute of Reservoir Characterization at the University of Oklahoma. The Equotip Bambino 2® hardness tester is a hand-held, portable, non-destructive device that uses the Leeb rebound principle that was developed by Proceq SA.

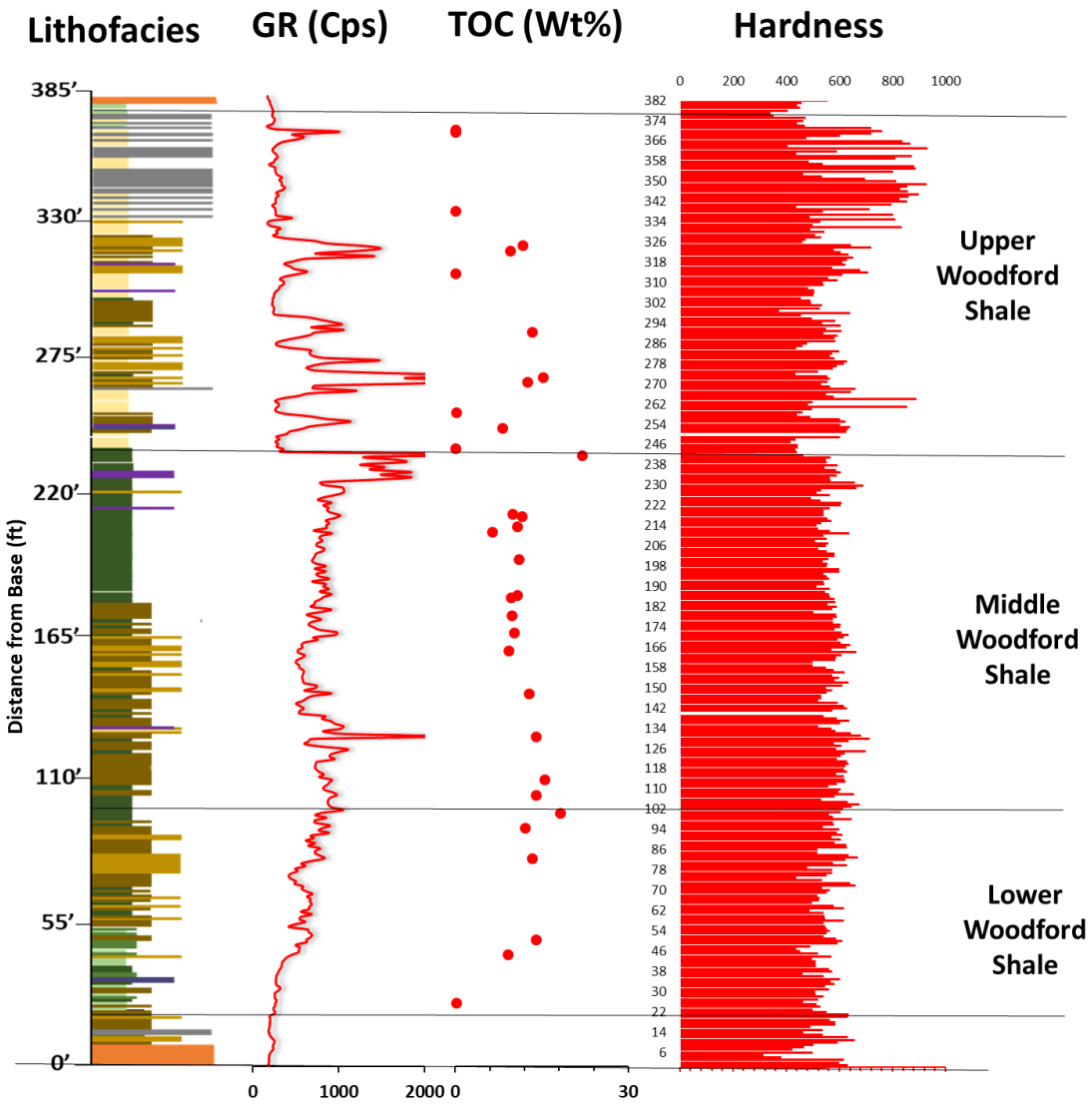

Figure 53. Stratigraphic hardness variation. Hardness variation with GR, lithofacies, and TOC.

Hardness data was excluded from this study because of the lack of correlation with other data available (i.e., XRF). This could be due to the degree of weathering of the Woodford Shale outcrop, or the heterogeneity within each sample, or as a result of both. It was observed that the type of lamination that is present within a sample can make a difference in the hardness values. Hence, it is important to take note of what type of laminations (if present) are observed in samples. For example, a silica-rich or clay rich lamination will make a difference. The inability to retrieve samples in some parts of the section due to weathering resulted in the underestimation of hardness values.